

1 **Review of “Tectono-thermal evolution of Oman’s Mesozoic passive**
2 **continental margin under the obducting Semail Ophiolite: a case study Jebel**
3 **Akhdar, Oman” by Arne Grobe et al. Author’s replies in green**

4 **Summarized comments of - M. Zattin (Referee) – Author’s replies in green**

5 Dear Prof. Zattin,

6 Thank you for your valid comment and feedback.

7 All comments made in the PDF were accepted as suggested and/or are commented below.

8 Especially, we extended on the meaning and importance of the study in the Introduction and revised and
9 extended the data description. The discussion now also elaborates on the errors associated with the temperature
10 predictions.

11 Moreover, we revised the Figures and Tables and enlarged the fonts.

12
13 1) First, the figures are in general not clear. The writings are very often too
14 small, keys for acronyms and colors are missing, and some diagrams should be added
15 (see annotated pdf for details). We revised the figures; please keep in mind that the figures appear smaller in the
16 automatically generated preview pdfs than in the later manuscript

17 2) Fig. 3 mixes stratigraphic and structural information We revised Figure 3

18 3) Revise tables DONE

19 4) Emphasize meaning of this work in the introduction – goals are not clear DONE

20 5) Description of results need improvement in text, figures and tables DONE

21 6) Relationship of map temperatures and stratigraphic age should be illustrated in a diagram with errors We
22 revised Figure 3 and updated the temperature data accordingly. To keep the number of total figures low,
23 we kept the information in one Figure.

24
25 L 54 – Rewrite first paragraph of introduction, expanding the concept DONE

26 L 72 – How can you say that peak temperatures reached by obduction have not been overprinted Rephrased

27 L75-79 - You should clear better the goals of the paper, especially focussing on the originality of the results.

28 Fig 2 – size depict... - Not clear what you mean Size was uniformed to prevent confusion and sentence in the
29 caption was deleted

30 L 106 - There is a big gap between this paragraph and the previous ones. DONE

31 L 111 – Batinah Coast - Not in figure DONE

32 L 112 – Ophiolite exposed subaerial - When? Since the early Paleogene? DONE, text now reads: The sedimentary
33 record in the Batinah coast and the foreland, as well as laterite formation on top of the ophiolite suggest subaerial
34 exposure and a slow-down or stopped obduction in the early Paleogene before lower marine conditions were
35 restored in the Maastrichtian

36 L129 - I suggest to merge the thermochronology studies in the more general discussion about exhumation that
37 started in the previous paragraph DONE

38 Figure 3

39 L 188-190 - This sentence is out of place Deleted as information was not essential for the manuscript

40 L 202-203 - This sentence is not clear Rewritten, now reads: Duretz et al. (2015) showed in a lithospheric scale
41 thermo-mechanical model that a thermal anomaly c. 100 km northwest of the Arabian margin is necessary to
42 initiate subsea thrusting (Duretz et al. 2015).

43

44 L 234 - Which are the errors associated to this equation and the following transformation into temperatures?

45 L 291/2 – sentence deleted as suggested DONE

46 L 310 - Actually, from what you write in the legend of figure S2, this is not an assumption but the result of a
47 sensitivity analysis. Text was changed accordingly

48 L 326 - The relationships between temperature and stratigraphic age are somehow visible in figure 3 but I suggest
49 to do a separate diagram. Figure was changed accordingly also taking other reviews into consideration

50

51 Table 1

52 Figures S3, S4 use different sample names, S4 is missing DONE

53

54 L 347 - Given the number of analyzed grains, it is difficult to say if two populations are really present or if the
55 broad range of ages is related to other causes (frequent with U-Th/He analysis)

56 We agree with the reviewer that a spread in ages is commonly observed in U-Th/He analysis. As the reviewer
57 rightly states, this may have multiple causes. We also agree that for a sound statistical analysis of presence of grain
58 age populations many more aliquots would be required (117 is a number determined by Vermeesch). The question
59 the reviewer poses is whether the observed populations are indeed geologically meaningful or may represent
60 factors independent of time-temperature history (such as inclusions, helium implantation or the like). We note that
61 in the data discussed here (i.e. T-5 and T-7), we find reproducing aliquots at roughly 58 and 100 Ma. It seems a
62 stretch to assign this to coincidence / errors in the method, but there have been weirder coincidences reported. We
63 address this in the new version of the manuscript: we do not call this populations anymore, but clusters, preventing
64 the misunderstanding that population implies the ages represent different cooling histories or different annealing
65 kinetics. Secondly, in the discussion, we added a paragraph on uncertainty and age spread of He data.

66 Figure 4

67

68 L 360 – How can you say that this is related to doming - Deleted

69 L 363 - Are you referring to thermal models obtained by HeFTy? If this is the case, the cooling rates are not
70 meaningful as lower temperature constraints (i.e. AFT and AHe) are missing. Minimum values deleted

71 L 365 - I see that this sample is a conglomerate. Did you analyze different clasts? If this is the case, it is a bit odd
72 that all the three grains give the same age if the degree of reset is only partial. This is an interesting point. Indeed
73 it came as a surprise the data reproduce so well despite being from a partially reset sample. However, as the
74 apparent age is as old as the formation's stratigraphic age, the data does not allow for post-depositional resetting.
75 If the grains had no reheating at all, they would show much older ages (depending on the lag time between cooling
76 in the orogeny + transportation and deposition). Consequently, the most straight-forward interpretation is a partial
77 reset. We speculate that the source of the dated grains has a rather uniform cooling history, or we dated by chance
78 only one of possibly many existing grain age populations. Here dating of a large amount of grains would provide

79 an answer how many different grain age populations are present. This is an exciting idea, which we leave for a
80 future study. In this manuscript we updated the text accordingly, stating that additional grain age populations could
81 be present.

82 changed to „ Even though all ages reproduce within error, this indicates partial reset of the ZHe system, as post-
83 depositional reheating above closure temperature would result in younger ages.”

84 L 368 - If only younger ages represent reset zircons (as stated in the previous sentence) the 110-95 age cannot be
85 related to any geological event as it is a partial reset age. A very good point. The question the reviewer rightly asks
86 is whether the obtained age can be a reduced older age instead of an unaffected 100 Ma population. Both
87 interpretations are valid, and only knowing the amount of radiation damage, chemical composition, and possibly
88 other yet unknown factors will be able to resolve this. Consequently, we rephrased the sentence accordingly to
89 “We note that the older ZHe population of 110 95 Ma coincides with timing of forebulge migration through the
90 area, as independently determined in the stratigraphic record in the Wasia-Aruma Break (Figure 3). This may be
91 either pure coincidence due to partial resetting of an older grain age population, or may be a grain age population
92 with higher closure temperature witnessing exhumation. We discuss reasons for different resetting temperatures
93 below. ”

94
95 L 440-447 This paragraph does not contain any data. I suggest to move these observations to the discussion chapter
96 Deleted and included in the discussion chapter as suggested

97 L 454 – change to figures 6 and 7 changed as suggested

98 L 460 - I would prefer to see this figure S5 in the main text rather than in the supplement. DONE

99
100 L 494 - I would not see any major difference between north and south It is a slightly earlier and stronger increase
101 in the thermal maturity data as shown in Figure 9b and 9c

102 L 566 - I do not understand what is the "sub-thrust thermal overprint" whose effects are limited to 10's of meters.
103 Rephrased to frictional thermal overprint

104 L 579 - This could be partly due also to an increase of the heat flow (as you show in figure S2). ADDED

105 L 600 - Why are you talking about extension? Top-to NNE shearing in the area is associated to tectonic
106 thinning/orogenic collapse and relates to an extensional event (added to clarify)

107 L 601-5 - This part is not clear. Which are the raw data you are talking about? Why "raw"? Rephrased to “used
108 calibration data” and references added

109 L 608 - Not clear how this paragraph is linked to the previous ones Better link established

110 L 641 - This sentence is not clear We rephrased the sentence. Now reads: “Zircon fission track ages witness cooling
111 of the Jebel Akhdar below c. 260 °C between 96 and 70 Ma (Saddiqi et al. 2006).”

112 L 643 - Why are you introducing the possibility of a Miocene event? References of earlier interpretations added

113 L 657 – Deleted as suggested

114

115

116 **Full comments of – L. Aldega (Referee) – Author’s replies in green**

117 Thank you for your valid and thoughtful feedback. We adapted the manuscript accordingly and all suggestions are
118 implemented and/or commented below. Especially, we extended on the meaning and importance of the study in
119 the Introduction and revised and extended the data description. The discussion now also elaborates on the errors
120 associated with the temperature predictions.

121 Moreover, we revised the Figures and Tables and enlarged the fonts.

122 We hope that after these modifications the manuscript can be accepted.

123 As most of your comments align with the review of Reviewer 1 we will provide one new document with tracked
124 changes together with our revised manuscript.

125

126 1) The introductory parts of the manuscript are weak in explaining the importance of the paper and why it is of
127 broad interest and scientific significance for the Solid Earth audience. It should be strongly highlighted what are
128 the aims and the implications of this work for the international community. **The introduction was rewritten, and**
129 **we extended on the importance of the paper.**

130

131 2) Results are not sufficiently described and are mixed with literature data. For instance, Section 4.1 provides a
132 mix of literature data (Grobe et al., 2016, Mozafari et al., 2015), that should be moved elsewhere **DONE**, and
133 undescribed original data. Authors should describe their solid bitumen data for the northern and southern flank of
134 the Jebel Akhdar anticline and then provide paleotemperature values. At the moment only a few lines 325-327 are
135 reported **Extended** and relationship between temperature and stratigraphic age in figure 3 is not clear **Figure was**
136 **updated**. Authors should find another way (different diagram, figure, map) to show their data that have been used
137 for calibrating numerical modelling. Also the results section “fluid inclusion” contains data from the literature and
138 original data. The authors should move data from literature elsewhere and result section should contain only
139 original data. **We adjusted most of the manuscript accordingly. For the fluid inclusion section we agree, that some**
140 **interpretations of other authors are stated to put the analyzed samples into context. Moving this to the Discussion**
141 **part of the chapter would lead to confusion and repetitions there as we would need to state the fluid inclusion**
142 **results three times (deepest burial S – deepest burial N and exhumation). Therefore, we kept the data with some**
143 **minor literature data and renamed the chapter “Results and Interpretation)**

144

145 3) Kerogen particles are scarce in the study samples due to the types of depositional environments and dominance
146 of carbonate rocks. Table 1 lists the results of measurements for a small number of solid bitumen particles
147 (converted to a vitrinite-reflectance equivalent values). Given the statistical nature of reflectance measurements
148 and the factors that can affect measured values (e.g. organic matter recycling, oxidation, oil staining, etc.), it is
149 desirable to have 50 individual readings per sample to obtain representative mean random reflectance and standard
150 deviation values. Most data in Table 1 have very low number of readings and it is unclear in how these
151 measurements are used or whether they are even used other than to provide qualitative support for the inferred
152 thermal maturity of the studied rock units and calibrate thermal modelling. It is necessary to show the thermal
153 maturity curve fitting the solid bitumen data (individual points with range bars) as a function of depth for the
154 northern and southern flank of the Jebel Akhdar Dome related to your 1D burial models. Without this information,
155 readers cannot be aware about the goodness of your calibrating data and your thermal modelling reconstruction.
156 1D burial models (now shown as supplementary material) should become part of the main text.

157 The reviewer suggests to show „the thermal maturity curve fitting, the solid bitumen data as a function of depth“.
158 Such information has been published in a previous paper in our group and would be a repetition here. Furthermore,
159 it should be noted that solid bitumen data do not cover a wide stratigraphic range; therefore, a depth plot is less
160 meaningful than in other regional settings. Moreover, the standard diagrams (e.g. VR vs depth) were developed in
161 “normal” sedimentary basins and cannot be applied at such a warm and by obduction overprinted basins. For
162 instance the thermal maturity modelling approach of Sweeney and Burnham’s Easy R0 is maxing out above 4.5
163 % so we had to show the calibration data in Temperature vs. time.

164

165 4) Converting solid bitumen data into vitrinite reflectance equivalent and subsequently into a paleotemperature
166 value is very tricky and can be inaccurate. Many studies generated regression equations that used the reflectance
167 of solid bitumen to calculate a vitrinite reflectance equivalent (Jacob, 1989; Bertrand, 1990, Bertrand, 1993;
168 Riediger 1993; Landis and Castano, 1995; Bertrand and Malo, 2001; Shoenherr et al., 2007, Wei et al., 2016; Liu
169 et al., 2017). These equations were derived from samples representing various maturity ranges, lithologies, and
170 basins, and as expected, their results differ from one another. Consequently, depending on which equation is used,
171 late mature and post-mature rocks within condensate-wet gas and dry gas windows may be misinterpreted, and
172 thus may lead to erroneous paleotemperature estimates. Recently, several papers show that solid bitumen is not
173 recommended as indicator of thermal maturity and may have not correlation with vitrinite reflectance values
174 (Petersen et al., 2013- international journal of coal geology, Gonçalves et al., 2015- international journal of coal
175 geology, Kus et al., 2016 – international journal of coal geology). Furthermore, paleotemperatures calculated by
176 Barker and Pawlewicz (1994)‘s equation may overestimate the “real” temperature when compared with Basin
177 Maturity Charts from the literature (e.g., Merriman and Frey, 1999 – very low grade metamorphism (book); and
178 Jaboyedoff and Th  lin, 1996 – European Journal of Mineralogy 8, 577-592) as the equation groups data from
179 different burial heating environments. I suggest to avoid to talk about temperature in the text but to talk about
180 levels of thermal maturity in terms of solid bitumen data. Temperature estimates may be extracted from your
181 modelling outputs (constrained by your thermal data) without using any equation.

182 The reviewer is completely correct: Transformation of solid bitumen reflectance to vitrinite reflectance has some
183 pitfalls and should be avoided when possible. However, this is mainly true at low levels of maturation where
184 uncertainties with respect to this transformation are much more important than at high levels of maturation. The
185 reviewer might keep in mind that optical properties of organic particles convert more and more at high levels of
186 maturity.

187 We think that temperature estimates are helpful, but we agree that we should discuss uncertainties.

188 5) I am not convinced by the age of the ophiolite emplacement, and Hawasina Nappe thrusting on top of the passive
189 margin units. In authors’ reconstruction, ophiolite obduction took place at 84 Ma (Fig. 6d) but its emplacement on
190 top of the Arabian passive margin units was dated 95 Ma by Tilton (1981), 95-93 Ma by Warren et al. (2003) or
191 88 Ma (Hacker, 1991). Any age chosen, would imply a shift to older ages for the Semail ophiolite and for the
192 Hawasina Nappe and consequently a decrease of tectonic burial.

193 This is an interesting point, which indeed requires clarification. As the reviewer states correctly, ages of roughly
194 95 Ma have been reported. However, these ages are formation of the metamorphic sole and initiation of obduction
195 at the mid oceanic ridge. Obduction of ophiolite onto the passive margin occurred only once the Hawasina Ocean
196 was completely overridden. Warren et al. estimate this to be roughly 15 Ma after obduction initiation, also in

197 agreement with the interpretation of Robertson et al. and the stratigraphic ages related to the moving forebulge.
198 This is in line with our modeling (actually we used these time constraints). Moreover, all the ages discussed above
199 are based on data of the Saih Hatat window and no one can predict for sure how to extrapolate this over the Semail
200 Gap to the Jebel Akhdar.

201 6) Some more details about the exhumation of the passive margin units in the Jebal Akhdar Dome should be
202 given to the readers. The removal by erosion or extensional tectonics of 8-10 km of ophiolite units should have
203 started in Danian time (Hansman et al., 2007) and be completed before the deposition of postobduction deposits
204 of the Jafnain and/or Russayl Formations (early Eocene) that experienced low levels of thermal maturity. To my
205 knowledge, only Late Maastrichtian-early Paleocene conglomerates of the Al Khawd Fm (maximum 350 m thick)
206 contain ophiolite clasts and they occur in depozones of the northern flank of Jebal Akhdar Dome. No occurrence
207 has been described for the southern flank of the anticline. Where has all the material coming from the dismantling
208 of such thick ophiolite overburden gone? Which sedimentary deposit has been formed in the southern and northern
209 flank of the Jebal Akhdar Dome? What is their thickness? Furthermore, the explanation about the juxtaposition
210 of the Hawasina and Muti sediments atop the carbonate platform units during extensional shearing sounds to me
211 to be contradicted by your numerical model of figure 6 where both units were buried at depths of 8-10 km since
212 84-79 Ma and should have experienced similar temperatures than those recorded by the Natih Fm.

213 We thank the reviewer for this remark. Indeed the Al Khawd Fm contains ophiolite clasts. However, this does not
214 suffice to explain the loss of several km of ophiolite. We argue elsewhere (Grobe et al. 2017, Tectonics) that the
215 ophiolite was significantly thinned during top-to-NNE shear, reducing the amount of material required to be eroded
216 by exogenic forces. Much of the material lost may have been transported to the Persian Gulf. We added a respective
217 sentence in the exhumation history. According to our data the Natih Formation experienced peak peak
218 temperatures of 225 – 260 °C (Natih B and deeper strata) & Hawasina and Muti below 170 °C.

219 7) Some parts of the discussion are overinterpreted or need clarification (see points line by line below). **DONE** In
220 general, the short duration of the heating event to explain the discrepancy between temperatures obtained by solid
221 bitumen and clay mineral assemblage fails as the ophiolite units remain atop the passive margin units from 79 to
222 55 Ma. The time span elapsing between ophiolite thrust stack emplacement and the beginning of tectonic
223 overburden removal is very long and both organic matter and clay minerals acquire similar thermal maturity. Only
224 for time of burials shorter than 1-2Ma and/or in hydrothermal/geothermal settings, clay minerals may have a slow
225 kinetic response when compared with vitrinite or bitumen reflectance, but this is not the case the evolution of
226 mixed layered minerals cannot be considered as an explanation for that discrepancy because I-S in Aldega et al.,
227 (2017) shows a trend as function of stratigraphic age either for carbonate or siliciclastic rocks. If the lack of
228 potassium is the key for explaining such discrepancy between paleotemperatures, I-S values would have been
229 scattered and they would not have shown any trend as function of stratigraphic age (or depth).

230 It is difficult for us to interpret the data in Aldega et. al 2017 but either lack of potassium or very short time heating
231 might be possible explanations. See also paper by Mählmann et. al 2015 , International Journal of Coal Geology.
232 The duration of emplaced ophiolite from 79-55 Ma probably does not exactly represent the time at thermal
233 equilibrium, especially after such deep and rapid burial...

234 8) It is hard to have confidence in the results presented in Figures 6 and 7 when the authors only provide some
235 general description of how they used Move 2D software for their geological reconstruction, how they use the
236 resulting structure geometries in Petromod 2D and how these results depend on the paleotemperature constraints
237 and 1D modelling method discussed above. We extended parts of the manuscript to clarify the conducted

238 modelling. The modelling conducted has to be seen as a general attempt, which is due to the uncertainties of the
239 available data.

240

241 Technical points:

242 1) The term “solid bitumen” should be replaced by “pyrobitumen” throughout the text as the reflectance boundary
243 between the two is placed at reflectance values of 0.7% (Hunt, 1978; Jacob, 1989; Landis and Castano, 1995) or
244 1.5% (Mastalerz et al., 2018). Solid bitumen is an oil window product generated by primary cracking whereas
245 pyrobitumen is a gas-window solid bitumen from secondary cracking,

246 Solid bitumen is a more general term and is also used in review papers and textbooks. However, we explained now
247 in the beginning that solid bitumen of high reflectance is often called pyrobitumen.

248 2) Which method of rock decompaction for the passive margin unit has been applied in numerical modelling? This
249 information should be added in the numerical basin modelling section PetroMod uses a forward, event-stepping
250 modeling, starting with the deposition of the oldest layer. Subsequent deposition and burial is leading to differential
251 compaction of the single rock units. Therefore, a decompaction algorithm is not necessary.

252

253 Other detailed comments and suggestions to text and figures are listed below.

254 Introduction

255 Line 51 – I would replace “sub-thrust sedimentary basin” with “subophiolite units” or “autochthonous passive
256 margin units” changed to subophiolite passive margin units

257 Line 63 – replace “full” with “whole” or “entire” and replace “Permo” with “Permian” DONE

258 Line 66- reference is quite old. Recent papers that deal with vitrinite reflectance or organic matter optical analysis
259 in other orogens are: Holy Cross Mountains: Schito et al., 2017 Marine and Petroleum Geology, 80, 112-132
260 Zagros: Mashhadi, et al., 2015. Marine and Petroleum Geology 66, 978-997. Apennines: Corrado et al., 2010 for
261 a review of the Apennines, Journal of the Virtual Explorer, Electronic Edition, ISSN 1441-8142, vol. 36, paper 15,
262 1-37 Line 70 – the reference is a bit old with only one paper dated, 2010. Updated accordingly

263 A selection of more recent papers that integrate thermal constraints and basin modelling to reconstruct tectonic
264 loads or overthrusts in fold-and-thrust belts is: Schito A. et al., 2018. Basin Research, 30, 532-549. Jirman et al.,
265 2018, Journal of Petroleum Geology, 41 (2), pp. 175-188. Aldega et al., 2018. Marine and Petroleum Geology, 93,
266 376-390 Duschl et al., 2016. Marine and Petroleum Geology, 77, 300-322 Caricchi et al., 2015. Geological Society
267 of American Bulletin, 127 (3-4), 428-442. Updated accordingly

268 Line 78 – replace “deepest burial” with “maximum burial” DONE

269 Tectonic setting Lines 90, 92, 98 – replace “Permo” with “Permian” see above DONE and checked in the rest of
270 the manuscript

271 Line 111-116. I would modify the sentence as the slowing down or ending of ophiolite obduction is early
272 Maastrichtian as indicated by the occurrence of a regional unconformity between the top of the allochthonous units
273 and overlying conglomerates and shales (Al Khawd Fm.). After that in Danian time post-obduction extension took
274 place (64±4 Ma; Hansman et al., 2018). DONE

275 Stratigraphic sequence

276 Line 155- Spell out Gp. DONE in whole manuscript

277 Line 167 – A more detailed description of the hawasina deposits is needed. The Hawasina deposits are not the
278 main focus of this manuscript, therefore we present the most relevant publications, but do not describe it in detail.

279 Temperature evolution of the autochthon - The title is misleading as the section does not describe any temperature
280 evolution through time of the passive margin units. You are reporting a set of temperatures from previous studies.
281 In this section you should provide paleotemperature data from other works that you discussed. I would re-title the
282 section "Previous paleothermal data" **DONE**

283 Line 177 – replace "is" with "are" and provide reference. **DONE**

284 Lines 188-190. I would delete these lines as they do not provide useful information in this section. **DONE**

285

286 Temperature evolution of the Semail ophiolite Nappe/allochthon

287 Lines 198-199. How much is the temperature? Please provide it **Rephrased**

288 Lines 199-203. You can use these sentence as well as all the information included in this paragraph in the
289 discussion section. **DONE**

290 Petroleum system: This section should be expanded providing information about, source, reservoir and seal rock
291 together with time of migration and accumulation of hydrocarbons. These information would be useful for
292 understanding and strengthening the discussion part about fluid migration. Adding thermal maturity data (vitrinite
293 reflectance or bitumen reflectance) about source rocks of the Natih and Fahoud fields would strengthen the
294 discussion of your solid bitumen data. At the moment information of solid bitumen can be moved to the
295 temperature evolution of the autochthon section. **Extended**

296

297 **Methods**

298 I would delete lines 216-217. **DONE**

299 Elemental analysis and thermal maturity

300 Line 218 – Thermal maturity is not a method. I would replace "elemental analysis and thermal maturity" with
301 "Raman spectroscopy of carbonaceous material" **DONE**

302 Line 219 – add "levels of" in front of "thermal maturity" **DONE**

303 Lines 220-221 – please define which stratigraphic units were analyzed for organic matter characterization **DONE**

304 Line 234 – please define "STA" in the equation. **STA is defined as scaled total area in the line prior to the equation**

305 Lines 236-238. Move these lines in the basin modelling section **DONE**

306

307 **Fluid inclusion thermometry**

308 Line 239 – replace "thermometry" with "microthermometry" **DONE**

309 Line 243- perhaps replace "mineralization" with "crystallization" **DONE**

310 Line 256- replace "of" with "for" **DONE**

311 Line 261 – define T_{fm} **DONE**

312

313 **Thermochronology**

314 Line 265- please define which stratigraphic units were analyzed for ZHe analysis. **DONE**

315

316 **Numerical basin modelling**

317 Line 287 – replace "R₀" with R_o%. O stands for oil. **DONE**

318 Line 290 – refer to the supplementary material for lithology and petrophysical rock properties **DONE**

319 Line 291 – Which seismic lines? Provide reference **DONE**

320 Lines 291-292. I would delete this sentence **DONE**

321 Lines 293-294. The sentence is cryptic. I would delete it as you will discuss this point in the discussion section

322 **DONE**

323 Lines 201-304. How can you calibrate burial depths for the Adam Foothills where thermal data are lacking?

324 **Clarified in the text – thermal data is lacking south of the foothills but not in the foothills**

325 Lines 309-310 – Is the increase of heat flow an assumption or a result of a sensitive analysis? There is a discrepancy

326 between the text and the supplementary material **extended: we assigned the here described heat flow trend and**

327 **tested it in sensitivity analysis.**

328

329 Results Thermal maturity and host rock burial temperatures

330 Lines 324-332. These results refer to previous works, Grobe et al., 2016 and Mozafari et al., 2015 and should be

331 moved in chapter “Temperature evolution of the autochthon”. **DONE**

332 Lines 325-327. This part should be expanded as it refers to your original data. Describe results for the northern

333 and southern flanks in terms of solid bitumen data **DONE but described in terms of STA and temperature (see**

334 **comment above)**

335 Line 330 – Provide vitrinite reflectance values, and then temperatures conversion. The sentence is not correct. In

336 Mozafari et al., 2015 there are only two VR data with values of 1.1% and their temperature estimate is 140_C.

337 There is no evidence of a Vr value of 1.8%. Please correct text and table 1. To my knowledge a vitrinite reflectance

338 value of 1.1% should be converted in a lower temperature range (100-130_C) as generally evidenced in other fold-

339 and-thrust belts and by basin maturity charts from literature (see Merriman and Frey, 1999 – very low grade

340 metamorphism book; and Jaboyedoff and Thélin, 1996 – European Journal of Mineralogy 8, 577-592) **DONE**

341

342 Thermochronology

343 Line 341 – delete “Figure 3” **DONE**

344 Line 360 – This part needs more details. How can you associated those ages with doming? **This is a good point.**

345 **We deleted the interpretation here, and interpret the ages in the discussion.**

346 Line 361 – I would not refer to figures S4 and S% as the burial history is not introduced yet. Furthermore see my

347 suggestions for figures S4 and S5. **DONE**

348 Line 371 - the zircon partial retention zone (PRZ, Reiners, 2005) is between 130 and 170 _C as you stated in the

349 method section. Please modify the sentence. **DONE**

350 Line 372 – I would replace “A magmatic sample of an intrusive” with “A sample from an intrusive body” **DONE**

351

352 Fluid inclusions

353 Lines 420-421. Why did you assume a depth of 2km? Please explain. Strike-slip faulting should be Paleocene or

354 Eocene in age and from your burial history you should have more than 5km thick overburden atop the Muti Fm.

355 **Rephrased – we now refer to the minimum thickness as evidenced by the preserved allochthonous thicknesses**

356 Line 430 – Replace “Sahtan Fm” with “Sahtan Group” **DONE and checked in the entire manuscript**

357

358 Structural observation

359 Lines 441-447. This section does not contain any data. I suggest to delete it or move it in the geological setting

360 **Deleted as suggested**

361 Basin Modelling

362 Line 454 – Replace “figures 8 and 9” with “figures 6 and 7” **DONE**

363 Line 455-How much is the eroded thickness of the Natih Formation? How much is the thickness of the Hawasina
364 Nappe? Add these information in the text **DONE**

365 Line 456- ophiolite emplacement is older than 84 Ma as shown in figure 6. The emplacement of Semail ophiolite
366 units onto the Arabian passive margine sediments is dated 88Ma (Hacker, 1991), 95-93 Ma (Warren et al., 2003),
367 95 Ma (Tilton, 1981). Any age chosen, implies a shift to older ages for the Hawasina Nappe. **See comment above**
368 **(point 6)**

369
370 Line 457 – it seems that maximum burial conditions are already reached at 84 Ma as shown in figure 6 **This age**
371 **varies along the transect**

372 Line 460 – I would like to see 1D burial histories for the northern and southern flank of the Jebel Akhdar described
373 as part of the main text. **DONE**

374 Lines 475- 476- delete 1.8% VR as it is not reported in Mozafari et al., 2015 and revise temperature range **DONE**

375 Line 475 – Replace “requires” with “require” **DONE**

376 Lines 494-497 – I do not see any difference in your modelling results for northern and southern flanks **Slight**
377 **differences exist, but as they are within the range of error we changed the manuscript accordingly**

378 Lines 507-512. The sentences are unclear to me. If you have a decrease of temperature by 60_C (0%
379 serpentinization) you should require a lower overburden thickness to fit that temperature decrease and not an
380 additional thickness. Please rephrase **If modelled temperatures decrease and thermal calibration data remains the**
381 **same we need to add additional thicknesses to equally match the calibration data (increase modelled temperature)**

382 Line 513 – replace “deepst” with “maximum” **DONE**

383

384 Discussion Burial history

385 Line 537. Please expand this part. Why? **DONE**

386 Lines 542-545. delete 1.8% VR as this value is not reported in Mozafari et al., 2015 and revise temperature
387 range/burial depths **DONE**

388 Lines 566-569. I did not understand these sentences. What is the sub-thrust thermal overprint? **Rephrased**

389 Line 570-574. This sentence is unclear to me. If 8-10 km of ophiolite units thrust over both passive margin and
390 Hawasina units, why are peak temperatures for these units so different? Peak temperature for the passive margin
391 units is up to 360_C (fluid inclusion data) but they are in the range of 130 to 170_C for the Hawasina sediments as
392 they have not reset the ZHe system. **Within their range of error the data is comparable as discussed. Please keep**
393 **in mind that the fluid inclusion data does not necessarily represent host rock but fluid temperature and we have to**
394 **compare with thermal maturity data instead.**

395 Line 575-577. This is a repetition. Information about heat flow has been already reported in line 513. Please delete
396 it. **DONE**

397 Lines 595–598. The short duration of the heating event to explain the discrepancy between temperatures obtained
398 by solid bitumen and clay mineral assemblage fails as the ophiolite units remain atop the passive margin units
399 from 79 to 55 Ma. The time span elapsing between ophiolite thrust stack emplacement and the beginning of
400 tectonic overburden removal should be shorter than 1-2Ma (hydrothermal/geothermal settings) in order to do not
401 allow clay minerals to record maximum temperature (Hoffman and Hower, 1979, Hillier et al., 1995). **Please see**

402 comment above (Point 6). It is highly improbable that the maximum temperatures in such a setting of rapid
403 obduction lasted long. Temperature equilibration takes several hundred thousand to few million years and while
404 this is happening as a consequence of ophiolite emplacement, tectonic thinning by top-to-NNE shear already starts.
405 Therefore, we think that short duration of heating is one possible explanation, but there may be other explanations
406 as well.

407

408 Line 598 – delete “dated” **DONE**

409 Lines 598-600. The interpretation that clay minerals formed during top-to-NNE shearing and does not record
410 maximum temperature associated to burial is a speculation. There are no K-Ar or other geochronological
411 constraints for clay minerals formation. **We completely agree with the reviewer. We note there is some discrepancy
412 between different T data, and this may be one explanation. We changed the sentence accordingly to “Alternatively,
413 we speculate that the dated clay minerals...”.**

414 Lines 600-606. I do not think the sentence adds value to the discussion and it seems to me very cryptic. I would
415 delete it. If the authors wants to keep the sentence they should expand this part and add more information about
416 that. **We rephrased the paragraph accordingly, to make it less cryptic.**

417

418 Pressure evolution and fluid migration I would delete “fluid migration” from the title as you describe fluid
419 migration in section 5.4. **DONE**

420 Lines 656-657- please delete the sentence written in german **DONE**

421

422 Figures and tables

423 Figure 1 – What is the difference between thrusts in red and thrusts in black in figure 1a? It should be explained
424 in the legend or in the figure caption. Add anticline symbol in the legend Please add latitude and longitude to figure
425 1b. Furthermore, why do thrusts in figure 1b have different stroke thickness? Please uniform them. **DONE**

426

427 Figure 3 – This figure is confusing and needs a restyling. **DONE** Thrusting of Hawasina and Semail ophiolite
428 should be placed before the synorogenic sediments of the Fiqa and Muti Fm. **DONE** It is seems that thrusting is
429 younger than 87 Ma. You can overcome this issue by deleting ages in the Group/Formation column. **DONE** Zircon
430 ages are too small. **DONE** Letter size is very small. A legend for lithology should be drawn. I would prefer to see
431 temperature values as points and error bars. **DONE**

432

433 Figure 4 – text in the legend is hardly visible. Please replace it. Provide a legend for the colours in the map. It
434 would be useful to add the trace of the anticline axial plane to better define northern and southern flank of the Jebel
435 Akhdar dome. **DONE**

436

437 Figure 6 – add a legend for the colours in the figure. **All units are explained in the figure** See my comments in the
438 text for the age of the ophiolite emplacement in order to modify the figure. The figure caption is confusing in the
439 last line as vertical lines show Wadi location as well and not only hydrocarbon fields. Please revise **DONE**

440 Figure 7 –vertical lines in the figure caption show Wadi location as well and not only

441 hydrocarbon fields. Please revise **DONE**

442

443 Figure 8- revise figure 8a on the basis of my comments on Vr values by Mozafari et al.,2015 **DONE now at 140°C**
444

445 Table 1 – replace ”,” with “.” in the calculate VR values. **DONE** Add longitude and latitude to sample location.
446 **DONE** What do you mean with “below the surface of the matrix”? What did you measure? Please rephrase. **DONE**
447 Spell out Kh2. **DONE** Mozafari et al., 2015 show only two data with 1.1 VR%. **DONE** Please correct the table I
448 would split table 1 into two tables. The first with literature data that can be moved to the temperature evolution
449 section and the other with your original data. **To enable a direct comparison of published data and our results we**
450 **kept the data in one Table, but we visually highlighted the new data and extended the table caption accordingly.**
451

452 Table 3 – “Replace “Thom” with “Th” in the fifth column. Replace in the figure caption “Data of Holland et al.
453 (2009) is added for comparison and we likewise corrected his homogenization temperatures” with ”Data by
454 Holland et al. (2009) are added for comparison and we likewise corrected their homogenization temperatures”.
455 **DONE**
456

457 Supplementary material

458 Figure S1 – Provide a better description of the table caption. Furthermore provide the amount of eroded thickness
459 simulated during the Wasia-Aruma break. Are those the inputs for Petromod 2D, 1D basin modelling or Move
460 2D? Please specify, Replace “dolomite” with “dolostones”. Dolomite is a mineral, dolostone is a rock. **Done – we**
461 **kept Dolomite as these are the officially defined lithologies as assigned in the software package to keep it**
462 **transparent.**
463

464 Figure S5 should become part of the main text and you should provide the thermal maturity curve fitting your solid
465 bitumen data as function of depth. Without this figure the thermal history may have no meaning. Readers must be
466 aware of calibrating data and fitting of the thermal maturity curve. In figure S5, ophiolite emplacement is not at
467 88 Ma as described in the figure caption. Label the figures as northern and southern flank. **Done**
468

469 Figures S9 and S10 have not been cited in the text. **Moved and cited in the main text**

Tectono-thermal evolution of Oman's Mesozoic passive continental margin under the obducting Semail Ophiolite: a case study [of](#) Jebel Akhdar, Oman

Arne Grobe^{1,2}, Christoph von Hagke¹, Ralf Littke², István Dunkl³, Franziska Wübbeler¹, Philippe Muchez⁴, Janos L. Urai^{1,5}

¹Structural Geology, Tectonics, and Geomechanics, EMR Group, RWTH Aachen University, Germany

²Geology and Geochemistry of Petroleum and Coal, EMR Group, RWTH Aachen University, Germany

³Sedimentology & Environmental Geology, Geoscience Center Georg-August-Universität Göttingen, Germany

⁴Geodynamics and Geofluids Research Group, Department of Earth and Environmental Sciences, KU Leuven, Belgium

⁵[Department of Applied Geoscience, German University of Technology in Oman GUtech, Muscat, Oman.](#)

Correspondence to: Arne Grobe, arne.grobe@rwth-aachen.de, ORCID: 0000-0001-6471-0624

Keywords: basin modeling, passive margin, obduction, burial, Raman spectroscopy, thermochronology, thermal maturity

Abstract. ~~The Mesozoic sequences of the Oman Mountains experienced only weak post-obduction overprint and deformation and, thus they offer a unique natural laboratory to study obduction.~~ We present a study of the pressure and temperature evolution in the passive continental margin under the Oman Ophiolite, using numerical basin models calibrated with thermal maturity data, fluid inclusion thermometry and low-temperature thermochronology. ~~Because the Oman Mountains experienced only weak post-obduction overprint, they offer a unique natural laboratory for this study.~~

Thermal maturity data from the Adam Foothills constrain burial in the ~~foredeep moving-tilt basin~~ in front of the advancing nappes ~~to-has been~~ at least 4 km. Peak temperature evolution in the carbonate platform under the ophiolite ~~is-dependes~~ only weakly ~~dependent~~ on the temperature of the overriding nappes which have cooled during transport from the oceanic subduction zone to emplacement. Fluid-inclusion thermometry yields pressure-corrected homogenization temperatures of 225 to 266 °C for veins formed during ~~progressing-progressive~~ burial, 296-364 °C for veins related to peak burial and 184 to 213 °C for veins associated with late-stage strike-slip faulting. In contrast, the overlying Hawasina nappes have not been heated above c. 170_°C, as witnessed by only partial resetting of the zircon (U-Th)/He thermochronometer.

In combination with independently determined temperatures from solid bitumen reflectance, we infer that the fluid inclusions of peak-burial-related veins formed at minimum pressures of 225-285 MPa. This implies that the rocks of the future Jebel Akhdar Dome were buried under 8-10 km of ophiolite on top of 2 km of sedimentary nappes, ~~which is~~ in agreement with thermal maturity data of solid bitumen reflectance and Raman spectroscopy.

~~B~~**Rapid** burial of the passive margin under the ophiolite results in sub-lithostatic pore pressures, ~~in agreement with observations on as indicated by~~ veins formed in dilatant fractures in the carbonates. We infer that overpressure is induced by rapid burial under the ophiolite ~~nappes~~. ~~Obduction-related tilt~~**Tilting** of the ~~passive margin carbonate platform~~ in combination with overpressure in the passive margin caused fluid migration towards the south in front of the ~~advancing~~ nappes.

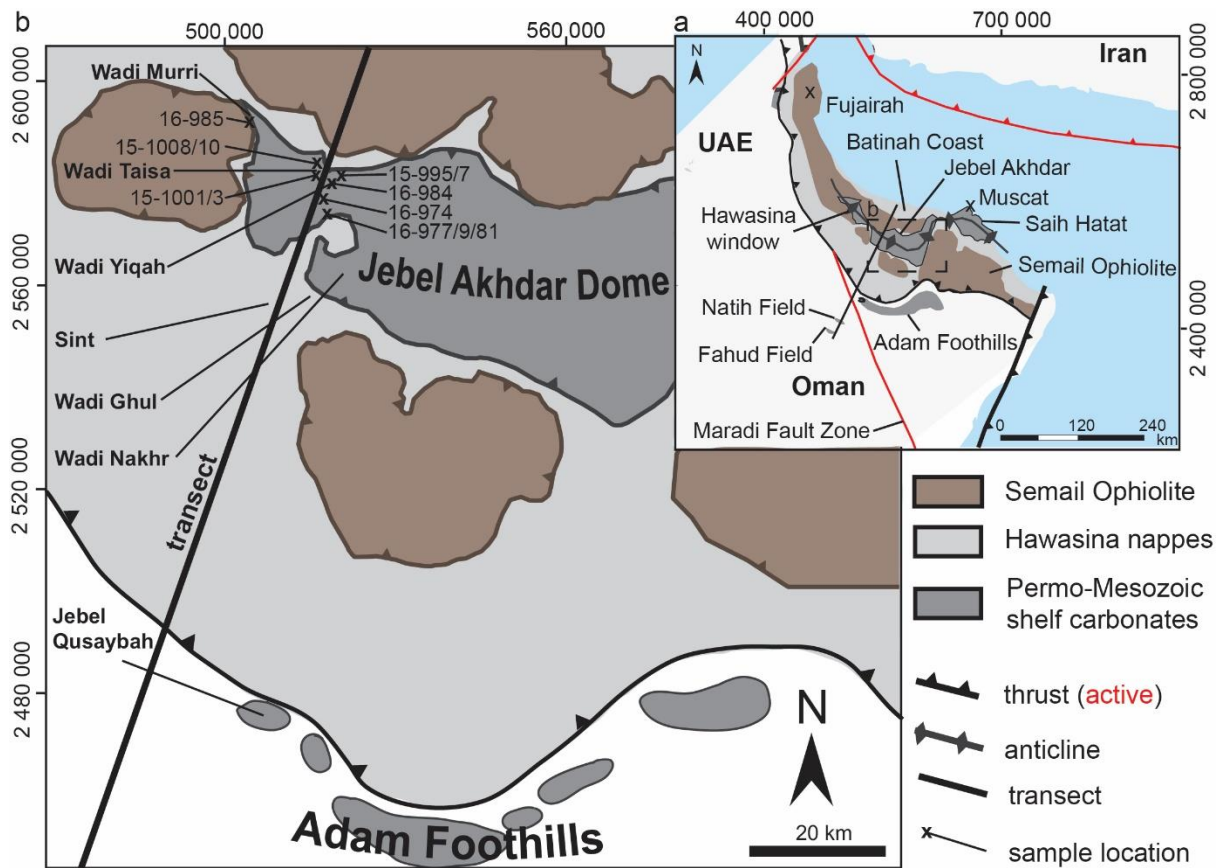
Exhumation of the Jebel Akhdar as indicated by our zircon (U-Th)/He data, integrated with existing data, started as early as the late Cretaceous to early Cenozoic, linked with extension ~~along-above~~ a major listric shear zone with top-to-NNE shear sense, ~~together with an early phase of extensional dome formation.~~ ~~In a second exhumation~~

42 ~~phase~~ the carbonate platform and obducted nappes of the ~~whole~~ Jebel Akhdar Dome cooled together below c.
43 170 °C between 50 and 40 Ma, before the final stage of anticline formation.

44 **1. Introduction**

45 The Permian-Mesozoic platform sediments of northern Oman (Figure 1; e.g. Beurrier et al., 1986; Glennie et al.,
46 1974; Lippard et al., 1982) with hydrocarbon accumulations in the southern foreland of the Jebel Akhdar Dome
47 (Figures 1 and 2) are overlain by the Semail ophiolite nappe complex, the largest and best-preserved ophiolite on
48 Earth. Limited tectonic extension after obduction followed by uplift, folding and deep erosion and the present-day
49 arid climate formed exceptional exposures in three tectonic windows and in the foreland fold-and-thrust belt of
50 the Oman Mountains (Figure 1). The Oman Mountains have been investigated in many studies focusing on tectonic
51 history (Breton et al., 2004; Cooper et al., 2014; Glennie et al., 1973, 1974; Grobe et al., 2018; Loosveld et al.,
52 1996; Searle, 2007), stratigraphic sequences (Van Buchem et al., 2002; Grelaud et al., 2006; Homewood et al.,
53 2008), geodynamic modelling (Duretz et al., 2015), hydrocarbon source rocks (Van Buchem et al., 1996; Philip et
54 al., 1995; Scott, 1990) and reservoir rocks (Arndt et al., 2014; De Keijzer et al., 2007; Koehrer et al., 2011; Virgo
55 et al., 2013). Less well known is the temperature and pressure evolution of the ~~sub-thrust sedimentary~~
56 ~~basin~~subophiolite passive margin units and the subsequent cooling history of the Jebel Akhdar (Aldega et al., 2017;
57 Grobe et al., 2018; Hansman et al., 2017; Poupeau et al., 1998; Saddiqi et al., 2006). This information is vital for
58 our understanding of. ~~A, a better understanding of this would further~~ further the time-temperature history ~~and~~
59 would allow to constrain ~~the obduction~~ dynamics. ~~of obduction~~ A differentiation of peak burial temperatures linked
60 to and forebulge migration and peak burial under the ophiolite obduction would allow to refine phases of
61 obduction stages. ~~Combining these~~ these peak temperatures evolution with cooling ages enables to integrate links
62 the burial history with ~~restoration of times and~~ phases of orogeny.

63



64
65
66
67
68
69
70

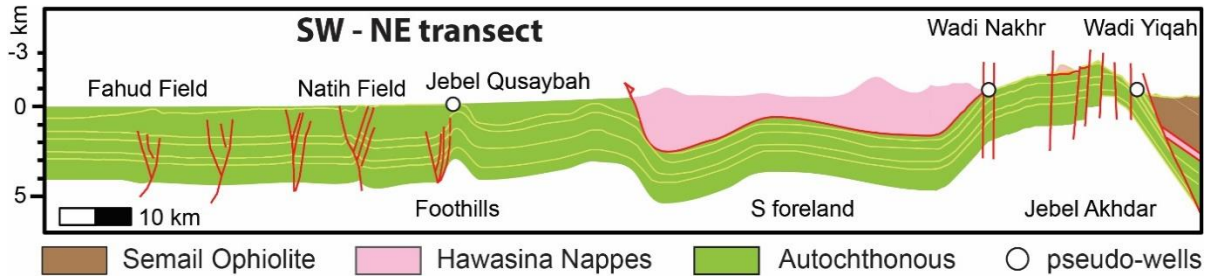
Figure 1: a) Tectonic setting of the Oman Mountains. Shaded in gray are the three tectonic windows of Hawasina, Jebel Akhdar and Saih Hatat as well as the Adam Foothills. Brown areas show the exposed Semail Ophiolite, black lines denote the obduction fronts of Semail and Masirah ophiolites, red lines denote lithosphere-scale, active structures. The modeled transect (black line) crosscuts the Jebel Akhdar window and continues to the Natih and Fahud oil fields in the southwestern mountain foreland. b) Geologic map of the Jebel Akhdar window with the location of the modeled transect (solid black line) and the locations of thermal maturity data (x).

71 ~~The full whole Permoian Mesozoic sequence of the carbonate platform below the ophiolite is well exposed,~~
 72 ~~providing outcrop samples to study the pressure and temperature history of this rapidly buried passive margin~~
 73 ~~sequence.~~

74 In other orogens, peak temperatures related to nappe emplacement were reconstructed by analyzing thermal
 75 maturity of finely dispersed organic material (e.g. Teichmüller and Teichmüller, 1986; Zagros: Mashhadi et al.,
 76 2015; Holy Cross Mountain: Schito et al., 2017; Eastern Alps: Lünsdorf et al., 2012; Southern Alps: Rantitsch
 77 and Rainer, 2003; Apennines: Reutter et al., 1988). However, the number of studies of thermal and pressure effects
 78 on overthrust sedimentary basins is limited and modeling approaches to reconstruct such large scale overthrusts
 79 are increasing but still rare-few (e.g. Aldega et al., 2018; Deville and Sassi, 2006; Ferreiro Mählmann, 2001; Jirman
 80 et al., 2018; Oxburgh and Turcotte, 1974; Roure et al., 2010; Schito et al., 2018; Wygrala, 1989). In these studies,
 81 a main difficulty is to differentiate between temperature history of obduction-overthrusting and overprinting by
 82 later phases of orogeny. In the Oman Mountains, peak temperatures reached by obduction have not been
 83 overprinted, ~~and fluid migration in the thrust belt is predominantly related to obduction.~~ ~~The whole Permian-~~
 84 ~~Mesozoic sequence of the carbonate platform below the ophiolite is well exposed, providing outcrop samples to~~
 85 ~~study the pressure and temperature history of this rapidly buried passive-margin sequence.~~

86 In this paper we present new thermal maturity, thermochronology and fluid inclusion data, and integrate them in
 87 a numerical basin model of the pressure-temperature evolution of-along a transect across the entire Jebel Akhdar
 88 extending from the undeformed passive margin sequence in the south to the Batinah coast in the north (Figure 2).

89 ~~This Our data~~ This integration allows helps to better constrain temperature and pressure conditions of deepest
 90 ~~maximum~~ burial as well as, and the time of dome formation and exhumation which we linked is linked to the
 91 structural and tectonic evolution of the area. Hence Presented results of, the Our results for the Oman Mountains
 92 can be used as analogue for to understand more deformed orogens, shed light to fluid migration in the early stages
 93 of orogeny and on exhumation related to orogenic collapse. and orogenic collapse related exhumation



95 **Figure 2: Structural transect used for modeling of the Jebel Akhdar Dome and its southern foreland (Al-Lazki et al.,**
 96 **2002; Filbrandt et al., 2006; Searle, 2007; Warburton et al., 1990). Highlighted are the locations of the pseudo-wells,**
 97 **(white circles, size depict area of sample interpolation) in Wadi Nakhr, Wadi Yiqah and at Jebel Qusaybah, Adam**
 98 **Foothills, which were used for model calibration.**
 99

100 2. Geological setting

101 2.1. Tectonic setting

102 Along the northeastern coast of Arabia, the NW-SE oriented Oman Mountains form a more than 400 km long
 103 anticlinal orogen (Figure 1). The mountain belt consists of allochthonous sedimentary and ophiolitic nappes thrust
 104 onto a Permian-Mesozoic passive continental margin (Breton et al., 2004; Glennie et al., 1973; Loosveld et al.,
 105 1996; Searle and Cox, 2002).

106 This continental margin was formed during opening of the Neotethyan ocean (Loosveld et al., 1996) and the
 107 formation of the Permian-Mesozoic Hawasina Basin (Béchenneq et al., 1988; Bernoulli et al., 1990). Cretaceous
 108 convergence of Arabia and Iran inverted the rifting and initiated subsea thrusting of the later
 109 future Semail Ophiolite on top of the Arabian Plate at 97-92 Ma, as is recorded by U-Pb geochronology (Rioux
 110 et al., 2013, 2016; Warren et al., 2005) and ⁴⁰Ar/³⁹Ar dating of the metamorphic sole (Hacker et al., 1996).
 111 Obduction initiation and the advancing ophiolite resulted in caused a flexural forebulge that moved
 112 southwestwards through the passive margin during the Upper Cretaceous (Robertson, 1987). Forebulge migration
 113 induced up to 1100 m of uplift of the Permian-Mesozoic Arabian Platform and erosion of the Cretaceous platform
 114 sediments (Searle, 2007). In the field this can be observed at, causing the Wasia-Aruma Break (Robertson, 1987).
 115 During northeastward directed subduction of the Arabian margin, During this convergence, parts of the Hawasina
 116 ocean sediments and volcanics units became detached and became accreted in front of and beneath the ophiolite
 117 nappe (Béchenneq et al., 1988, 1990; Glennie et al., 1974; Searle et al., 2003; Warburton et al., 1990). Palinspastic
 118 reconstructions of the Hawasina Nappes locate the position of the initial ophiolite thrusting 300-400 km offshore
 119 the Arabian coast (Béchenneq et al., 1988; Glennie et al., 1974).

120 Initiated B In the carbonate platform, burial under the Hawasina and ophiolite advancing nappes, the
 121 allochthonous sequences led to the generation of overpressure cells and the formation of three crack-seal calcite
 122 vein generations in the margin sequence, which represent overpressure build ups and releases (Gomez-Rivas et
 123 al., 2014; Grobe et al., 2018; Hilgers et al., 2006; Holland et al., 2009; Virgo, 2015). Peak The highest grades of

124 metamorphism ~~of the subducted margin~~ is recorded by eclogites exposed in ~~the~~ As Sifah ~~region~~ (E-Saih Hatat,
125 Figure 1a), ~~where the burial triggered thermal climax resulted in zircon and rutile recrystallization~~ at c. 79 Ma
126 (Warren et al., 2003).

127 The sedimentary record in the Batinah coast and the foreland, as well as laterite formation on top of the ophiolite
128 ~~suggest subaerial exposure and a slow-down or stopped obduction before lower marine conditions were restored~~
129 ~~in the Maastrichtian suggest that obduction slowed or stopped in the early Paleogene, and the ophiolite was~~
130 ~~exposed subaerially~~ (Coleman, 1981; Forbes et al., 2010; Nolan et al., 1990). This slowdown might relate to the
131 formation of the Makran subduction zone at c. 35 Ma (Agard et al., 2005; Grobe et al., 2018; Hassanzadeh and
132 Wernicke, 2016; Jacobs et al., 2015; Mouthereau, 2011). ~~This shift of deformation to the north resulted in~~
133 ~~preservation~~ing the ~~initial-early~~ stage of the obduction orogen in ~~northern~~ Oman.

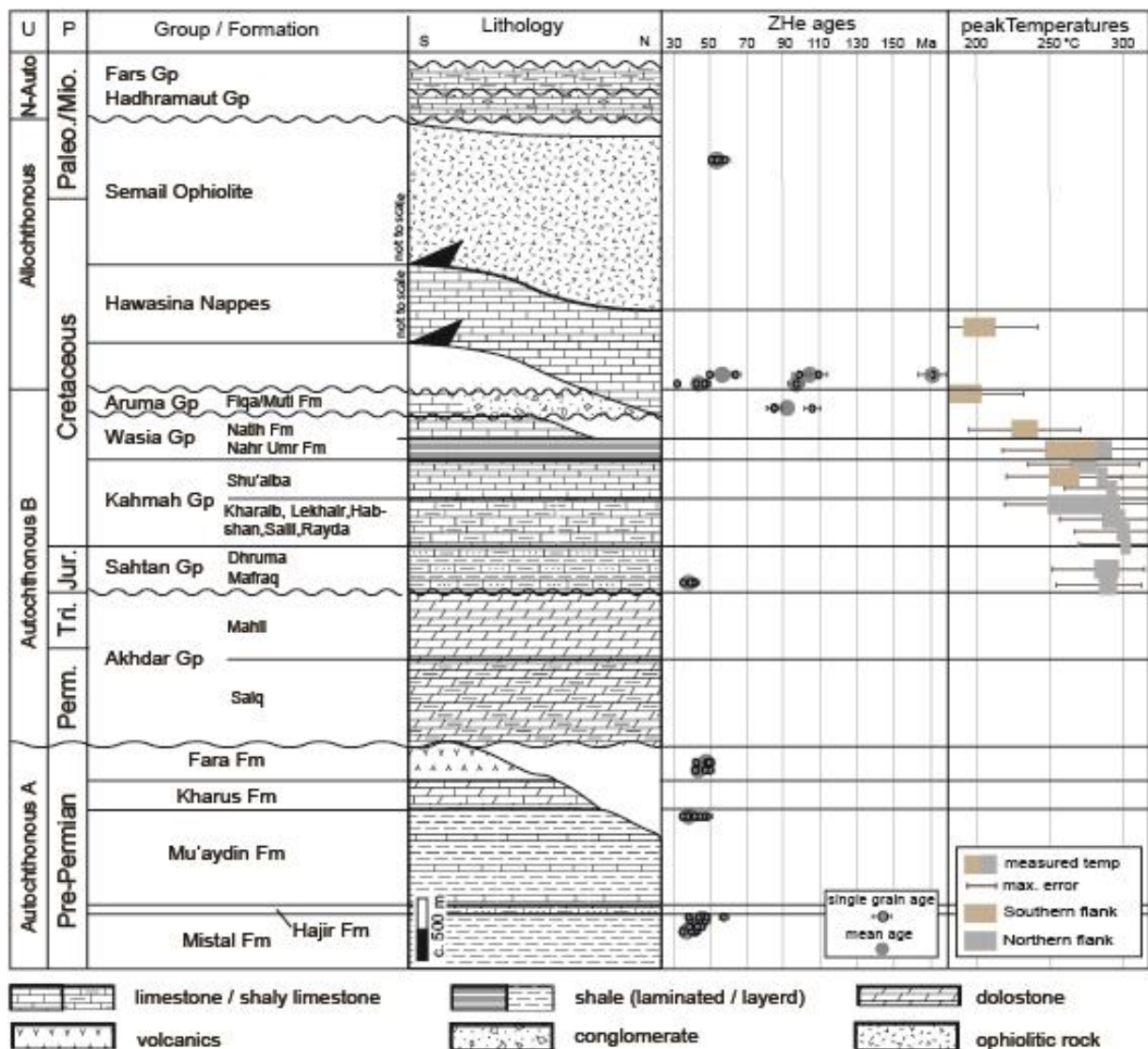
134 ~~Regional~~In the Jebel Akhdar, post-obduction extension took place along ductile top-to-NNE shear zones, ~~dated~~
135 ~~at~~ 64 ± 4 Ma (Grobe et al., 2018; Hansman et al., 2018), followed by NW-SE striking normal fault systems (Al-
136 Wardi and Butler, 2007; Fournier et al., 2006; Grobe et al., 2018; Hanna, 1990; Hilgers et al., 2006; Holland et al.,
137 2009 [a and b](#); Loosveld et al., 1996; Mattern and Scharf, 2018; Virgo, 2015).

138 Renewed Arabia-Eurasia convergence during the Cenozoic formed the three dome structures ~~with the associated~~
139 ~~tectonic windows~~. Timing of formation and exhumation of the Jebel Akhdar Dome is still debated. Stratigraphic
140 arguments for a late Cretaceous doming are Maastrichtian rocks unconformably deposited on Hawasina (Bernoulli
141 et al., 1990; Fournier et al., 2006; Hanna, 1990; Nolan et al., 1990), while inclined Miocene strata at the northern
142 fringes of the dome points to a ~~younger~~ Miocene doming (Glennie et al., 1973). Consequently, some models
143 suggest a two-phased exhumation in Cretaceous and Miocene (Grobe et al., 2018; Searle, 1985, 2007), in
144 agreement with ~~thermochronological constrains and an interpreted two-stage cooling with possible reheating in~~
145 ~~late Miocene~~ (Poupeau et al., 1998; Saddiqi et al., 2006). ~~More recent studies, however, have shown that the data~~
146 ~~of Poupeau et al. (1998) and Saddiqi et al. (2006) can also be explained by a cooling-only scenario with exhumation~~
147 ~~in the Eocene~~ (Hansman et al., 2017). ~~This is in agreement with~~ structural observations suggesting early dome
148 formation and later amplification of the structure (Grobe et al., 2018).

149 2.2. Stratigraphic sequence

150 Sediments in the Jebel Akhdar area consist of a pre-Permian sequence (Autochthonous A, Figure 3) unconformably
151 overlain by a ~~Permian~~-Mesozoic sequence (Autochthonous B, Figure 3; Beurrier et al., 1986; Breton et al., 2004;
152 Glennie et al., 1974; Rabu et al., 1990). During the late Cretaceous, Hawasina nappes and the Semail Ophiolite
153 were emplaced onto the passive margin, and neo-autochthonous rocks of Cenozoic age were deposited on top of
154 the ophiolite after obduction (Béchenec et al., 1988; Forbes et al., 2010; Loosveld et al., 1996).

155



156
157
158
159
160
161
162
163
164

Figure 3: Stratigraphy of the Jebel Akhdar area with its two passive margin sequences Autochthonous A and B overthrust by Hawasina and Semail Nappes and unconformably overlain by neo-autochthonous units. **Ages (Forbes et al., 2010) are basin modeling input data. In addition, thermal calibration data is shown: ZHe ages (Table 2) show two different grain age populations clusters. Maximum-Peak** burial temperatures from organic matter maturity (black, Table 1) outline the temperature increase with stratigraphic age. Temperature data was supplemented by values from *Mozafari et al. (2015) and *Grobe et al. (2016). (U = Unit, P =Period). Note that the Semail and Hawasina nappes are shown in their structural rather than stratigraphic positions; **-D**lithological data is compiled from Beurrier et al. (1986), Loosveld et al. (1996), Terken et al. (2001) and Forbes et al. (2010).

165
166
167
168
169
170
171
172
173
174

Autochthonous A deposits are exposed in the Jebel Akhdar window down to the Mistal Fm. (Beurrier et al., 1986). Black limestones of the Hajir Fm., mudstone rich carbonate beds of the Mu'aydin Fm. and lime- and dolostones of the Kharus Fm. conformably overlie the Mistal Fm. (Beurrier et al., 1986; Glennie et al., 1974). Platform break-up is recorded by laminated cherts and volcanoclastics of the Fara Fm. (Beurrier et al., 1986) followed by an unconformity representing a gap from Cambrian to Permian times (Loosveld et al., 1996). After establishment of the Neotethyan Ocean during the Permian, northern Oman returned to stable passive margin conditions and the carbonate platform of the Autochthonous B developed, with the Akhdar Gp at its base (Koehrer et al., 2010; Pöppelreiter et al., 2011). This is unconformably overlain by limestones with clastic interlayers of the Jurassic Sahtan Group (Beurrier et al., 1986; Pratt et al., 1990). Limestones with marly, frequently organic-rich intercalations of the Cretaceous Kahmah (Habsi et al., 2014; Vahrenkamp, 2010) and Wasia groups (Grelaud et

175 al., 2006; Homewood et al., 2008; Philip et al., 1995) form the youngest platform sediments (Robertson, 1987;
176 Warburton et al., 1990).

177 The obduction-related moving forebulge and associated uplift ended passive margin deposition and eroded the
178 topmost Wasia ~~Group Gp.~~ (Natih Fm.) in the Jebel Akhdhar (Figure 3), and deeper in the Saih Hatat region.
179 Deposition in the foredeep basins in front and behind the forebulge was dominated by the syn- and postorogenic,
180 conglomerate-rich sediments of the Muti Fm., Aruma ~~Gp. Group~~ (Beurrier et al., 1986; Robertson, 1987). Towards
181 the south, in the Adam Foothills, this laterally grades to calcareous foreland sediments of the Fiqa Fm. (Forbes et
182 al., 2010; Robertson, 1987; Warburton et al., 1990).

183 Hawasina sediments accreted in front and beneath the ophiolite represent marine slope and basin facies, time
184 equivalent to the Autochthonous B (Béchenec et al., 1990). After obduction of oceanic crust on-top of the passive
185 margin, neo-autochthonous evaporites and carbonates of the Paleocene to Eocene Hadhramaut Gp. and bivalve-
186 rich dolomites and limestones of the Oligo- to Pliocene Fars ~~Group Gp.~~ were deposited south of the mountains
187 (Béchenec et al., 1990; Forbes et al., 2010). Paleogeographical reconstructions show that the Oman Mountains
188 had high relief after obduction, followed by a low relief landscape until the early Eocene (Nolan et al., 1990). In
189 the middle Eocene marine transgression caused widespread deposition of limestones, as witnessed e.g. by the Seeb
190 and Ruwaydah Formations (Nolan et al., 1990). Post Eocene times show renewed relief development and
191 continued uplift until recent times (Glennie et al., 1974; Searle, 2007).

192 **2.3. ~~Temperature evolution of the Autochthon~~ Previous paleothermal data of the Autochthon**

193 Only limited paleo-temperature data ~~are is~~ available from the carbonate platform (Fink et al., 2015; Grobe et al.,
194 2016; Holland et al., 2009; Stenhouse, 2014). Peak-burial temperatures of 226-239 °C for the top of the platform
195 were measured using solid bitumen reflectance (also referred to as pyrobitumen reflectance) and Raman
196 spectroscopy of carbonaceous material (RSCM) in the Jebel Akhdar (Grobe et al., 2016). Data correspond
197 to Results indicate peak-burial temperatures of 266 to 300 °C (Grobe et al., 2016; Table 1). Temperature estimates
198 based on RSCM and solid bitumen reflectance (Grobe et al., 2016) yielded similar temperatures for the southern
199 flank of 248-280 °C for the Nahr Umr, 226-239 °C for the Natih B and 172-206 °C for the Muti, respectively
200 (Table 1, Figure 3).

201 Vein crystallization temperatures of 166-205 °C at the top of the Natih A (near Al Hamra) were measured by
202 quartz-calcite thermometry in veins formed during ophiolite-induced burial (Gen. III of Grobe et al., 2018), and
203 approximately 255 °C for veins associated with a later normal fault network (Gen V of Grobe et al., 2018;
204 Stenhouse, 2014). Fluid inclusions (FI) of bedding parallel pinch-and-swell veins (top-to-NNE shear after peak
205 burial, Gen. IV of Grobe et al., 2018) show uncorrected minimum trapping temperatures of 134-221 °C in the
206 lower beds of the Sahtan Group at Wadi Nakhr (Holland et al., 2009). Reflectance measurements of solid-bitumen-
207 containing veins in the Wadi Ghul (Gen I of Grobe et al., 2018), which are interpreted to be associated with fluid
208 mobilization during forebulge migration, showed maximum temperatures of 230 °C (Fink et al., 2015).

209 Vitrinite reflectance data of Mozafari et al. (2015) shows temperatures of c. 140 °C for the Natih B in the Jebel
210 Qusaybah, Adam Foothills, an area not overthrust by the ophiolite complex.

211 ~~Reconstructions of the thermal history using numerical basin modeling were presented for the southern~~
212 ~~foreland and the contained Natih Fm. outlining its extreme efficiency interpreted to be a result of thrusting-~~

213 ~~induced lateral migration (Terken, 1999; Terken et al., 2001) and the Proterozoic hydrocarbon source rocks~~
214 ~~(Visser, 1991).~~

215 2.4. Temperature evolution of the Semail Ophiolite nappe / Allochthon

216 Initial intra-oceanic ophiolite thrusting and associated metamorphism at its sole took place at peak temperatures
217 of 840 ± 70 °C at 97-92 Ma measured at several locations in the Oman Mountains (Gnos and Peters, 1993; Hacker
218 and Mosenfelder, 1996; Rioux et al., 2013; Searle and Cox, 2002; Warren et al., 2003). At 90-85 Ma the base of
219 the ophiolite cooled to 350 ± 50 °C (white mica Ar/Ar dating, Gnos and Peters, 1993). At around 80 Ma the deepest
220 burial of the Oman margin beneath the ophiolite was reached (Hacker and Mosenfelder, 1996; Warren et al., 2005)
221 with temperatures in the metamorphic sole below 300 °C (Le Metour et al., 1990; Saddiqi et al., 2006). ~~Due to the~~
222 ~~at least 2 km thick imbricated Hawasina Nappes between the ophiolite and the passive margin sequence, the~~
223 ~~thermal overprint did not affect the of the nappe temperature on the top of the carbonate platform was low. Limited~~
224 ~~thermal overprinting of the units underlying the ophiolite is supported by the fact that the sediments of the nappes~~
225 ~~directly below the ophiolite do not show signs of regional metamorphism in the Jebel Akhdar region~~ (Searle,
226 1985). ~~Duretz et al. (2015) showed in~~ A lithospheric scale thermo-mechanical model of the thrusting in
227 northwestern Oman includes a thermal anomaly c. 100 km northwest offshore the Arabian margin to initiate subsea
228 thrusting (Duretz et al., 2015).

229 2.5. Petroleum system elements

230 Several petroleum systems developed in the carbonate platform of northern Oman with important source rock
231 horizons in the Natih Fm. (~~Natih~~ Members B and E). Both members contain Type I/II kerogen with total organic
232 carbon contents up to 15 % in the Natih B and up to 5 % in the Natih E, respectively (Terken, 1999). Source rock
233 maturity is restored based on biomarker analysis to c. 0.7 % VR within the Fahud reservoir and c. 0.9 % VR in the
234 Natih reservoir (Terken, 1999). In the southern mountain foreland Natih oil generation started in the middle
235 Cretaceous and continuous until present (Terken, 1999). Ophiolite obduction in the Jebel Akhdar area of northern
236 Oman led to over-mature Natih source rocks (Grobe et al., 2016). The Natih Fm. is classified as supercharged,
237 laterally drained, foreland petroleum system (Terken et al., 2001). However, the thermal impact of the moving
238 forebulge and the importance of tectonic processes for fluid migration below and in front of the obduction orogen
239 are not clear. At least three different generations of solid bitumen particles in veins and source rocks on the
240 southern slope of the Jebel Akhdar suggest pulses of hydrocarbon generation and migration in front of the Oman
241 Mountains (Fink et al., 2015; Grobe et al., 2016). In central Oman, Shu'aiba and Tuwaiq oils are produced out of
242 Kahmah and Sahtan ~~Gp. Group~~ reservoirs, sealed by argillaceous shales of the Nahr Umr Fm. (Terken et al., 2001).
243 All ~~T~~ these units are ~~all~~ well-exposed in the Oman Mountains.

244 3. Methods

245 ~~Samples for thermal reconstruction were collected during several field campaigns between 2013 and 2016~~
246 ~~in the Jebel Akhdar Dome (Figure 2).~~

247 3.1. Elemental analysis and thermal maturity Raman spectroscopy of carbonaceous material

248 To determine levels of thermal maturity, over 100 dark, unweathered and organic-rich samples were taken from
249 different stratigraphic units in the Jebel Akhdar (ADD Sahtan Group, Kharaib Fm., Shu'aiba Fm., Nahr Umr Fm.,
250 Natih Fm., Muti Fm. STRATIGRAPHIC LEVELS., Figure 3). Based on total organic carbon (TOC) content as
20

251 determined by Grobe et al. (2016), 13 samples were selected for thermal maturity analysis on surfaces cut
252 perpendicular to bedding. Results were used to calibrate peak-burial temperatures of the numerical basin models.
253 The organic particles lack sufficient size or surface quality for reflectance measurements and are therefore
254 investigated by confocal Raman spectroscopy of carbonaceous material. The technique measures vibrational
255 energies of chemical bonds which change during temperature induced reorganization of amorphous carbonaceous
256 material (kerogen) to graphite (e.g. Aoya et al., 2010; Beyssac et al., 2002; Kouketsu et al., 2014; Mair et al.,
257 2018). Measurements were conducted at the Geoscience Center, Göttingen, on a Horiba Jobin Yvon HR800 UV
258 spectrometer attached to an Olympus BX-41 microscope and a 100× objective. A high-power diode laser with a
259 wavelength of 488 nm and an output power of 50 mW was installed and a D1 filter avoided sample alteration by
260 heating. Each spectral window (center at 1399.82 cm⁻¹, grid of 600 lines/mm) was measured 5 to 10 times for 2
261 to 10 seconds with a Peltier CCD detector at activated intensity correction. For quality control, the 520.4 cm⁻¹ line
262 of a Si-wafer was measured every 30 minutes without observable drift of the measurements. To transform the
263 measured data into VR_r values the scaled total area (STA) approach of Lünsdorf (2016) was applied with the
264 equation of Grobe et al. (2016):

$$VR_r = -\frac{STA - 280.13}{24.71} \quad [\%]$$

265 Absolute errors of the applied calibration are in the order of ±40 °C, based on comparing neighboring samples
266 (Grobe et al., 2016) we can resolve the relative differences down to ±30 °C which also represents the residual error
267 interpreted to relate to within-sample heterogeneity (Lünsdorf et al., 2017; Nibourel et al., 2018).
268

269

270 3.2. Fluid inclusion thermometry

271 Doubly-polished wafers (c. 200 μm thick) of four vein samples (FI-N1, -N2, -M1, -M2) have been prepared
272 according to the procedure described by Muchez et al. (1994). Fluid inclusion (FI) petrography and
273 microthermometry was performed to analyze the temperature-pressure conditions and fluid's salinity. FIs represent
274 paleofluids accidentally trapped in a crystalline or amorphous solid during mineralizationcrystallization,
275 lithification or both (Diamond, 2003). If unaffected by later changes, trapping pressure and temperature is given
276 by the homogenization temperature (Barker and Goldstein, 1990). Based on the time of trapping primary (mineral
277 growth), secondary (fracture-related) and pseudosecondary inclusions are distinguished (Barker and Goldstein,
278 1990; Diamond, 2003; Goldstein, 2001; Van Den Kerkhof and Hein, 2001):

279 Two calcite vein samples of the Natih Fm. (FI-N1 and 2, Locations Figure 4) represent conditions related to early
280 burial (FI-N2, structural generation I of Grobe et al., 2018), and burial beneath the ophiolite (FI-N1, structural
281 generation III of Grobe et al., 2018). Two quartz-rich calcite veins of the Muti Fm. (FI-M1 and 2, Locations Figure
282 4) are related to late, NE-SW striking strike slip faults (generation IX of Grobe et al., 2018). FI assemblages were
283 defined and fluid inclusions measured with a Linkam THMSG600 thermostage (accuracy ± 0.1 °C) attached to an
284 Olympus BX60 microscope at the KU Leuven, Belgium. Calibration was performed using CO₂, H₂O-NaCl, H₂O-
285 KCl, and H₂O standards. Homogenization temperatures (T_h) were measured prior to temperatures of complete
286 freezing (T_f), first melt (T_{fm}), and complete melting of ice (T_{m(ice)}) to avoid stretching or leakage due to the volume
287 increase during ice formation. All measured temperatures were recorded during heating, except ~~of~~ for the freezing
288 temperature (T_f). Pressure corrections of T_h were conducted with the program FLINCOR (Brown, 1989) for
289 280 and 340 MPa, assuming 8 to 10 km of ophiolite overburden (see model results, ρ= c. 3070 kg/m³) and 2 km

290 of sedimentary Hawasina Nappes ($\rho = c. 2450 \text{ kg/m}^3$), and for 45 MPa, assuming 2°km of sedimentary overburden
291 (Al-Lazki et al., 2002; Grobe et al., 2016). Fluid salinities were calculated from the $T_{m(\text{ice})}$ values considering a
292 $\text{H}_2\text{O-NaCl}$ composition (Bodnar, 1993), which is based on the T_{fm} values.

293 **3.3. Thermochronology**

294 Zircon (U-Th)/He (ZHe) dating allows to reconstruct the ~~tectono~~-thermal history of the topmost few kilometers of
295 the Earth's crust. Helium retention in less metamict zircon crystals is sensitive in the temperature range between
296 c. 130 and 170 °C, i.e. the zircon partial retention zone (PRZ, Reiners, 2005). 11 rocks sampled above (Muti Fm.,
297 Hawasina and Semail nappes), below (Mistal Fm., Muaydin Fm., Fara Fm.) and within (Sahtan Gp.) the carbonate
298 platform were selected for ZHe dating. Zircon crystals were released using high voltage pulse crushing
299 (<http://www.selfrag.com>) and concentrated by standard mineral separation processes (drying, dry sieving,
300 magnetic and heavy liquid separation). Three to eight clear, intact, euhedral single crystals were selected per
301 sample and transferred into platinum micro-capsules. They were degassed under high vacuum by heating with an
302 infrared diode and extracted gas purified using a SAES Ti-Zr getter at 450 °C. Helium was analyzed with a Hiden
303 triple-filter quadrupole mass spectrometer. Degassed zircons were subsequently dissolved in pressurized teflon
304 bombs, spiked and U, Th and Sm measured with a Perkin Elmer Elan DRC II ICP-MS equipped with an APEX
305 micro flow nebulizer.

306 Time-temperature histories were reconstructed using the HeFTy 1.8.3 software package (Ketcham, 2005) applying
307 kinetic zircon properties of Guenther et al. (2013). For samples with reset zircons the only constraint used was a
308 minimum temperature above 200 °C between deposition and the calculated ZHe age. Thermal modeling was
309 conducted until 100 statistically good time-temperature paths were achieved (goodness of fit: 0.5, value for
310 acceptable fit: 0.05). In cases where this was not possible, at least 10,000 independent paths were calculated.

311 **3.4. Numerical basin modeling**

312 Structural evolution was palinspastically reconstructed starting from the present-day profile using Move 2D
313 (2016.1, Midland Valley Exploration). Geometries and relative ages of the structures were supplemented with
314 subsurface data (Al-Lazki et al., 2002; Filbrandt et al., 2006; Searle et al., 2004; Warburton et al., 1990). The
315 reconstruction workflow ~~is based on restoring the pre-deformation layer continuity was~~ as follows: (1) faulted
316 layers in the southern foreland were restored, (2) doming was retro-deformed by vertical simple shear, before (3)
317 normal faults in the Jebel Akhdar were restored. This sequence is based on our tectonic model (Grobe et al., 2018).
318 The resulting geometries were used as pre-thrusting input geometries for 2D PetroMod 2014.1 (Schlumberger)
319 basin modeling, enabling thermal maturity reconstruction for vitrinite reflectance values of 0.3 to 4.7 % by the use
320 of the EASY % $R_{0\%}$ approach (Sweeney and Burnham, 1990). The numerical basin model is based on a
321 conceptual definition of events. Based on this sequence of events (sedimentation, erosion, hiatus) a forward,
322 event-stepping modeling ~~is-was~~ performed, starting with the deposition of the oldest layer. Subsequent deposition
323 and burial is leading to differential compaction of the single rock units. For each event lithologies and related
324 petrophysical rock properties ~~are-were~~ assigned (Figures S1, S2). ~~The final basin model (representing the present~~
325 ~~day) fits the geometries deduced from seismic interpretation and geology. This is the first time that~~ ophiolite
326 ~~obduction is reconstructed using a petroleum system modelling software such as PetroMod. To simulate obduction~~
327 ~~we used a rapid, stepwise laterally advancing emplacement, i.e. sedimentation, of ophiolitic rocks. This is~~
328 ~~reasonable, as we will show that the ophiolite did not thermally overprint the passive margin sequence from above.~~

329 For our conceptual model the following sequence of events was implemented (Figure 3): (1) passive margin
330 carbonate sedimentation from Permian until late Cenomanian times (Forbes et al., 2010; Loosveld et al., 1996),
331 interrupted by a short erosional period at the Triassic-Jurassic boundary (Koehrer et al., 2010; Loosveld et al.,
332 1996), (2) a moving forebulge associated with a paleo-water depth increase in its foredeep and erosion of the top
333 of the carbonate platform in the north of the transect (Robertson, 1987), (3) the emplacement of allochthonous
334 sedimentary nappes and (4) subsequent obduction, i.e. stepwise, rapid sedimentation, of the ophiolite with deepest
335 burial reached at c. 79 Ma (Warren et al., 2005). The area of the Adam Foothills, represented in the transect by ~~the~~
336 Jebel Qusaybah, is a relic of the moving forebulge not overthrust by allochthonous units – this was used to calibrate
337 burial depth of the foredeep at this point in the transect. The south of the foothills is unaffected by foredeep and
338 obduction, but also lacks thermal calibration data. Absolute ages, thicknesses, lithologies and related petrophysical
339 properties as well as source rock properties were associated according to results of our own field mapping and the
340 compiled data from Forbes et al. (2010; Figure S1).

341 Thermal boundary conditions of the model have been defined for each time step by the basal heat flow (HF) and
342 the sediment water interface temperature (SWIT), representing the upper thermal boundary (Figure S3). To
343 account for active margin tectonics and uplift and exhumation of the Jebel Akhdar, we assume an increase in basal
344 heat flow since the late Cretaceous. The resulting heat flow trend (Figure S3, Terken et al., 2001; Visser, 1991)
345 has been assigned to the entire transect and was tested in the sensitivity analysis. Paleo-surface temperatures were
346 estimated based on Oman's paleo-latitude (after Wygrala, 1989) corrected by the effect of the paleo-water depth
347 (PWD) derived from the facies record (Van Buchem et al., 2002; Immenhauser et al., 1999; Immenhauser and
348 Scott, 2002; Koehrer et al., 2010; Pratt et al., 1990; Robertson, 1987).

349 This set-up has been iterated until modeling results fit the thermal calibration data (Table 1). From VR_r calculations
350 peak-burial temperatures were determined following the approach of Barker and Pawlewicz (1994). For calibration
351 of the numerical basin models, data was supplemented by thermal maturity and peak-burial temperature data of
352 63 Natih B source rock samples, taken around the Jebel Akhdar Dome (Grobe et al., 2016), and two data points in
353 the Adam Foothills on Jebel Qusaybah (Mozafari et al., 2015).

354 Main modelling uncertainties derive from the unknown thickness of paleo-overburden (Muti Fm., Ophiolite,
355 Hawasina Nappes) and uncertainty of paleo-basal heat flow. Present-day heat flow was calibrated by data and
356 borehole temperatures of Visser (1991) and Rolandone et al. (2013) and peak-burial temperatures determined by
357 Raman spectroscopy and solid bitumen reflectance data (Table 1). From surface samples and their position in the
358 stratigraphic column various pseudo-wells were created (e.g. Nöth et al., 2001) and used as control points for the
359 2D model (Figure 2). The model was used for sensitivity analyses of different input parameters.

360 **4. Results and Interpretation**

361 **4.1. Thermal maturity and host rock burial temperatures**

362 New Raman spectroscopy data of the northern flank give scaled total areas of 78-172. This correspond to peak
363 temperatures of 270-300 °C in the Shu'aiba Fm., 268-305 °C in the Kahmah Group, 283-286 °C in the Sahtan Gp.,
364 270-288 °C in the Nahr Umr Fm. and 266 °C at the base of the Natih Fm. Based on the calculation to VR_r and
365 temperature an absolute error of ± 30 °C has to be considered for the single values.

366

367 **Table 1: Thermal maturity data and calculated peak temperatures of northern Oman (new data highlighted by bold**
 368 **sample name).** Temperatures from Raman spectroscopy of carbonaceous material are calculated based on the STA
 369 **approach of Lünsdorf (2016) and the formula equation published by of Grobe et. al (2016).** M/P indicate if measurement
 370 **was conducted on solid bitumen particles (P) or below the surface of their organic rich matrix (M).** **Errors shown are**
 371 **related to the measurement, calculation errors are in the order of +/-30 °C.** Data of Mozafari et al. (2015) are used for
 372 **Jebel Qusaybah, Adam Foothills.**

373 **From Raman spectroscopy, integrated deformation peaks (D peaks) give scaled total areas of 90-156 which**
 374 **correspond to peak-burial temperatures of 266 to 300 °C (Grobe et al., 2016; Table 1). The maximum temperatures**
 375 **increase with stratigraphic age and are similar on the northern and southern flanks of the Jebel Akhdar Dome (e.g.**
 376 **Natih Fm.). Nahr Umr and Shu'aiba Fm. show slightly higher peak temperatures in the north of the transect (Figure**
 377 **3). Temperature estimates based on RSCM and solid bitumen reflectance (Grobe et al., 2016) yielded similar**
 378 **temperatures for the southern flank of 248-280 °C for the Nahr Umr, 226-239 °C for the Natih B and 172-206 °C**
 379 **for the Muti, respectively (Table 1, Figure 3). Vitrinite reflectance data of Mozafari et al. (2015) shows**
 380 **temperatures of c. 145-182 °C for Natih B in the Jebel Qusaybah, Adam Foothills, an area not overthrust by the**
 381 **ophiolite complex.**

sample No.	location (UTM 40Q)					No. of measurements	mean D_STA	calculated VR, [%]	mean Temp.
15_995	Wadi Yiqah	516683	2582911	Sahtan Gp.	M	14	113 +/- 14	6.52	286 +/- 6 °C
15_997	Wadi Yiqah	517815	2583645	Shu'aiba Fm.	M	10	115 +/- 5	6.69	289 +/- 3 °C
15_1001	Wadi Taisa	516538	2584640	Kahmah Gp.	M	1	78	8.19	305 °C
15_1003	Wadi Taisa	516538	2584640	Kahmah Gp.	M	8	96 +/- 9	7.44	297 +/- 4 °C
15_1008	Wadi Taisa	516562	2584727	Kahmah Gp. (top)	M	8	113 +/- 15	6.78	290 +/- 7 °C
15_1010	Wadi Taisa	516693	2584882	Shu'aiba Fm.	M	13	98 +/- 11	7.28	295 +/- 5 °C
15_1010	Wadi Taisa	516693	2584882	Shu'aiba Fm.	P	4	149 +/- 15	5.31	270 +/- 9 °C
16_974	Tr- Jur fault	515839	2582229	base Sahtan Gp.	P	6	125 +/- 17	6.29	283 +/- 9 °C
16_977	Kharb Plateau	520420	2577490	base Natih Fm.	M	10	156 +/- 9	5.04	266 +/- 6 °C
16_979	Kharb Plateau	519305	2577363	top Nahr Umr Fm.	M	2	117 +/- 4	6.60	288 +/- 2 °C
16_981	Kharb Plateau	519933	2577201	top Nahr Umr Fm.	M	1	149	5.30	270 °C
16_984	Wadi Taisa	518069	2583462	Kahmah Gp.	M	3	172 +/- 26	5.29	268 +/- 22 °C
16_985	Wadi Murri	505508	2592709	Shu'aiba Fm.	M	2	90 +/- 4	7.69	300 +/- 2 °C
Grobe et al. (2016)_SV10	Wadi Nakhr	521260	2560364	Natih	P	6	-	2.83	227-231 °C
Grobe et al. (2016)_AG22	Wadi Nakhr	521255	2560362	Natih	M	4	-	3.72	225-260 °C
Grobe et al. (2016)_AG01	Wadi Nakhr	520375	2562026	Shu'aiba (Kh 3)	M	4	-	4.49	251-269 °C
Grobe et al. (2016)_AG11	Sint	505627	2564136	Hawasina	P	5	-	2.45	193-213 °C
Grobe et al. (2016)_AG25	Balcony Walk Nakhr	520913	2565658	Nahr Umr	M	4	-	4.23	226-267 °C
Grobe et al. (2016)_AG26_1	Balcony Walk Nakhr	521052	2565560	Nahr Umr	P	2	-	(2.58)	(211-213 °C)
Grobe et al. (2016)_AG26_3	Balcony Walk Nakhr	521052	2565560	Nahr Umr	M	2	-	4.96	275-280 °C
Grobe et al. (2016)_AG27	Balcony Walk Nakhr	520879	2565342	Nahr Umr	M	3	-	4.61	248-266 °C
Grobe et al. (2016)_AG30	Balcony Walk Nakhr	520756	2565030	Nahr Umr	M	3	-	4.25	248-257 °C
Grobe et al. (2016)_AG37	Jebel Shams	514821	2568047	Muti	P	3	-	2.16	191-208 °C
Grobe et al. (2016)_AG38	Jebel Shams	514930	2567334	Muti	P	2	-	1.99	172-206 °C
reference	location (UTM 40Q)					No. of measured particles	measured BR, [%]	calculated / measured VR, [%]	calculated T _{peak} (Barker and Pawlewicz, 1994)
Grobe et al. (2016)	Wadi Nakhr area	521216	2560308	Natih B	BR _i	253	3.08-3.59	3.08-3.59	226-239 °C
Fink et al. (2015)	Wadi Nakhr area	518550	2561000	Natih B	BR _i	200	3.10-3.14	-	c. 225 °C
Fink et al. (2015)	Wadi Nakhr area	514800	2565950	Natih A Vein	BR _i	c. 250	3.40-3.76	-	-
Grobe et al. (2016)	Al Hamra area	531024	2557020	Natih B	BR _i	20	2.95-3.34	2.95-3.34	223-233 °C
Grobe et al. (2016)	Wadi Sahtan	531010	2585640	Natih B	BR _i	6	3.32	3.32	232 °C
Mozafari et al. (2015), measured at RWTH	Jebel Qusaybah	507930	2491600	Natih B	VR _i	20	-	1.1	c. 140 °C

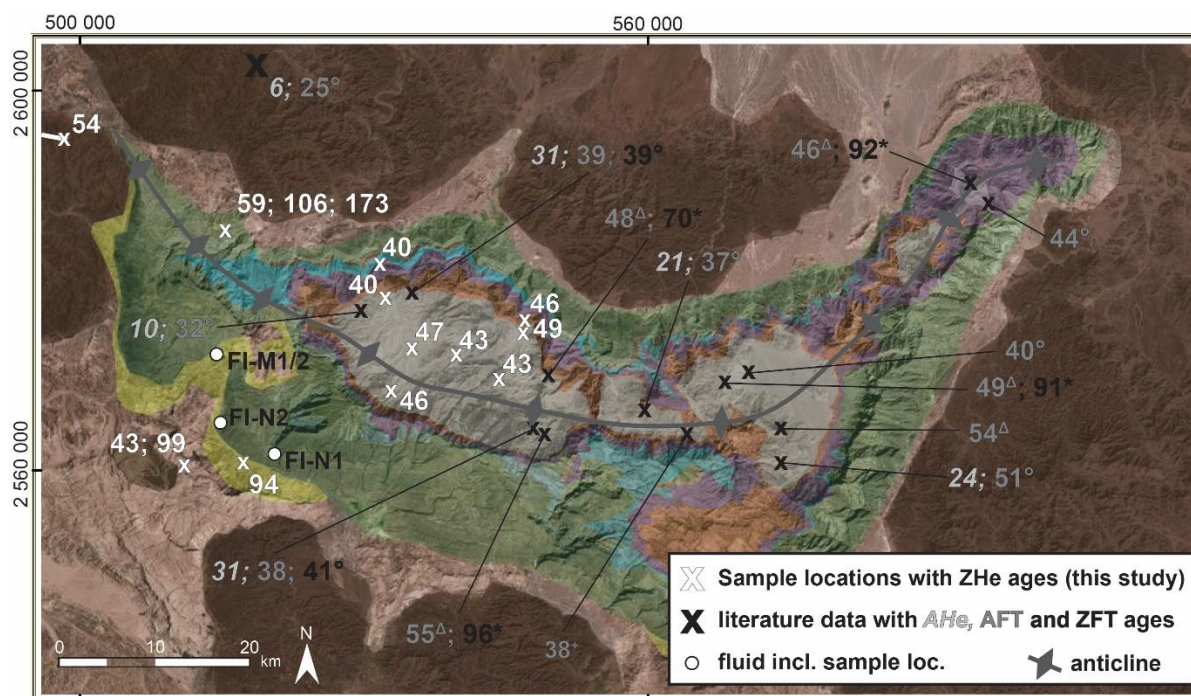
382

383

384 4.2. Thermochronology

385 Results of the ZHe dating are shown in Figures 3 and 4; time-temperature paths modeled with HeFTy are included
 386 in the electronic supplement (Figures S4 and S5). Samples from the carbonate platform (stratigraphically older
 387 than Muti Fm.) have been entirely reset after deposition, as witnessed by Neogene apparent ages (Figure 3). This
 388 Similarly, cooling ages from coincides with the center of the Jebel Akhdar Dome in which all cooling ages fall in
 389 the range of 48.7 ± 1.8 to 39.8 ± 3.0 Ma (Table 2, Figure 4). Sample T4, collected in the Muti Fm., yields an
 390 apparent mean age of 93.8 ± 6.9 Ma and samples T5 and T7 of the Hawasina Nappes collected at the northern and
 391 the southern slope of the dome, show two grain age populations-clusters of $43.0 \pm 3.7 / 99.2 \pm 8.5$ Ma, and
 392 $58.9 \pm 7.0 / 106.0 \pm 5.2$ Ma, respectively. In sample T5, an additional single grain age population—of
 393 172.9 ± 14.9 Ma was obtained.

394



395

396 **Figure 4: Map view of ZHe ages (in Ma) sampled below, in and above the carbonate platform of the Jebel Akhdar**
 397 **Dome.** Data outlines a general cooling between 58.9 ± 7.0 and 39.8 ± 3.0 Ma. Some samples outside of the dome show
 398 two age populationsclusters, with an additional age population—of c. 100 Ma. Additional temperature data refers to
 399 zircon fission track ages of (*) Saddiqi et al. (2006), Apatite fission track ages of (Δ) Poupeau et al. (1998) and (+) Mount
 400 et al. (1998), and AHe, AFT and ZFT ages of (+, grey) Hansmann et al. (2017). Moreover, the locations of samples used
 401 for fluid inclusion measurements are shown. Colors in the background depict geological units (brown: ophiolite, pink:
 402 Hawasina units, light green: Muti Fm., dark green: Wasia and Kahmah Gp., blue: Sahtan Gp., purple: Mahil Fm,
 403 orange: Saiq Fm, grey: pre-Permian, shaded DEM from Esri, Digital Globe, swisstopo, and the GIS user Community).

404

405 **Table 2: Results of zircon (U-Th)/He dating.**

sample aliquot	lithology / location Easting Northing		He		²³⁸ U			²³² Th			Th/U ratio	Sm			ejection correct. (Ft)	uncorrected He age [Ma]	FT corrected				mean age [Ma]	
			vol. [ncc]	1 σ [%]	mass [ng]	1 σ [%]	conc. [ppm]	mass [ng]	1 σ [%]	conc. [ppm]		mass [ng]	1 σ [%]	conc. [ppm]			He age [Ma]	He age [Ma]	2σ [%]	2σ [Ma]		
T1-Z1	sandstone		5.31	0.83	1.04	1.81	212.00	0.38	2.41	77.66	0.37	0.03	10.43	6.44	0.754	38.90	51.60	8.20	4.20	48.70	+/-	1.80
T1-Z2	547533	2574875	6.05	0.84	1.31	1.81	323.34	0.33	2.41	80.49	0.25	0.01	21.24	2.97	0.737	36.10	49.10	8.70	4.30			
T1-Z3	Fara Fm.	Autochthon A	3.45	0.87	0.84	1.81	212.21	0.30	2.41	74.73	0.35	0.02	14.08	3.83	0.719	31.30	43.60	9.20	4.00			
T1-Z4			3.15	0.86	0.64	1.82	178.10	0.34	2.41	95.86	0.54	0.01	15.61	4.16	0.72	36.30	50.50	9.10	4.60			
T2-Z1	tuffite		9.23	0.83	2.04	1.81	352.85	1.03	2.41	178.16	0.50	0.04	9.53	7.26	0.778	33.40	42.90	7.60	3.20	46.10	+/-	2.00
T2-Z2	547533	2574875	8.58	0.83	1.99	1.81	376.54	0.88	2.41	166.07	0.44	0.07	7.63	14.20	0.757	32.30	42.70	8.10	3.50			
T2-Z3	Fara Fm.	Autochthon A	12.48	0.83	2.32	1.81	377.81	1.01	2.41	163.95	0.43	0.03	11.07	5.44	0.789	40.20	51.00	7.30	3.70			
T2-Z4			6.16	0.83	1.26	1.81	186.92	0.52	2.41	76.65	0.41	0.03	10.98	4.83	0.768	36.80	48.00	7.80	3.80			
T3-Z1	sandstone		3.69	0.86	1.04	1.81	361.71	0.41	2.41	142.73	0.39	0.02	15.90	6.29	0.689	26.90	39.10	10.00	3.90	42.60	+/-	1.70
T3-Z2	544722	2570255	2.82	0.88	0.63	1.82	254.57	0.22	2.42	87.47	0.34	0.02	12.85	9.07	0.694	34.20	49.40	9.90	4.90			
T3-Z3	Muaydin Fm.	Autochthon A	1.54	0.90	0.35	1.85	116.01	0.23	2.42	75.70	0.65	0.02	17.64	5.19	0.67	31.80	47.50	10.50	5.00			
T3-Z4			4.71	0.84	1.20	1.81	309.13	0.70	2.41	180.18	0.58	0.05	9.18	12.12	0.74	28.50	38.50	8.60	3.30			
T3-Z5			8.91	0.83	1.95	1.81	262.57	1.30	2.41	175.08	0.67	0.07	9.00	9.29	0.761	32.60	42.90	8.00	3.40			
T3-Z6			9.80	0.83	2.52	1.81	283.31	1.13	2.41	127.16	0.45	0.06	7.80	6.56	0.816	29.00	35.60	6.60	2.30			
T3-Z7			11.83	0.83	2.41	1.81	219.27	1.23	2.41	111.66	0.51	0.11	7.31	10.01	0.794	36.10	45.50	7.10	3.20			
T3-Z8			8.41	0.83	1.85	1.81	224.86	1.04	2.41	125.92	0.56	0.07	9.09	8.40	0.784	33.10	42.20	7.40	3.10			
T4-Z1	conglomerate		18.23	0.83	1.79	1.81	380.98	0.44	2.41	93.57	0.25	0.02	13.79	3.77	0.736	79.30	107.60	8.70	9.40	93.80	+/-	6.90
T4-Z2	517510	2560808	10.68	0.83	1.36	1.81	392.55	0.35	2.41	100.65	0.26	0.02	15.99	5.30	0.703	61.20	86.90	9.60	8.40			
T4-Z3	Muti Fm.	Autochthon B	5.24	0.85	0.56	1.82	137.78	0.48	2.41	118.23	0.86	0.04	8.48	11.06	0.738	64.20	86.90	8.60	7.50			
T5-Z1	turbiditic sandstone		34.15	0.82	3.38	1.81	502.17	0.79	2.41	117.95	0.23	0.10	7.97	14.16	0.781	78.70	100.80	7.50	7.60	106.00	+/-	5.20
T5-Z2	512934	2561691	13.52	0.83	1.28	1.81	333.42	0.27	2.41	69.42	0.21	0.02	16.57	4.11	0.744	82.70	111.20	8.50	9.50			
T5-Z3	Matbat Fm.	Hawasina N.	8.95	0.83	1.30	1.81	254.43	0.78	2.41	153.35	0.60	0.01	16.47	2.78	0.754	49.70	65.90	8.20	5.40			
T5-Z4			9.21	0.84	1.75	1.81	416.93	0.69	2.41	163.29	0.39	0.04	9.44	9.25	0.766	39.80	51.90	7.90	4.10			
T5-Z5			37.88	0.80	51.13	2.33	1.81	561.72	0.37	2.41	90.14	0.16	0.02	11.59	0.741	0.741	128.10	172.90	8.60			
T6-Z1	granodiorite		6.55	0.83	1.00	1.81	241.80	1.28	2.41	311.91	1.29	0.29	5.62	69.36	0.747	41.60	55.60	8.30	4.60	53.70	+/-	1.20
T6-Z2	478301	2592360	6.39	0.85	0.97	1.81	288.96	1.32	2.41	394.16	1.36	0.28	5.31	84.38	0.719	41.10	57.20	9.10	5.20			
T6-Z3	Trondjemite	Semail Ophio.	7.07	0.83	1.06	1.81	314.75	1.79	2.41	528.55	1.68	0.19	5.49	57.19	0.751	39.20	52.30	8.20	4.30			
T6-Z4			12.11	0.84	1.79	1.81	347.26	3.35	2.41	649.55	1.87	0.31	5.55	61.00	0.769	38.60	50.20	7.70	3.80			
T6-Z5			6.78	0.84	1.08	1.81	273.36	1.46	2.41	368.85	1.35	0.27	5.75	68.70	0.738	39.10	53.00	8.60	4.50			
T7-Z1	quartzite		14.91	0.84	1.56	1.81	427.30	0.43	2.41	118.20	0.28	0.05	9.26	12.45	0.744	73.80	99.20	8.50	8.50	99.20		
T7-Z2	514817	2586049	4.14	0.87	1.35	1.81	428.75	0.38	2.41	119.50	0.28	0.02	12.47	7.90	0.729	23.70	32.50	8.90	2.90			
T7-Z3	Matbat Fm.	Hawasina N.	6.37	0.85	1.33	1.81	274.36	0.30	2.41	62.67	0.23	0.03	10.62	6.71	0.769	37.50	48.80	7.90	3.80			
T7-Z4			9.66	0.81	12.43	2.13	1.81	539.06	0.15	2.45	38.38	0.07	0.01	17.24	0.777	36.90	47.50	7.70	3.70			
T7-Z5			4.03	0.83	5.46	0.94	1.81	232.12	0.47	2.41	115.05	0.50	0.02	12.63	0.738	31.70	43.00	8.60	3.70			
T8-Z1	tuffitic sandstone		4.60	0.86	1.34	1.81	450.89	1.11	2.41	374.66	0.83	0.16	5.81	53.52	0.759	23.70	31.20	8.00	2.50	39.80	+/-	3.00
T8-Z2	532600	2578681	2.92	0.85	0.56	1.82	147.09	0.86	2.41	226.75	1.54	0.28	5.14	73.06	0.715	31.40	44.00	9.20	4.00			
T8-Z3	Mistal Fm.	Autochthon A	2.21	0.89	0.46	1.83	168.48	0.57	2.41	208.48	1.24	0.05	8.65	16.66	0.716	30.90	43.20	9.20	4.00			
T8-Z4			3.46	0.85	0.85	1.81	212.57	0.41	2.41	103.10	0.49	0.01	14.27	3.65	0.74	30.30	41.00	8.60	3.50			
T9-Z1	quartzite		2.90	0.86	0.61	1.82	238.35	0.50	2.41	198.12	0.83	0.01	16.09	5.23	0.705	33.10	46.90	9.50	4.50	45.50	+/-	2.40
T9-Z2	532595	2568258	0.72	0.98	0.18	1.94	109.52	0.13	2.43	76.58	0.70	0.05	10.52	29.38	0.674	27.50	40.80	10.50	4.30			
T9-Z3	Mistal Fm.	Autochthon A	2.04	0.89	0.41	1.84	147.39	0.28	2.41	101.51	0.69	0.01	18.70	3.60	0.718	35.10	48.80	9.20	4.50			
T10-Z1	sandstone		5.09	0.85	0.93	1.81	213.39	0.95	2.41	217.83	1.02	0.02	13.41	4.93	0.754	36.40	48.20	8.10	3.90	46.90	+/-	4.10
T10-Z2	534779	2572636	6.71	0.83	1.37	1.81	267.61	1.24	2.41	241.07	0.90	0.04	9.18	8.32	0.763	33.30	43.70	7.90	3.40			
T10-Z3	Mistal Fm.	Autochthon A	8.97	0.83	2.25	1.81	568.33	1.79	2.41	452.52	0.80	0.04	8.74	10.22	0.723	27.70	38.40	9.00	3.50			
T10-Z4			2.26	0.88	0.35	1.85	118.10	0.39	2.41	131.18	1.11	0.02	14.08	5.39	0.727	41.80	57.50	8.90	5.10			
T11-Z1	quartzite		4.70	0.84	1.01	1.81	188.02	0.57	2.41	106.02	0.56	0.01	19.39	2.18	0.746	34.00	45.60	8.40	3.80	42.50	+/-	2.00
T11-Z2	540394	2572230	1.55	0.90	0.39	1.84	109.55	0.33	2.41	93.99	0.86	0.01	20.85	2.31	0.706	27.30	38.80	17.60	6.80			
T11-Z3	Mistal Fm.	Autochthon A	1.50	0.94	0.37	1.84	110.19	0.19	2.42	56.69	0.51	0.01	17.25	3.39	0.693	29.90	43.20	9.90	4.30			
T12-Z1	sandstone		5.35	0.85	1.21	1.81	355.93	1.09	2.41	320.43	0.90	0.02	16.47	5.58	0.706	30.10	42.70	9.50	4.00	40.10	+/-	1.50
T12-Z2	531776	2582871	4.28	0.86	1.12	1.81	286.68	0.16	2.42	40.59	0.14	0.01	27.93	1.79	0.736	30.70	41.70	8.80	3.70			
T12-Z3	Sahtan Gp.	Autochthon B	3.80	0.86	1.06	1.81	349.54	0.14	2.43	44.41	0.13	0.01	22.03	2.70	0.719	28.70	39.90	9.20	3.70			
T12-Z4			1.51	0.89	0.38	1.84	92.50	0.32	2.41	76.60	0.83	0.01	15.61	3.53	0.758	27.30	36.10	8.10	2.90			

407 These ages indicate a large-scale cooling signal that affects the entire ~~study~~ Jebel Akhdar area ~~area and is associated~~
408 ~~with doming~~. The ZHe age pattern and 1D thermal models (~~Figures S3 and S4~~) indicate a phase of rapid cooling
409 below 170 °C in the early Cenozoic (58.9 ± 7.0 and 39.8 ± 3.0 Ma). The range of modeled cooling paths outline
410 ~~minimum and~~ maximum cooling rates of 2-8 °C/Myr. This is followed by slower cooling until the present day.
411 Data from the Muti Fm. and the Hawasina units differ partly from this trend: the apparent ZHe ages of clast in the
412 Muti sample T4 (mean: 93.8 ± 6.9 Ma) is as old as its respective stratigraphic age (Robertson, 1987) ~~indicating~~
413 ~~only partial reset of the ZHe system~~. Even though all ages reproduce within error, this indicates partial reset of the
414 ZHe system, as post-depositional reheating above closure temperature would result in younger ages. Samples of
415 the lower Hawasina Nappes contain two grain age ~~populations~~ clusters. Older ages coincide with higher uranium
416 concentrations suggesting that only the younger ages represent thermally reset zircons. Even though, The We note
417 that the older ZHe population ages of 110-95 Ma coincides with timing of forebulge migration through the area,
418 as independently determined in the stratigraphic record in by the Wasia-Aruma Break (Figure 3). This may be
419 either pure coincidence, due to partial resetting of an older grain age population, or may be a grain age population
420 with higher closure temperature witnessing exhumation. We discuss reasons for different resetting temperatures
421 below. However, Ppartial reset of ZHe ages suggests that the Hawasina samples have not experienced temperatures
422 exceeding the partial retention zone (PRZ) of ~~1350~~ 170 °C.

423 A ~~magmatic~~ sample ~~of from~~ an intrusive ~~body of from~~ the Semail Ophiolite yields ZHe ages of 53.7 ± 1.2 Ma (T6)
424 with a modeled cooling path gradually decreasing into the PRZ until c. 55 Ma. This time interval of passing the
425 PRZ is comparable to the Hawasina nappe samples beneath the ophiolite but occurs slightly earlier than cooling
426 of the Autochthonous. Nevertheless, Semail Ophiolite, Hawasina Nappes and the autochthonous margin sequence
427 were affected by the same cooling event that was possibly initiated by exhumation of the Jebel Akhdar Dome.

428 4.3. Fluid inclusions

429 The Muti veins' samples FI-M1 and M2 of the southern Jebel Akhdar show evidence of crack and seal processes
430 (youngest parts in the center of the vein, Ma-2010-11b and 14a of Arndt 2015) with blocky quartz grains that
431 contain two kinds of roundish primary FIs with sizes of 3-20 μm . They are mainly aligned along dark zones and
432 are interpreted as growth zones or form bright clusters in the central part of the crystals. A third set of fluid
433 inclusions (FIs) appears in large, grain-crosscutting trails interpreted to be of secondary origin. Calcite crystals
434 within the Natih veins contain bright FIs with sizes of 2-20 μm and are edgy, often rectangular or trapezoidal in
435 shape. Identified primary FIs are aligned parallel to crystal growth zones.

436 All measured FIs are two-phase, liquid-vapor inclusions with ice as last phase to melt. The Muti samples show
437 $T_{\text{fm(ice)}}$ between -5.1 ± 0.5 and -4.6 ± 0.3 °C and $T_{\text{m(ice)}}$ at -2.2 ± 0.2 to -1.9 ± 0.1 °C, the Natih sample T_{fm} of -
438 18.4 ± 1.9 to -20.2 ± 2.1 °C and $T_{\text{m(ice)}}$ of -7.1 ± 0.3 to -8.9 ± 1.8 °C (Table 3). First melting temperatures of all
439 inclusions correspond to an H₂O-NaCl system and complete melting temperatures of ice indicate salinities similar
440 to seawater (3.0 ± 0.5 to 3.5 ± 0.3 wt.-% NaCl eq., Muti Fm., Figure S6) or three times higher (10.3 ± 0.3 to
441 12.5 ± 2.0 wt.-% NaCl eq., Natih Fm., Figure S6).

442
443 **Table 3: Results of FI microthermometry. Identified FI types, their measured homogenization temperatures and results**
444 **of the pressure correction for 280 and 340 MPa accounting for 8 and 10 km of ophiolite with partly serpentinized mantle**
445 **sequence and 2 km of sedimentary nappes, and for 45 MPa accounting for 2 km of sedimentary overburden for samples**
446 **unaffected by ophiolite obduction. First melting (T_{fm}) and final melting of ice ($T_{\text{m(ice)}}$) temperatures and salinities are**
447 **given. Data by Holland et al. (2009) are added for comparison and we likewise corrected their homogenization**
448 **temperatures**~~Data of Holland et al. (2009) is added for comparison and we likewise corrected his homogenization~~

449
450

temperatures for pressures of 280 and 340 MPa, as his samples were originally covered by the ophiolite complex. (* further heating was avoided to prevent fluid inclusion damage)

sample No.	vein orient., location and host mineral	FI kind	No. of FIA	T _h [°C]	pressure corrected T [°C] for 45 MPa		T _m [°C]	T _{m ice} [°C]	salinity [wt.-% NaCl]
FI-M1	NE-SW striking	primary	21	166 +/- 7	189 +/- 7		-4.7 +/- 0.2	-2.2 +/- 0.2	3.5 +/- 0.3
	strike-slip vein (IX), Muti Fm.	primary	22	189 +/- 3	213 +/- 3		-4.6 +/- 0.3	-2.0 +/- 0.3	3.2 +/- 0.4
	Gorge area, quartz	secondary	18	> 200*	> 224		-4.6 +/- 0.2	-2.0 +/- 0	3.2 +/- 0
					pressure corrected T [°C] for 45 MPa				
FI-M2	NE-SW striking	primary	24	161 +/- 3	184 +/- 3		-5.1 +/- 0.5	-1.9 +/- 0.1	3.0 +/- 0.2
	strike-slip vein (IX), Muti Fm.	secondary	12	116 +/- 12	138 +/- 12		-	-	-
	Gorge area, quartz	secondary	24	150 +/- 2	172 +/- 2		-	-	-
					for 280 MPa	for 340 MPa			
FI-N1	Natih Fm., NW-SE	primary	14	90 +/- 5	235 +/- 5	266 +/- 5	-18.4 +/- 1.9	-7.1 +/- 0.3	10.3 +/- 0.3
	burial vein (III), Wadi Nakhr, calcite	primary	26	(114 +/- 7)	(264 +/- 7)	(297 +/- 7)	-20.2 +/- 2.1	-8.9 +/- 1.8	12.5 +/- 2.0
FI-N2	Natih Fm., early E-W vein (I)	primary	10	80 +/- 4	225 +/- 4	256 +/- 4	-	-	-
	Al Raheba, calcite								
					for 280 MPa	for 340 MPa			
Holland et al. (2009)	Sahtan Gp., bedding parallel shear vein, top-to-NE (IV), Wadi Nakhr, quartz	primary and pseudosec.	n.a.	134-141	296-303	357-364	from -19	-3.7 to -2.3	3.8 to 6.0

451

452

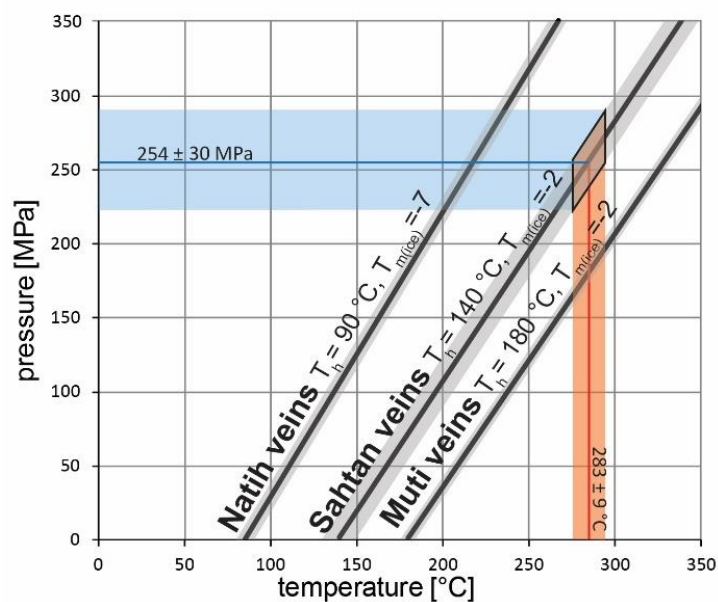
453 Primary inclusions in quartz crystals from the Muti Fm. show minimum trapping temperatures of 161 ± 3 to
454 166 ± 7 °C (Table 3, FI-M2 and middle of FI-M1) with a second primary population of 189 ± 3 °C (sides of vein
455 FI-M1). T_h of secondary inclusions in FI-M1 are above 200 °C. In sample FI-M2, two generations of secondary
456 inclusions were observed, both reflecting lower T_h than the primary inclusions. No hints of necking down, leakage
457 or stretching were observed at the measured inclusions and over 90 % of the measured FIs in one assemblage are
458 in the range of 10-15 °C representing a good quality of the measurements (Goldstein, 2001).

459 Samples FI-N1 and N2 of the Natih Fm. in the southern Jebel Akhdar (Figure 4) contain primary inclusions hosted
460 by calcite crystals giving T_h of 80 ± 4, 90 ± 5 and 114 ± 7 °C (Table 3). The latter population is often characterized
461 by elongated, possibly stretched FI, and is not considered for further interpretations. Assuming vein formation
462 during burial (Grobe et al., 2018; Hilgers et al., 2006; Holland et al., 2009; Virgo, 2015) under 8 to 10 km of
463 ophiolite including partially serpentinized peridotite and 2 km of Hawasina Nappes, results were pressure
464 corrected for 280 and 340 MPa leading to corrected homogenization temperatures of 235 ± 5 and 266 ± 5 °C (FI-
465 N1), and 225 ± 4 and 256 ± 4 °C (FI-N2, Table 3). Signs of strong deformation such as twinning or cleavage were
466 not observed in the measured inclusions; secondary inclusions were present but not measured.

467 These temperatures represent minimum trapping conditions of a paleo-fluid and do not necessarily represent burial
468 temperatures of the host rock. It should be noted that the analyzed Natih veins formed bedding confined (Grobe et
469 al., 2018; Holland et al., 2009; Virgo, 2015) and show host rock buffered carbonate isotope signatures (Arndt et
470 al., 2014; Hilgers et al., 2006). This corroborates the idea that analyzed veins were in thermal equilibrium with
471 their host rocks.

472 FI microthermometry of late strike-slip veins in the Muti Fm. are interpreted to have formed after dome formation
 473 (Grobe et al., 2018; Virgo, 2015) at an assumed minimum depth of 2 km (preserved allochthonous thickness). A
 474 pressure correction for the related 45 MPa corresponds to minimum fluid trapping temperatures of 184 ± 3 °C (FI-
 475 M2) and 213 ± 3 °C (FI-M1) with a later phase of primary inclusions outlining 189 ± 7 °C and even cooler
 476 secondary inclusions of 138 ± 12 to 172 ± 2 °C (FI-M1 and M2, Table 3). These cooler fluid temperatures can be
 477 explained by further exhumation of the Jebel Akhdar and, hence, cooling of the fluids' reservoir during crack-seal
 478 vein formation. Isotope studies on the vein calcite do not support an open system with fluid exchange (Stenhouse,
 479 2014; Virgo and Arndt, 2010), hence, we interpret the formation of strike-slip related veins as having formed
 480 during exhumation following peak burial.

481 Based on the assumption that fluid and host rock were in thermal equilibrium, we can use maturity data in
 482 combination with fluid inclusion data to estimate the pressure at vein formation. Peak temperatures of the Sahtan
 483 Fm Group- revealed by RSCM reached 283 ± 9 to 286 ± 6 °C (Table 1, Figure 5 red line) and enable to solve the
 484 pressure-temperature couples of FIs measured in Sahtan veins formed at deepest burial by Holland et al. (2009,
 485 black line). This results in minimum trapping pressures of 254 ± 30 MPa at times of vein formation (Figure 5 blue
 486 line), which correspond to times close to or at deepest burial of the carbonate platform.



487
 488 **Figure 5: Fluid inclusion isochores (solid black lines) of analyzed fluid inclusion populations with corresponding std.**
 489 **deviations (shaded areas, for Sahtan Gp. Group data of Holland et al., 2009, conservatively ± 10 °C are assumed). To**
 490 **estimate the pressure conditions during vein formation, calculated temperatures from thermal maturity data are added**
 491 **for the Sahtan Gp. Group (red line with error) and result in minimum trapping pressures of 254 ± 30 MPa during peak**
 492 **burial (blue line with error).**

493 **4.4. Structural observations**

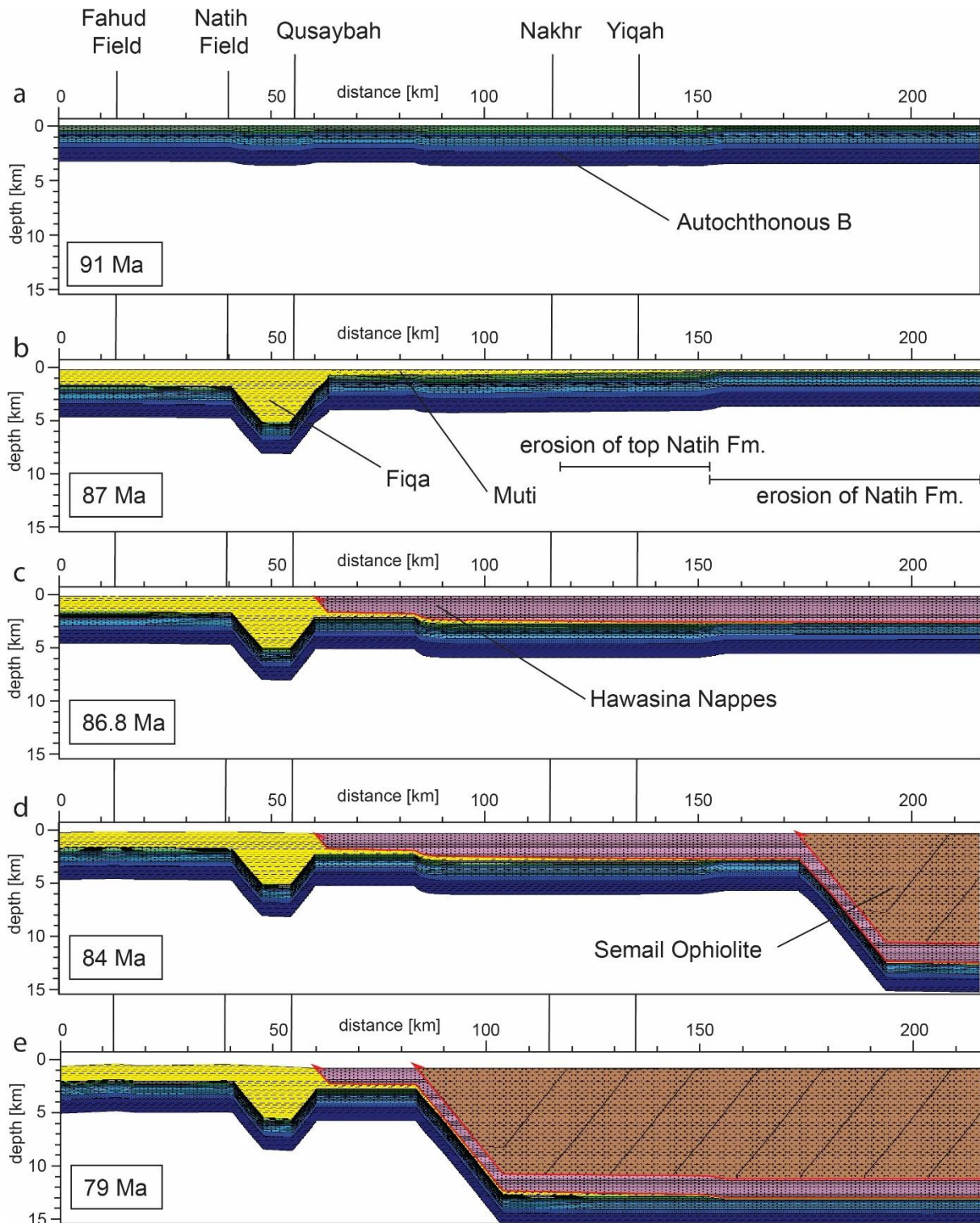
494 **The reconstructed transect (Figure 2) shows the dome structure of the Jebel Akhdar covered with ophiolite**
 495 **nappe remnants in the northeast, the thrustured southern foreland and the salt basins in the southeast that**
 496 **contain the fault-bound hydrocarbon reservoirs of the Fahud and Natih fields. Structures shown are related**
 497 **to large scale normal faulting in the mountain area, where faults are subsequently rotated and bent by**
 498 **doming (Jebel Akhdar), and later strike-slip faulting crosscut domed layers (Gomez-Rivas et al., 2014;**

499 ~~Grobe et al., 2018; Virgo, 2015). Reactivation and inversion of some of the strike-slip faults caused formation~~
500 ~~of hydrocarbon traps in the southern foreland (Natih and Fahud field, e.g. Al-Kindi and Richard, 2014).~~

501 4.5.4.4. Basin modeling

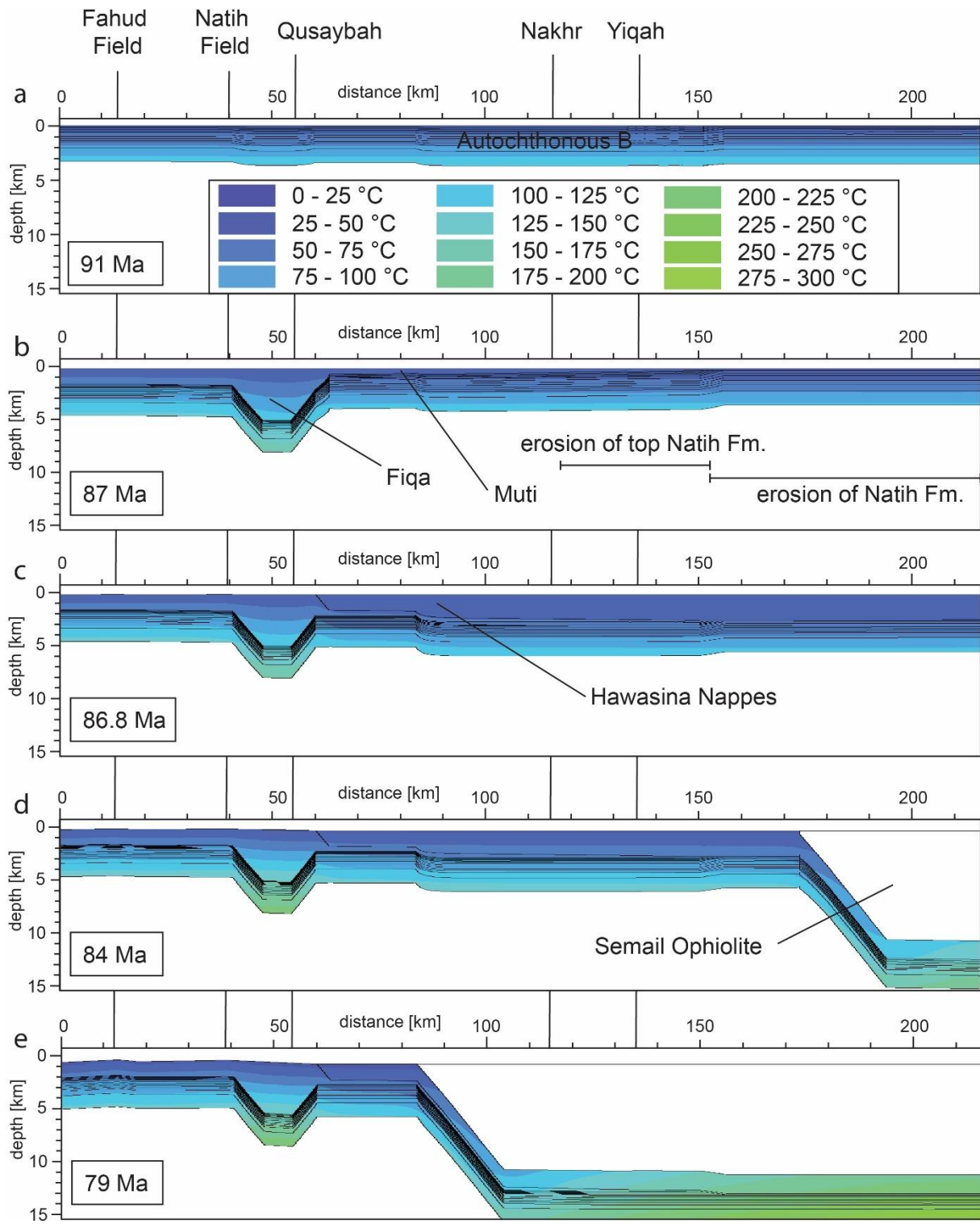
502 Numerical basin modeling integrates all data and tests the individual interpretations in the thermal and geodynamic
503 framework. Deepest burial was constrained with thermal maturity data and exhumation with thermochronological
504 data. In the following we present our best fit model, considering a mixed ophiolite lithology (Searle and Cox,
505 2002) consisting of strongly serpentinized peridotites. Then, the sensitivity of important results to changes of
506 relevant input parameters are discussed.

507 Modeled evolution of the transect over time is given in Figures 8-6 and 97, showing (a) final deposition of the
508 Autochthonous B, (b) erosion of the Natih Fm. in the North by a moving foredeep (no erosion in S, full erosion in
509 N), (c) emplacement of 1400-m of Hawasina Nappes, and d-e) ophiolite obduction reconstructed by rapid,
510 stepwise sedimentation. After maximum burial beneath the ophiolite complex at c. 80 Ma (Warren et al., 2005)
511 exhumation is assumed to start slightly prior to 55 Ma (Saddiqi et al., 2006) with a rapid phase of cooling below
512 c. 200 °C at 55 Ma leading to lower temperatures in the Jebel Akhdar region. 1D burial plots of two pseudo-wells
513 created out of point data in Wadi Nakhr and Wadi Yiqah are shown in Figure 8.



515
516

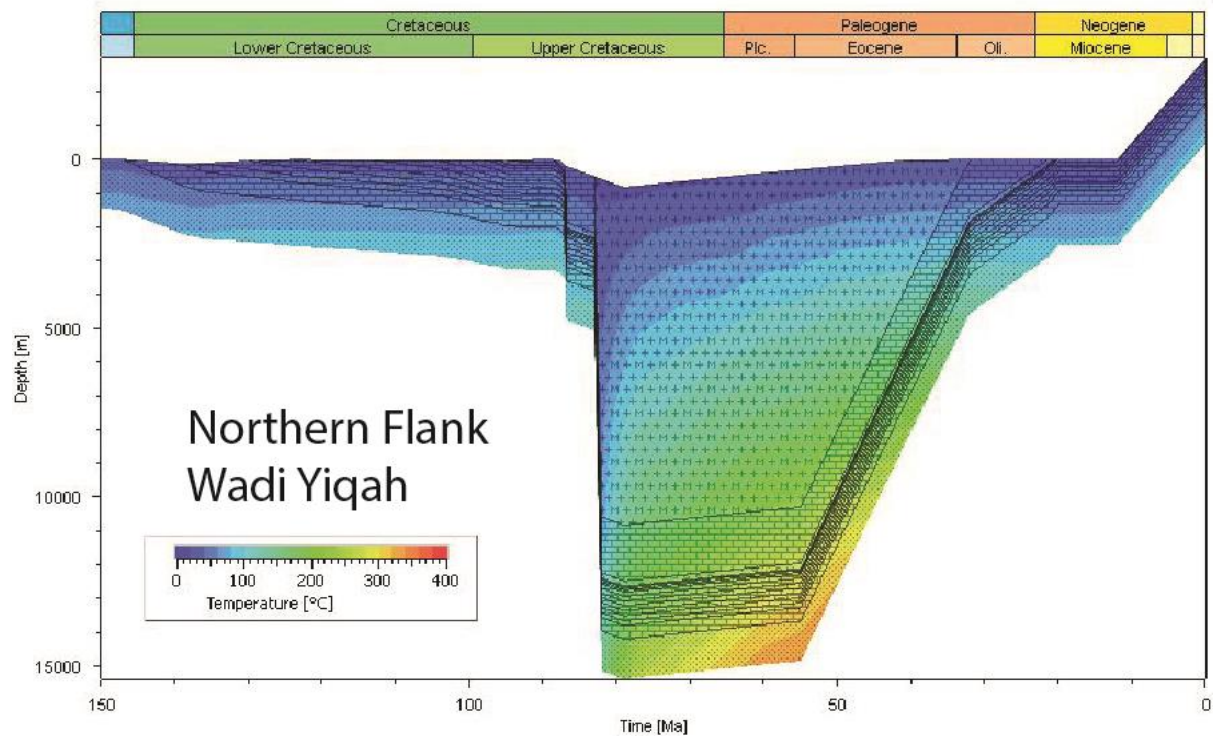
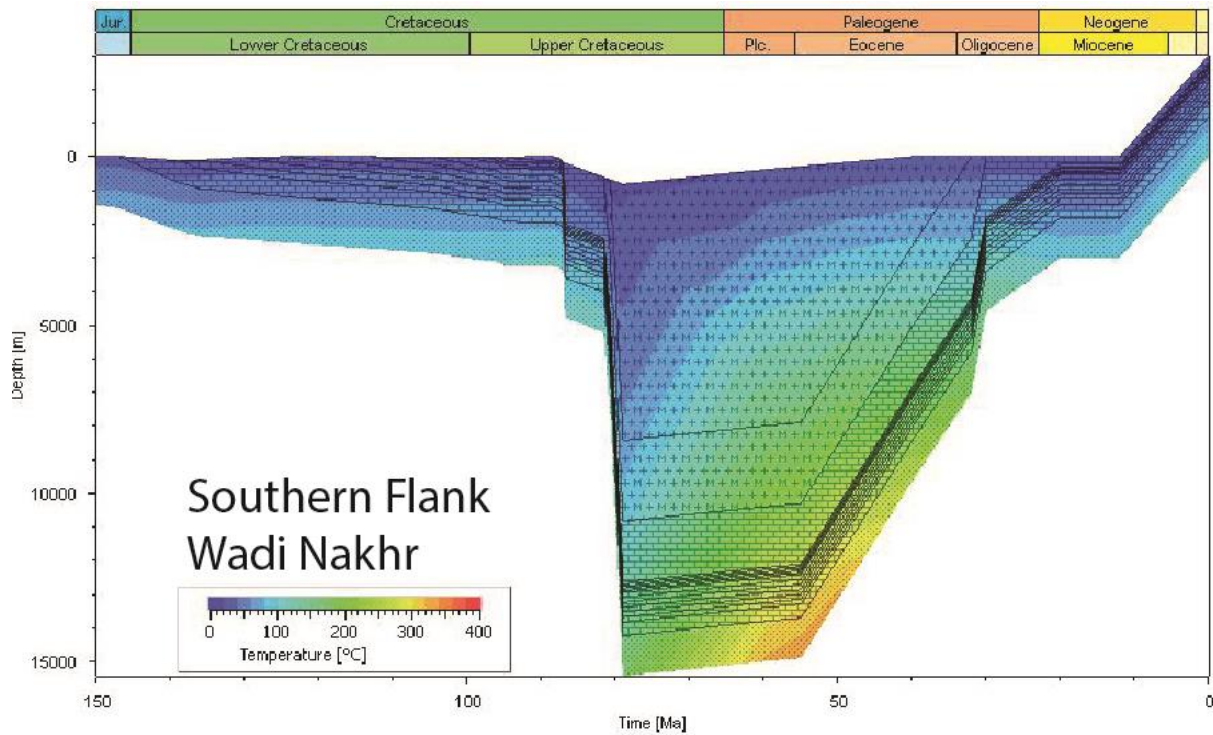
517 **Figure 6: Modeling results: Transect evolution from sedimentation of the Autochthonous B at stable passive margin**
 518 **conditions (a), to moving foredeep that finally filled with Fiqa sediments (b, peak burial as calibrated by thermal**
 519 **maturity data), Hawasina Nappe (c) and ophiolite emplacement (d) leading to deepest burial (e). Highlighted with**
 520 **vertical lines in the background are the locations of present-day oil fields and sampled valley locations.**



521

522 **Figure 7: Modeling results: Temperature distribution and temporal evolution along of the transect of Figure 6.**
 523 **Highlighted with vertical lines in the background are the locations of present-day oil fields and and sampled valley**
 524 **locations sampling sites.**

525



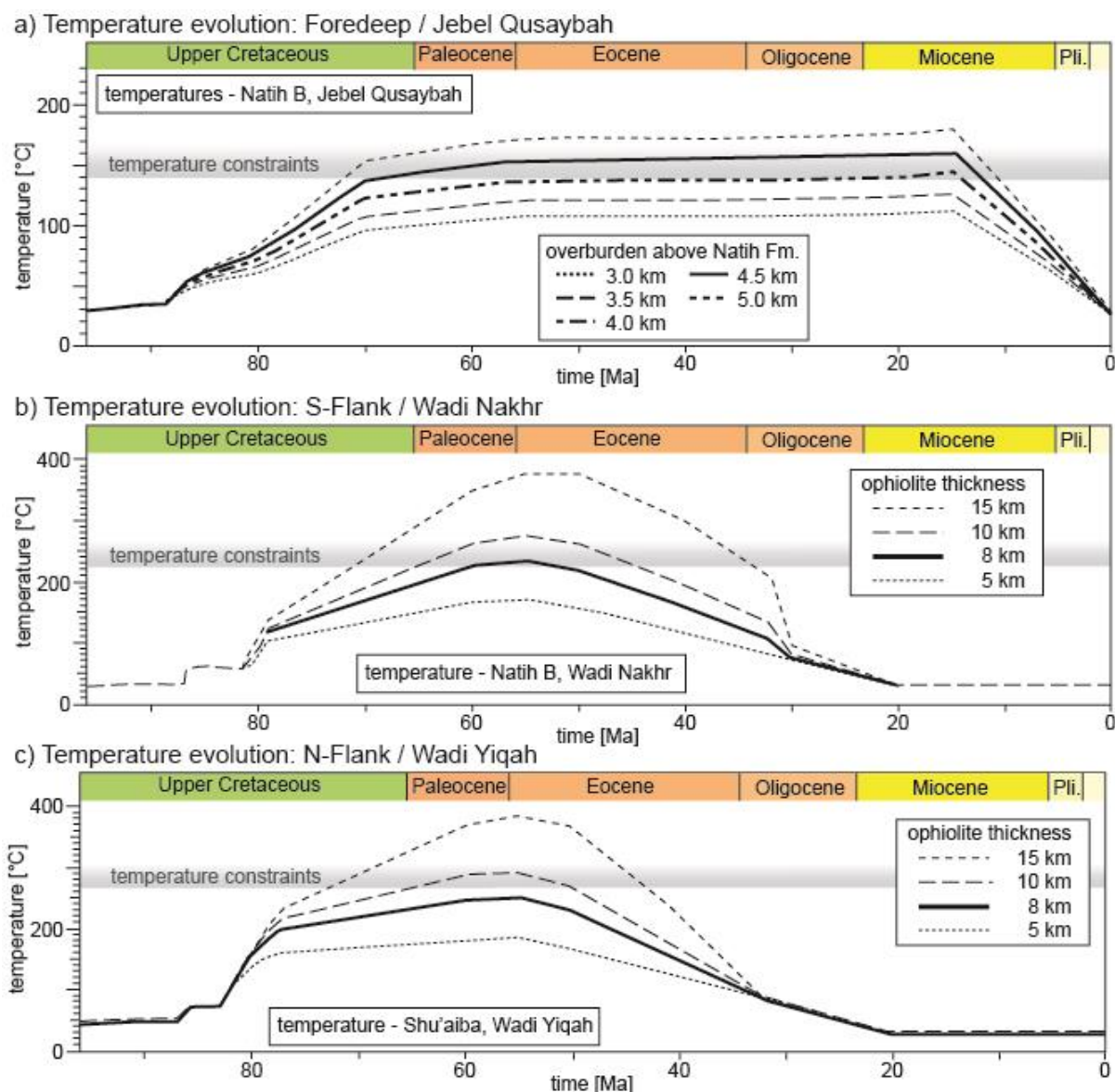
526
527
528
529
530
531

Figure 8 Modeling results: Two representative burial plots for two pseudo-wells created near the entrances of Wadi Nakhr and Yiqah (Figures 1, 6 and 7) show two phases of rapid burial related to Hawasina and Semail Nappe emplacement and c. 88 Ma and ophiolite emplacement at c. 78 Ma. Burial in the North (Wadi Yiqah) starts c. 2 Myra earlier due to ophiolite obduction taking place from N to S.

532 As a model set up only presents one possible solution out of several, sensitivity analyses with varying paleo-
 533 overburden thicknesses (Figures 9 and 10), changing degree of serpentinization of the ophiolite and varying basal
 534 heat flow during deepest burial (Figure 11) are presented and discussed below.

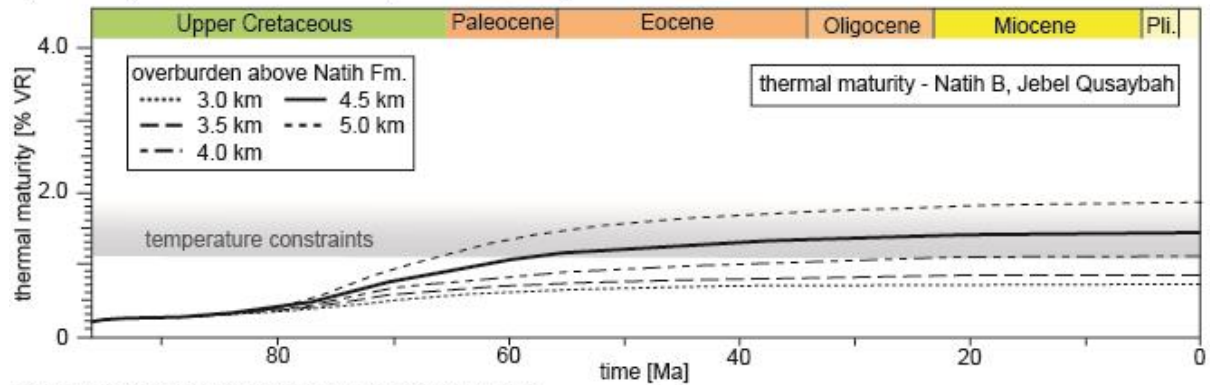
535 Thermal maturity data of the Natih B at Jebel Qusaybah (1.1 % VR_r), Adam Foothills, requires peak temperatures
 536 of c. 145–1820 °C (Table 1). Sensitivity analyses of the overburden above the Natih Fm. outlined-show that at
 537 least 4 to 4.5 km of sedimentary overburden (Figures 9a and 10a) are-is needed to match the calibration data
 538 (Figures 9a and 10a).

539

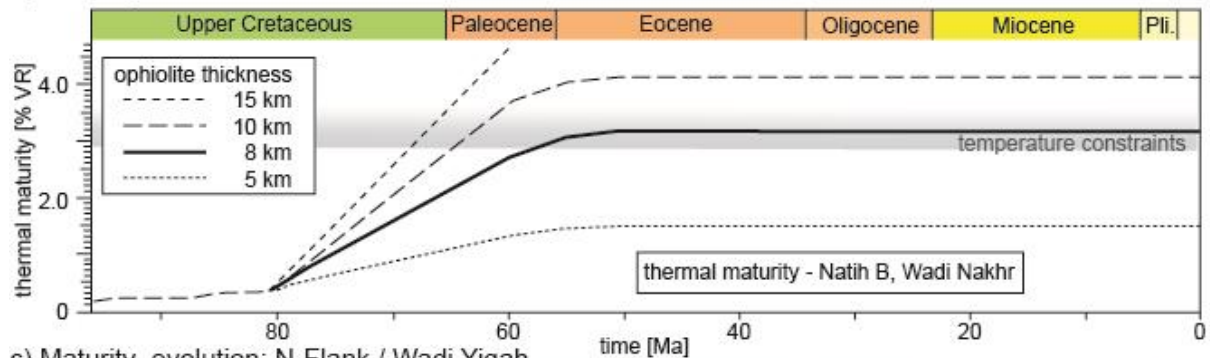


540
 541 **Figure 9: Sensitivity analysis of paleo-overburden and its influences on temperature in comparison to calculated peak**
 542 **temperatures (gray area) for pseudo-wells at Jebel Qusaybah (a), Wadi Nakhr (b) and Wadi Yiqah (c).**

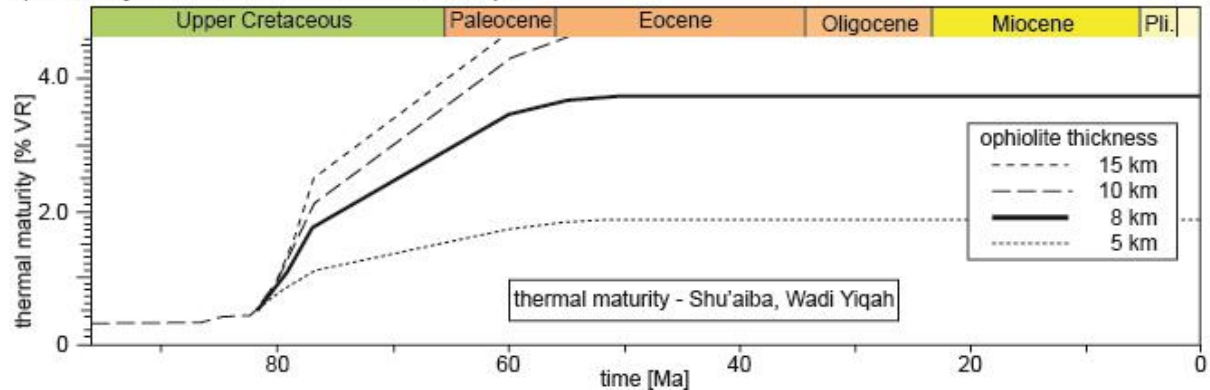
a) Maturity calibration: Foredeep / Jebel Qusaybah



b) Maturity calibration: S-Flank / Wadi Nakhr



c) Maturity evolution: N-Flank / Wadi Yiqah



543

544 Figure 10: Sensitivity analysis of paleo-overburden and its influences on thermal maturity in comparison to calibration
 545 data (gray area). Data is used to calibrate burial depth of the foredeep at the Jebel Qusaybah (a) and the paleo-ophiolite
 546 thickness at the southern flank of the Mountains at Nakhr (b), -and at its northern counterpart at Yiqah (c) is in
 547 agreement with the temperature data of Figure 9, however to mature to be reconstructed by standard maturity
 548 modelling (Sweeney and Burnham, 1990).

549

550 To restore the former minimum thickness of the Semail Ophiolite, the thickness of the Hawasina Nappes
 551 along the transect was fixed to 2 km, representing its minimum thickness as suggested by the maximum
 552 present-day thickness of the Jebel Misht exotics. To reach the required thermal conditions measured at the
 553 entrance of the Wadi Nakhr (Natih B: 2.83-3.72 % VR_r, 225-260 °C; Grobe et al., 2016), 8-10 km of original,
 554 total thickness of strongly serpentinized ophiolite sequence are needed in addition to the assumed 2 km of
 555 Hawasina Nappes (Figures 9b and 10b). These thicknesses are also sufficient to reach peak temperatures
 556 calculated for older stratigraphy at the northern flank of the Jebel Akhdar Dome (Shu'aiba Fm. at Wadi
 557 Yiqah: 270-295 °C by RSCM, Figures 9c and 10c). Modeling results show an earlier heating and onsetting
 558 longer-lasting, quicker-more rapid increase in maturity and temperature in the north. We associate this,
 559 which we interpret as associated with the 2 Mys earlier onset of obduction and, hence, a longer burial of the

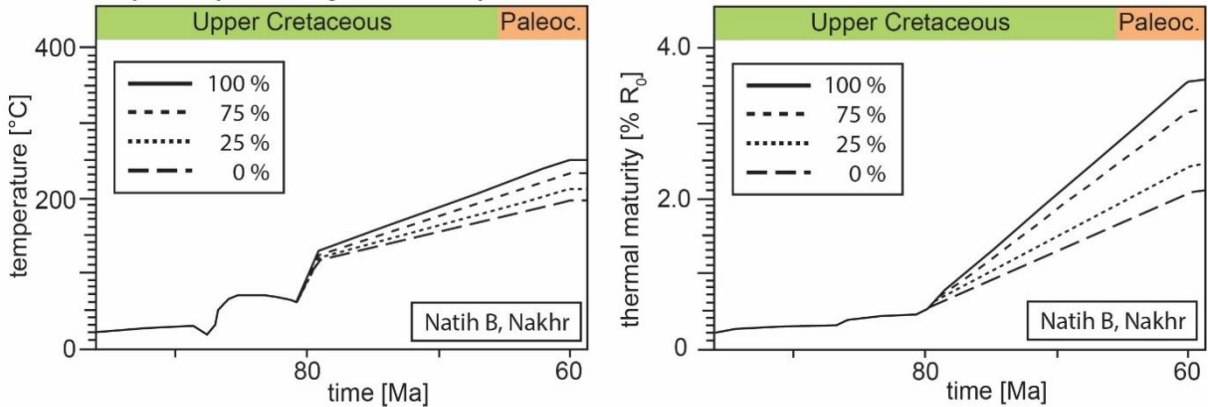
560 **northern carbonate platform (Wadi Yiqah) under the active ophiolite obduction compared to its southern**
561 **counterpart (Béchenec et al., 1990; Cowan et al., 2014).**

562 Another factor influencing the modeling results is related to the lithology of the overburden and its compaction.
563 In the special case of burial under an ophiolite, serpentinization of peridotite and its impact on ophiolite density
564 and thermal conductivity must be considered. Sensitivity analysis of ophiolite serpentinization shows the
565 temperature and thermal maturity effects on our model (Figure 11). A model-case of ophiolite without any
566 serpentinized peridotite (0 %-case, $\rho_{\text{ophio}}=3133 \text{ kg/m}^3$) would represent the largest deviation compared to our best-
567 case model assuming complete ophiolite serpentinization (100 %-case, $\rho_{\text{ophio}}=3069 \text{ kg/m}^3$). This density is based
568 on Al-Lazki et al. (2002). Even if the upper part of the ophiolite ~~is-was~~ missing in the Jebel Akhdar area (Nicolas
569 and Boudier, 2015), this and the ~~observations-field data~~ of Searle and Cox (2002) in the Saih Hatat support strong
570 serpentinization. A less serpentinized ophiolite means higher densities and related higher thermal conductivities
571 of the overburden and thus lower peak temperatures in the sediments below. In ~~a-the case of~~ no- serpentinization
572 ~~case~~, peak temperature of Natih B in the Wadi Nakhr would decrease by c. 60 °C resulting in a maximum thermal
573 maturity decrease of 1.5 % VR. The best fit model with an ophiolite thickness of 8-10 km would need additional
574 3 km of overburden at 0 % serpentinization to equally match the measured thermal maturities. Additional
575 thicknesses of 0.75 km (75 % serpentinization), 1.5 km (50 % serpentinization) and 2.25 km (25 %
576 serpentinization) apply for lower degrees of serpentinization, respectively.

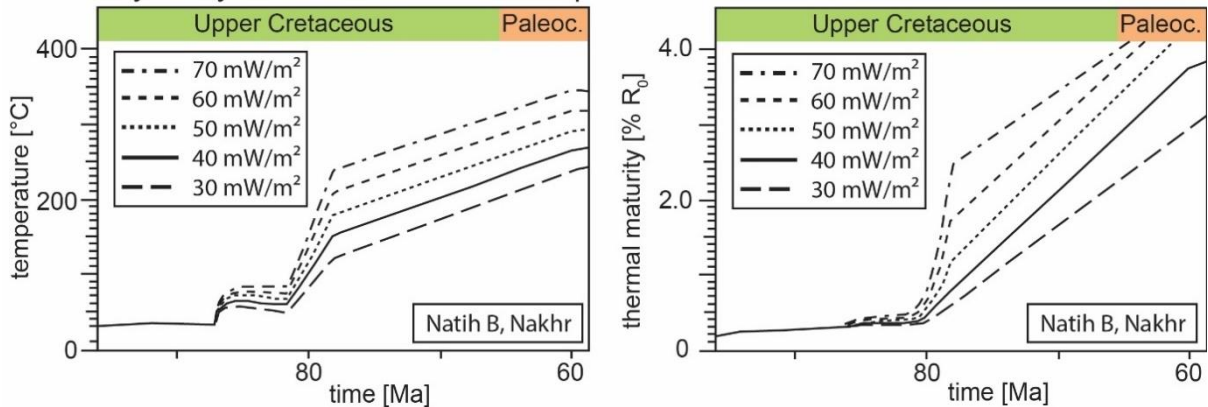
577 Results depend strongly on basal heat flow (Figure S3). The best fit model of 40 mW/m² at ~~deepest-maximum~~ burial
578 is typical for a passive continental margin setting. If this heat flow at peak burial would be lowered to 30 mW/m²
579 an additional amount of 1.2 km of ophiolitic overburden would be required to achieve a match with thermal
580 calibration data (Figure 11). Increased heat flow values to 50, 60 or 70 mW/m² would result in ~~less-lowering of~~
581 ~~of-by~~ -1.3, -2.4 and -3.5 km, respectively (Figure 11).

582

Sensitivity Analysis: Degree of Serpentinization



Sensitivity Analysis: Heatflow variation at peak burial



583

584 **Figure 11: Sensitivity analysis: Top: Different degrees of serpentinization of the peridotite within the Semail Ophiolite**
 585 **affect the temperature (left) and thermal maturity (right) evolution (modeled for Natih B Fm. at Wadi Nakhr). Pure**
 586 **peridotite (0 % serpentinization) require additional 3 km of ophiolite in addition to the 8-10 km of the best-fit model to**
 587 **equally match the calibration data. 100 % refers to complete serpentinization of the peridotite in the ophiolite. Bottom:**
 588 **The influence of variable heat flow values at peak burial on temperature (left) and thermal maturity (right).**

589 5. Discussion

590 [AnyEvaluating uncertainties in basin and petroleum system models has to deal with uncertainties, inis especially](#)
 591 [important particular](#)—for complex areas such as the Jebel Akhdar, where sedimentary rocks reached high
 592 temperatures and maturities due to deep and rapid burial. In the following, we discuss these uncertainties with
 593 respect to temperature and burial history, overpressure build-up and induced fluid flow. For all presented basin
 594 models of the study area, the following [limitations—assumptions](#) apply: (1) decompacting the present-day
 595 lithologies does not consider rock volume lost by pressure solution. This is probably of minor importance in our
 596 study area as host-rock buffered isotope ratios of the veins were interpreted as local sinks for nearby dissolved
 597 calcite (Arndt et al., 2014; Hilgers et al., 2006), so that the overall rock volume remains approximately constant,
 598 (2) decompaction only accounts for burial, whereas a possible tectonic compaction is neglected (Neumaier, 2015)
 599 and (3) calculated overpressure does not include a rock volume decrease due to pressure solution.

600 5.1. Burial history

601 Little is known about the very early phase of burial, before 91 Ma (Figures 6 and 7, Grobe et al., 2018). The
 602 assumptions for this period are based on hypotheses on the tectonic evolution of the passive continental margin as
 603 well as data on thickness of sedimentary units but are not strongly constrained by petrographic data.

604 In Turonian times (Robertson, 1987) a southwest-ward-moving forebulge, related to plate convergence, affected
605 northern Oman. It eroded the northeastern platform edge and migrated southwest-ward to the present-day position
606 of the Adam Foothills (Robertson, 1987). Measured thermal maturities of 1.1–1.8 % VR_r were used to reconstruct
607 peak temperatures during burial in Jebel Qusaybah, Adam Foothills ~~to c. , which range between 145 and~~
608 ~~182~~140 °C. Numerical basin modeling results reveal that additional paleo-overburden of at least 4 to 4.5 km (Natih
609 B, Qusaybah, Figure 10) is required to reach these temperatures. The exhumation history of the Adam Foothills is
610 not well known; our model is based on an interpreted late exhumation during the Miocene (Claringbould et al.,
611 2013). Earlier exhumation would shorten the time span of the rock at higher temperatures (Figure 7), lead to
612 decreased thermal maturity and, hence, would require additional overburden to match the measured thermal
613 maturity data. Therefore, the resulting burial of 4 to 4.5 km has to be regarded as minimum value, ~~which would~~
614 ~~increase by pre-Miocene exhumation of the Jebel Qusaybah.~~ South of the Adam Foothills basin geometries ~~do not~~
615 ~~show tilting and~~ are ~~interpreted as~~ not affected by the moving foredeep. Here peak burial was reached under c. 3 km
616 of Fiqa, Hadhramaut and Fars formations. This is based on the assumption that present-day burial equals deepest
617 burial as no thermal calibration data of the area south of Jebel Qusaybah was achieved, which is in agreement with
618 interpretations of Terken (1999) and Warburton et al. (1990).

619 In case of the Jebel Akhdar, peak temperatures were reached as a consequence of burial below the ophiolite
620 (Loosveld et al., 1996; Searle et al., 2003; Searle, 2007; Warren et al., 2005). Here the sedimentary rocks reached
621 high temperatures and maturities as shown by solid bitumen reflectance, RSCM, FT-IR and Rock-Eval pyrolysis
622 data (Fink et al., 2015; Grobe et al., 2016). Pre-obduction burial by sedimentation is not sufficient for such high
623 thermal maturities, and it likewise cannot be explained by increased basal heat flow before 91 Ma or after 55 Ma.
624 Influence of local hydrothermal effects cannot be excluded, but because the entire Jebel Akhdar reached high
625 temperatures, short-term, local events are unlikely to have been dominant. A regional thermal overprint on the
626 passive margin sediments by warm ophiolite obduction can be excluded ~~as the peak temperatures in the Jebel~~
627 ~~Akhdar Dome are increasing with stratigraphic age. Due to the at least 2 km thick imbricated Hawasina Nappes~~
628 ~~between the ophiolite and the passive margin sequence, the thermal overprint did not affect the top of the carbonate~~
629 ~~platform. Limited thermal overprinting of the units underlying the ophiolite is supported by the fact that the~~
630 ~~sediments of the nappes directly below the ophiolite do not show signs of regional metamorphism in the Jebel~~
631 ~~Akhdar region (Searle, 1985).~~ This is in agreement with models of Lutz et al. (Lutz et al., 2004) ~~outlining that~~
632 ~~show that even in subduction zones the isotherms of the thermal evolution of rapidly buried sediments are not~~
633 ~~adjusting to the surrounding temperatures instantaneously.~~ Moreover, the thermal imprint as observed by the
634 metamorphic sole in northern Oman ~~is only affecting~~ 10's of meters in the sub-thrust Hawasina Nappes (Searle
635 and Cox, 2002) and not the carbonate platform sediments below. This ~~only minor sub-thrust thermal/frictional~~
636 ~~thermal~~ overprint ~~is~~ also observed in other ~~thrust zones/areas~~ (e.g. Wygrala, 1989).

637 To reach ~~the~~ measured maturity ~~data values~~ in the ~~Jebel Akhdar mountain_ area of the transect~~ a paleo-thickness
638 of the ophiolite in the order of 8-10 km on top of 2 km of Hawasina Nappes is required (Figure 10); this ~~would~~
639 ~~account for~~ ~~corresponds to~~ 280 to 320 MPa of lithostatic pressure ~~and is,~~ in rough agreement with the pressure
640 reconstructed by combining fluid inclusion data and independently determined thermal rock maturity temperatures
641 (cf. FI results: 254 ± 30 MPa). ~~Depending on lithological effects, such as a less pronounced serpentinization of the~~
642 ~~ophiolite, this value might increase by up to 3 km (Figure 10). Basal heat flow values at deepest burial are estimated~~
643 ~~to c. 40 mW/m². This seems realistic as passive margin conditions prevail, and no magmatism or rifting is reported~~
644 ~~in the area.~~

645 Basin modeling indicates that highest temperatures were reached much later than deepest burial under the ophiolite
646 (Figure 7), directly prior to uplift. This difference is interpreted as the time the rock needed for thermal
647 equilibration after rapid burial. Deep burial under the ophiolite represents the only time ~~in~~in the basin's evolution
648 when ductile limestone deformation was possible (Grobe et al., 2018). However, there is uncertainty concerning
649 the exact timing of deepest burial in the Jebel Akhdar (we used 79 Ma according to U-Pb dating of eclogites in the
650 Saih Hatat window; Warren et al., 2005), the related basal heat flow (discussion, Fig. S2) and the beginning of
651 early uplift (we used 55 Ma, as discussed below).

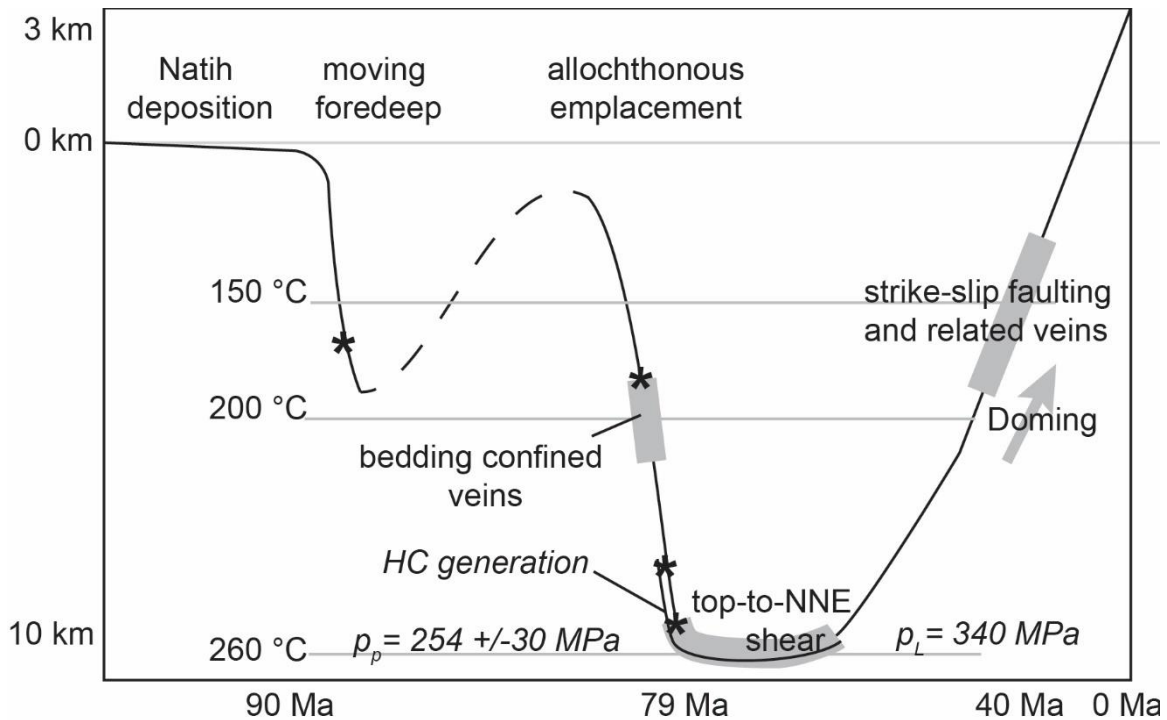
652 Our peak temperatures are in ~~principal~~-agreement with temperatures of c. 200 °C suggested for the top of the
653 carbonate platform by Breton et al. (2004), and non-reset zircon fission tracks in the pre-Permian basement
654 indicating peak temperatures up to 280 °C (Saddiqi et al., 2006). Moreover, thermal maturities of the same
655 stratigraphic units show similar values along the transect and around the dome (Grobe et al., 2016). Hence, we
656 assume a similar burial history for the entire Jebel Akhdar. The temperatures used in our models are in contrast
657 with recent results on mixed illite-smectite layers and clay mineral assemblages from the Jebel Akhdar by Aldega
658 et al. (2017) who argue for peak temperatures of 150-200 °C on the northern flank of the Jebel Akhdar and 120-
659 150 °C on the southern flank. These values are incompatible with our solid bitumen and Raman spectroscopy data,
660 as well as with the overmature Natih B source rock on the southern flank (data presented here and in Grobe et al.,
661 2016). Independent data on temperatures from fluid inclusions confirm the higher temperature range. At present,
662 there is no clear explanation for this discrepancy. However, it has been shown that the vitrinite reflectance system
663 is more sensitive to rapid temperature changes than clay mineralogy (e.g. Hillier et al., 1995; Velde and Lanson,
664 1993). If burial was short enough, the clay minerals may not have time to recrystallize, possibly due to a lack of
665 potassium, whereas vitrinite reflectance increases. Alternatively, we speculate~~Another possible explanation may~~
666 ~~be~~ that the ~~dated~~ clay minerals were transformed during top-to-NNE shearing, thus their state do not show peak
667 burial. Indeed it has been shown that deformation associated with this early extension reaches deeply into the
668 passive margin sequence, and includes the Rayda and Shuaiba Formations (Grobe et al., 2018; Mattern and Scharf,
669 2018). Furthermore, Aldega et al. (2017) ~~suggest~~argue that the ~~thermal evolution during uplift of~~cooling history
670 proposed by Grobe et al. (2016) indicates temperature in the basement < 70°C during the Eocene-Oligocene, thus
671 not does not accounting for thermochronological data in pre-Permian basement rocks, ~~(Poupeau et al., 1998;~~
672 ~~Saddiqi et al., 2006), arguing the 1D thermal models indicate temperature in the basement had to be lower than~~
673 ~~70°C during the Eocene-Oligocene.~~ In fact, the ~~raw used~~calibration data we used ~~from~~off for the basement indicate
674 rapid cooling at 55 ± 5 Ma (Poupeau et al., 1998; Saddiqi et al., 2006), in agreement with models of Grobe et al.
675 (2016) and the exhumation presented in this work.

676 This exhumation might be a result~~Temperatures~~ of the ductile top-to-NNE shearing event (64 ± 4 Ma, Hansman
677 et al., 2018). Its onset, ~~markings~~ the time of deepest burial and related peak temperatures measured in bedding
678 parallel veins, ~~were reconstructed to~~estimated at 186-221 °C by Holland et al. (2009) assuming an ophiolitic
679 overburden of 5 km (Sahtan Fm., Wadi Nakhr). If we adjust this pressure correction for higher values of 280 to
680 340 MPa accounting for the here elaborated 8 to 10 km of ophiolite and 2 km of sedimentary nappes, trapping
681 temperatures would increase to c. 296-364 °C (Table 3), which are in the order of the maximum burial temperatures
682 as deduced from organic matter maturity.

683 Figure 12 presents a summary burial ~~plot~~graph indicating temperature and age constraints. Highlighted in gray is
684 additional information gained by fluid inclusion thermometry. These data indicate paleo-fluid temperatures in the
685 range of 225 ± 4 (280 MPa) to 266 ± 5 °C (340 MPa) during burial under the ophiolite (bedding-confined veins),

686 c. 296-364 °C at peak burial (top-to-NNE sheared veins) and 213 ± 3 °C during exhumation with a later phase of
 687 primary inclusion outlining 184 ± 3 to 189 ± 7 °C (both strike-slip related veins). Temperature decrease within the
 688 latter formed parts of the strike-slip veins might relate to a change of fluid source or to exhumation during vein
 689 formation. In combination with our thermochronology data the second possibility appears more likely and would
 690 imply strike-slip faults developed after c. 55 Ma.

691



692

693 **Figure 12: Summary burial sketch for the top of the carbonate platform (Natih Fm.).** Shown temperatures are based
 694 on RSCM and FI thermometry, pressure data calculated out of FI measurements and independently determined
 695 temperature data. The uplift-exhumation history is restored by ZHe ages. (* indicate times of overpressure formation,
 696 gray areas depict vein formation)

697 5.2. Exhumation history

698 Our new thermochronology data from the central part of the Jebel Akhdar Dome suggests cooling below the reset
 699 temperature of the ZHe thermochronometer (c. 130-170 °C) between 48.7 ± 1.8 and 39.8 ± 3.0 Ma (Table 2, Figure
 700 4). The small variation in cooling ages for the different stratigraphic levels indicates rapid passage of the entire
 701 rock suite through the ZHe partial retention zone, and consequently rapid exhumation of the Jebel Akhdar Dome.
 702 This Eocene cooling is in agreement with ZHe ages of pre-Permian strata of Hansman et al. (2017) ranging between
 703 62 ± 3 and 39 ± 2 Ma. Apatite fission track (AFT) ages measured in the basement of the Jebel Akhdar range
 704 between 55 ± 5 Ma and 48 ± 7 Ma (4 samples, Poupeau et al., 1998) and 51 ± 8 Ma to 32 ± 4 Ma (Hansman et al.,
 705 2017). The temperature of resetting the AFT system (i.e. the depth of the base of the partial annealing zone) may
 706 vary depending on annealing kinetics. For different apatite crystals this temperature ranges between 100 and 120
 707 °C (Carlson et al., 1999; Fitzgerald et al., 2006). Hence, these AFT ages reproduce within error with our ZHe
 708 results, despite the fact that both systems are sensitive to different temperature intervals (100-120 °C and 130-
 709 170 °C, respectively This supports the interpretation of rapid exhumation of the Jebel Akhdar at c. 55 Ma. Zircon
 710 fission track ages witness cooling of the Jebel Akhdar below c. 260 °C between 96 and 70 Ma (Saddiqi et al.,
 711 2006). This implies slow cooling thereafter (c. 100° between 70 and 55 Ma) until rapid exhumation at c. 55 Ma. ->
 712 This supports the interpretation of rapid exhumation of the Jebel Akhdar. In combination with zircon fission track

713 ~~ages of Saddiqi et al. (2006), indicating the rocks cooled below c. 260 °C between 70 and 96 Ma, modeled cooling~~
714 ~~paths indicate rapid exhumation initiated at c. 55 Ma.~~ Earlier exhumation would not result in required thermal
715 maturities as exposure of the rock to highest temperatures would be too short for thermal equilibration. A reheating
716 event in the late Miocene is not required to explain the data.

717
718 Our ZHe data from the Muti Formation and the Hawasina Nappes show a spread in ages, ~~between 173 and ranging~~
719 ~~from 43 to 173~~ Ma, i.e. partly much older than the ages observed in the stratigraphically lower units in the center
720 of the dome.

721 ~~A spread in (U-Th)/He-ages is often observed, and has been attributed to radiation damage density, uneven~~
722 ~~distribution of mother isotopes in the dated crystal, broken grains, grain chemistry, among other causes (e.g.~~
723 ~~Flowers et al., 2009; Guenther et al., 2013). Several studies show that samples from sedimentary rocks are~~
724 ~~particularly prone to spread in ages (e.g. von Hagke et al., 2012; Ketcham et al., 2018; Levina et al., 2014). This~~
725 ~~is because transported grains are subject to abrasion, which influences age correction for grain geometry and may~~
726 ~~obscure presence of inclusions within the crystal. Additionally, dated grains can originate from different sources,~~
727 ~~and thus have a different chemical composition and a different pre-depositional ~~time~~ temperature history. This~~
728 ~~may result in different ~~resetting~~ temperatures, and consequently different grains (or grain age populations)~~
729 ~~represent different thermochronometers.~~

730
731 ~~It is difficult to prove the existence of such multiple thermochronometers, as independent parameters indicative~~
732 ~~for different kinetics have not yet been established. Indeed, statistical analysis of different grain age populations~~
733 ~~requires dating of multiple grains (e.g. to be 95 % certain that a population representing 5 % of the grains is not~~
734 ~~missed 117 single grain ages need to be dated, Vermeesch (2004)). In any case, reproducing ages determined in~~
735 ~~different samples indicates the data is geologically meaningful, i.e. the observed spread is the result of partial~~
736 ~~resetting and/or different kinetics and not the result of factors independent of the time-temperature history, such~~
737 ~~as undetected inclusions or external helium implantation. We thus interpret the system as ~~This indicates the system~~~~
738 ~~has been only partially reset, implying these units were not heated above the reset temperature (approximately~~
739 ~~130-170 °C) after deposition. This interpretation is corroborated by ~~Units exposed in the Hawasina Window~~~~
740 ~~(Figure 1) also show unreset ZHe ages in the Hawasina Window (Figure 1f, Csontos, pers. comm.).~~ The top of the
741 Natih Formation has seen temperatures above 220 °C. We suggest ~~that~~ this apparent contradiction may be
742 explained by juxtaposition of the colder Muti and Hawasina units against the top of the carbonate platform during
743 extensional top-to-NNE shearing. This implies that at least 50 °C of cooling are associated with post obduction
744 extension, i.e. before doming. A two-stage exhumation history of the Jebel Akhdar Dome has also been inferred
745 from structural data (Grobe et al., 2018; Mattern and Scharf, 2018) and the stratigraphic record (Fournier et al.,
746 2006; Mann et al., 1990). ~~Top-to-NNE shearing is associated with tectonic thinning of the ophiolite (Grobe et al.,~~
747 ~~2018). This tectonic denudation will also result in cooling, and may explain why so little ophiolite is found in the~~
748 ~~post-obduction sediments. Additionally, ophiolitic material may have been lost to the ~~Persian Gulf of Oman.~~~~

749 750 **5.3. Pressure evolution ~~and fluid migration~~**

751 Evolution of pore pressures was modelled (Figures S7 and S8) assuming a ~~perfect~~ seal on top of the Natih Fm.
752 ($k_{\text{Muti}}=10^{-23}$ m²). Porosity was lost during Muti deposition in the moving forebulge (top seal) and related burial, the

753 emplacement of the Hawasina Nappes and the ophiolite, which induced compaction and a remaining very low
754 porosity of c. 1 %. Hydrostatic pressure increased with burial under the moving forebulge at 88 Ma to 40 MPa,
755 after Muti deposition to 60 MPa and after ophiolite emplacement to 120 MPa. Calculated pore pressure ~~exceeded~~
756 rise above hydrostatic pressure in response to Hawasina Nappe and ophiolite emplacement.
757 Formation of tensile fractures, as inferred from bedding confined, Mode-I veins in the Natih Fm. (Arndt et al.,
758 2014; Grobe et al., 2018; Holland et al., 2009; Virgo, 2015), require internal fluid pressures (P_f) exceeding the sum
759 of the stress acting normal on the fracture surface (σ_3) and the tensile stress of the rock (T): $P_f > \sigma_3 + T$, and
760 a differential stress ($\sigma_1 - \sigma_3$) below 4T (Secor, 1965). Host-rock buffered vein isotope compositions indicate that
761 the veins were formed by local fluids (Arndt et al., 2014) and, hence, require local overpressure cells.
762 Sensitivity analyses of reduced permeabilities of Muti, Natih and Nahr Umr formations show that overpressure
763 generation, necessary for rock fracturing, requires a very good top seal and also a reduced horizontal permeability
764 of the Natih Fm. of 10^{-23} m² (Figure S7 and S8). A top seal on its own is not sufficient for overpressures initiating
765 rock failure. This case results in pore pressures up to 300 MPa within the top Natih and localized overpressures of
766 195 MPa in front of the obducting ophiolite.
767 All results indicate that without low horizontal permeabilities of the Natih Fm. $\leq 10^{-23}$ m² overpressure cells
768 required for vein formation cannot be generated. The reduced permeabilities in the Natih Fm. are necessary to
769 prevent an early, tectonically-driven horizontal pressure release.

770 **5.4. Fluid migration**

771 Numerical basin modeling shows that rapid burial of sedimentary rocks below the ophiolite (88-80 Ma) caused
772 under-compaction, i.e. a porosity too high with respect to burial depth, and consequent pore pressure increase.
773 Two example model results of fluid migration in front of the obducting ophiolite are shown in the electronic
774 supplement Figure S9. If low permeabilities are assigned to the non-source-rock members of the Natih Fm.,
775 migration will mainly take place within the source rocks and at layer interfaces within the Natih Fm. If the complete
776 Natih Fm. has low permeabilities, fluids will leave the source rock vertically first, before lateral migration localizes
777 along layer boundaries. The pressure gradient between overpressures below the allochthonous nappes and the less
778 deeply buried southern foreland initiates tectonically-driven fluid migration in front of the obducting nappes, an
779 idea that was first introduced by Oliver (1986). Solid bitumen accumulations in black stained calcite veins are in
780 agreement with this interpretation (Fink et al., 2015).
781 Dome formation of the Jebel Akhdar anticline around 55 Ma initiated layer tilting and consequent southward
782 migration of the generated hydrocarbons as observed by secondary low reflective solid bitumen generations in
783 Natih veins and host rocks at the southern flank of the Oman Mountains (Fink et al., 2015; Grobe et al., 2016).

784 **6. Conclusions**

785 This study provides insights into the temperature evolution during obduction, prior to subsequent orogenesis.
786 Arabia's passive continental margin was buried to at least 4 km at times of foredeep migration and afterwards
787 under 8-10 km of Semail Ophiolite and 2 km of sedimentary Hawasina Nappes. Burial under the ophiolite resulted
788 in peak temperatures of up to 300 °C (Shu'aiba Fm.) with sub-lithostatic pore pressures. Ophiolite obduction and
789 overpressure cells expelled fluids towards the foreland, through matrix and fracture porosity.
790 ZHe data show cooling associated with forebulge migration, as well as with exhumation of the Jebel Akhdar Dome.

791 Exhumation of the Jebel Akhdar Dome took place in two stages. A first stage is associated with top-to-NNE
792 shearing, which is responsible for at least 50 °C of cooling, as witnessed by juxtaposition of units including
793 partially reset ZHe ages against units that experienced more than 220 °C. ZHe data show the second exhumation
794 phase, associated with doming of the Jebel Akhdar occurred between 49 and 39 Ma.

795 **Author contribution**

796 JLU, RL and AG ~~conceived of~~[initiated and planned](#) the study. AG planned and carried out fieldwork as well as
797 thermal maturity measurements (VR, solid bitumen reflectance, Raman spectroscopy), structural interpretations
798 and basin modelling. [AG, CvH, JU, ID](#) and FW carried out fieldwork and structural interpretations. FW and ID
799 conducted the thermochronological measurements with help of CvH. PM and AG performed fluid inclusion
800 thermometry.

801 AG and CvH prepared the manuscript with contributions from all co-authors.

802 **Acknowledgements**

803 We acknowledge the highly-appreciated help of Donka Macherey (sample preparation, RWTH Aachen), the team
804 of the KU Leuven (fluid inclusion measurements) and Keno Lünsdorf (Raman spectroscopy, Georg-August-
805 University, Göttingen). Sample crushing was realized by the team of SELFRAG, Switzerland. Wiekert Visser and
806 Victoria Sachse are thanked for fruitful discussions; Gösta Hoffmann and Wilfried Bauer [of GUTech are](#) thanked
807 for helping with field logistics. We are grateful for comments of Edwin Gnos, Andreas Scharf, Bruce Levell, Wolf-
808 Christian Dullo and Mark Handy on earlier versions of this manuscript.

809 **References**

- 810 Agard, P., Omrani, J., Jolivet, L. and Mouthereau, F.: Convergence history across Zagros (Iran): constraints from
811 collisional and earlier deformation, *Int. J. Earth Sci.*, 94(3), 401–419, doi:10.1007/s00531-005-0481-4, 2005.
- 812 Al-Lazki, A. I., Seber, D., Sandvol, E. and Barazangi, M.: A crustal transect across the Oman Mountains on the
813 eastern margin of Arabia, *GeoArabia*, 7(1), 47–78, 2002.
- 814 Al-Wardi, M. and Butler, R. W. H.: Constrictional extensional tectonics in the northern Oman mountains, its role
815 in culmination development and the exhumation of the subducted Arabian continental margin, *Geol. Soc. London,*
816 *Spec. Publ.*, 272(1), 187–202, doi:10.1144/GSL.SP.2007.272.01.11, 2007.
- 817 Aldega, L., Carminati, E., Scharf, A., Mattern, F. and Al-Wardi, M.: Estimating original thickness and extent of
818 the Semail Ophiolite in the eastern Oman Mountains by paleothermal indicators, *Mar. Pet. Geol.*, 84, 18–33,
819 doi:10.1016/j.marpetgeo.2017.03.024, 2017.
- 820 Aldega, L., Bigi, S., Carminati, E., Trippetta, F., Corrado, S. and Kavoosi, M. A.: The Zagros fold-and-thrust belt
821 in the Fars province (Iran): II. Thermal evolution, *Mar. Pet. Geol.*, 93, 376–390,
822 doi:10.1016/J.MARPETGEO.2018.03.022, 2018.
- 823 Aoya, M., Kouketsu, Y., Endo, S., Shimizu, H., Mizukami, T., Nakamura, D. and Wallis, S.: Extending the
824 applicability of the Raman carbonaceous-material geothermometer using data from contact metamorphic rocks, *J.*
825 *Metamorph. Geol.*, 28(9), 895–914, doi:10.1111/j.1525-1314.2010.00896.x, 2010.
- 826 Arndt, M., Virgo, S., Cox, S. F. and Urai, J. L.: Changes in fluid pathways in a calcite vein mesh (Natih Fm, Oman

827 Mountains): insights from stable isotopes, *Geofluids*, 14(4), 391–418, doi:10.1111/gfl.12083, 2014.

828 Barker, C. E. E. and Pawlewicz, M. J. J.: Calculation of vitrinite reflectance from thermal histories and peak
829 temperatures, in *Vitrinite Reflectance as a Maturity Parameter*, vol. 570, edited by P. Mukhopadhyay and W. Dow,
830 pp. 216–229, American Chemical Society., 1994.

831 Béchenec, F., Metour, J. L. E., Rabu, D., Villey, M. and Beurrier, M.: The Hawasina Basin: A fragment of a
832 starved passive continental margin, thrust over the Arabian Platform during obduction of the Sumail Nappe,
833 *Tectonophysics*, 151(1–4), 323–343, doi:10.1016/0040-1951(88)90251-X, 1988.

834 Béchenec, F., Le Metour, J., Rabu, D., Bourdillon-de-Grissac, C., de Wever, P., Beurrier, M. and Villey, M.: The
835 Hawasina Nappes: stratigraphy, palaeogeography and structural evolution of a fragment of the south-Tethyan
836 passive continental margin, *Geol. Soc. London, Spec. Publ.*, 49(1), 213–223,
837 doi:10.1144/GSL.SP.1992.049.01.14, 1990.

838 Bernoulli, D., Weissert, H. and Blome, C. D.: Evolution of the Triassic Hawasina Basin, Central Oman Mountains,
839 *Geol. Soc. London, Spec. Publ.*, 49(1), 189–202, doi:10.1144/GSL.SP.1992.049.01.12, 1990.

840 Beurrier, M., Bechenec, F., Rabu, D. and Hutin, G.: Geological Map of Rustaq - explanatory notes, Sultanat
841 Oman, *Minist. Pet. Miner.*, 1986.

842 Beyssac, O., Goffé, B., Chopin, C. and Rouzaud, J. N.: Raman spectra of carbonaceous material in metasediments:
843 A new geothermometer, *J. Metamorph. Geol.*, 20, 859–871, doi:10.1046/j.1525-1314.2002.00408.x, 2002.

844 Bodnar, R. J.: Revised equation and table for determining the freezing point depression of H₂O-NaCl solutions,
845 *Geochimica Cosmochim. Acta*, 57, 683–684, 1993.

846 Breton, J. P., Béchenec, F., Le Métour, J., Moen-Maurel, L. and Razin, P.: Eoalpine (Cretaceous) evolution of
847 the Oman Tethyan continental margin: Insights from a structural field study in Jabal Akhdar (Oman Mountains),
848 *GeoArabia*, 9(2), 41–58, 2004.

849 Brown, P. E.: FLINCOR; a microcomputer program for the reduction and investigation of fluid-inclusion data,
850 *Am. Mineral.*, 74, 1390–1393, 1989.

851 Van Buchem, F. S. P., Razin, P., Homewood, P. W., Philip, J. M., Eberli, G. P., Platel, J. P., Roger, J., Eschard,
852 R., Desaubliaux, G. M. J., Boisseau, T., Leduc, J. P., Labourdette, R. and Cantaloube, S.: High resolution sequence
853 stratigraphy of the Natih Formation (Cenomanian/Turonian) in northern Oman: distribution of source rocks and
854 reservoir facies, *GeoArabia*, 1(1), 65–91, 1996.

855 Van Buchem, F. S. P., Razin, P., Homewood, P. W., Oterdoom, W. H. and Philip, J.: Stratigraphic organization of
856 carbonate ramps and organic- rich intrashelf basins: Natih Formation (middle Cretaceous) of northern Oman, *Am.*
857 *Assoc. Pet. Geol. Bull.*, 86(1), 21–53, doi:10.1306/61EEDA30-173E-11D7-8645000102C1865D, 2002.

858 Carlson, W. D., Donelick, R. A. and Ketcham, R. A.: Variability of apatite fission-track annealing kinetics: I.
859 Experimental results, *Am. Mineral.*, 84(9), 1213–1223, doi:10.2138/am-1999-0901, 1999.

860 Claringbould, J. S., Hyden, B. B., Sarg, J. F. and Trudgill, B. D.: Structural evolution of a salt-cored, domed,
861 reactivated fault complex, Jebel Madar, Oman, *J. Struct. Geol.*, 51, 118–131, doi:10.1016/j.jsg.2013.03.001, 2013.

862 Coleman, R. G.: Tectonic Setting for Ophiolite Obduction in Oman, *J. Geophys. Res.*, 86(B4), 2497–2508, 1981.

863 Cooper, D. J. W., Ali, M. Y. and Searle, M. P.: Structure of the northern Oman Mountains from the Semail
864 Ophiolite to the Foreland Basin, *Geol. Soc. London, Spec. Publ.*, 392, 129–153, 2014.

865 Cowan, R. J., Searle, M. P. and Waters, D. J.: Structure of the metamorphic sole to the Oman Ophiolite, Sumeini
866 Window and Wadi Tayyin: implications for ophiolite obduction processes, *Geol. Soc. London, Spec. Publ.*, 392(1),
867 155–175, doi:10.1144/SP392.8, 2014.

868 Deville, E. and Sassi, W.: Contrasting thermal evolution of thrust systems: An analytical and modeling approach
869 in the front of the western Alps, *Am. Assoc. Pet. Geol. Bull.*, 90(6), 887–907, doi:10.1306/01090605046, 2006.

870 Duretz, T., Agard, P., Yamato, P., Ducassou, C. C. C., Burov, E. B. and Gerya, T. V.: Thermo-mechanical
871 modeling of the obduction process based on the Oman Ophiolite case, *Gondwana Res.*,
872 doi:10.1016/j.gr.2015.02.002, 2015.

873 Ferreiro Mählmann, R.: Correlation of very low grade data to calibrate a thermal maturity model in a nappe tectonic
874 setting, a case study from the Alps, *Tectonophysics*, 334, 1–33, 2001.

875 Filbrandt, J. B., Al-Dhahab, S., Al-Habsy, A., Harris, K., Keating, J., Al-mahruqi, S., Ozkaya, S. I., Richard, P. D.
876 and Robertson, T.: Kinematic interpretation and structural evolution of North Oman, Block 6, since the Late
877 Cretaceous and implications for timing of hydrocarbon migration into Cretaceous reservoirs, *GeoArabia*, 11(1),
878 97–115, 2006.

879 Fink, R., Virgo, S., Arndt, M., Visser, W., Littke, R. and Urai, J. L. L.: Solid bitumen in calcite veins from the
880 Natih Formation in the Oman Mountains: multiple phases of petroleum migration in a changing stress field, *Int. J.*
881 *Coal Geol.*, 157, 39–51, doi:10.1016/j.coal.2015.07.012, 2015.

882 Fitzgerald, P. G., Baldwin, S. L., Webb, L. E. and O’Sullivan, P. .: He data from slowly cooled crustal terranes
883 and the interpretation of intra-sample variations of single crystal apatite ages from vertical profiles., *Chem. Geol.*,
884 225, 91–120, 2006.

885 Flowers, R. M., Ketcham, R. A., Shuster, D. L. and Farley, K. A.: Apatite (U–Th)/He thermochronometry using a
886 radiation damage accumulation and annealing model, *Geochim. Cosmochim. Acta*, 73(8), 2347–2365,
887 doi:10.1016/J.GCA.2009.01.015, 2009.

888 Forbes, G. A., Jansen, H. S. M. and Schreurs, J.: *Lexicon of Oman - Subsurface Stratigraphy - Reference Guide*
889 *to the Stratigraphy of Oman’s Hydrocarbon Basins*, *GeoArabia Spec. Publ.* 5, 2010.

890 Fournier, M., Lepvrier, C., Razin, P. and Jolivet, L.: Late Cretaceous to Paleogene post-obduction extension and
891 subsequent Neogene compression in the Oman Mountains, *GeoArabia*, 11(4), 17–40, 2006.

892 Glennie, K. W., Boeuf, M. G. A., Clarke, M. W. H., Moody-Stuart, M., Pilaar, W. F. H. and Reinhardt, B. M.:
893 Late Cretaceous Nappes in Oman Mountains and Their Geologic Evolution : Reply, *Am. Assoc. Pet. Geol. Bull.*,
894 57(1), 5–27, 1973.

895 Glennie, K. W., Boeuf, M. G. A., Hughes Clarke, M. W., Moody-Stuart, M., Pilaar, W. F. H. and Reinhardt, B.
896 M.: *Geology of the Oman Mountains*, *Verh. van het K. Ned. Geol. Mijnbouwkd. Genoot.*, 31, 432, 1974.

897 Gnos, E. and Peters, T.: K-Ar ages of the metamorphic sole of the Semail Ophiolite: implications for ophiolite
898 cooling history, *Contrib. to Mineral. Petrol.*, 113, 325–332, 1993.

899 Goldstein, R. H.: Fluid inclusions in sedimentary and diagenetic systems, *Lithos*, 55(1–4), 159–193,
900 doi:10.1016/S0024-4937(00)00044-X, 2001.

901 Gomez-Rivas, E., Bons, P. D., Koehn, D., Urai, J. L., Arndt, M., Virgo, S., Laurich, B., Zeeb, C., Stark, L. and
902 Blum, P.: The Jabal Akhdar Dome in the Oman mountains: Evolution of a dynamic fracture system, *Am. J. Sci.*,
903 314(7), 1104–1139, doi:10.2475/07.2014.02, 2014.

904 Grelaud, C., Razin, P., Homewood, P. W. and Schwab, a. M.: Development of Incisions on a Periodically
905 Emergent Carbonate Platform (Natih Formation, Late Cretaceous, Oman), *J. Sediment. Res.*, 76(4), 647–669,
906 doi:10.2110/jsr.2006.058, 2006.

907 Grobe, A., Littke, R., Urai, J. L. J. L. L., Lünsdorf, N. K. K., Littke, R. and Lünsdorf, N. K. K.: Hydrocarbon
908 generation and migration under a large overthrust: The carbonate platform under the Semail Ophiolite, *Jebel*

909 Akhdar, Oman, *Int. J. Coal Geol.*, 168, 1–17, doi:10.1016/j.coal.2016.02.007, 2016.

910 Grobe, A., Virgo, S., von Hagke, C., Urai, J. L. L. and Littke, R.: Multiphase Structural Evolution of a Continental
911 Margin During Obduction Orogeny: Insights From the Jebel Akhdar Dome, Oman Mountains, *Tectonics*, 37(3),
912 888–913, doi:10.1002/2016TC004442, 2018.

913 Guenther, W. R., Reiners, P. W., Ketcham, R. A., Nasdala, L. and Giester, G.: *American Journal of Science*, Am.
914 J. Sci., 313(March), 145–198, doi:10.2475/03.2013.01, 2013.

915 Habsi, N. Al, Shukaili, M. Al, Tooqi, S. Al, Ehrenberg, S. N. and Bernecker, M.: Lithofacies, diagenesis and
916 reservoir quality of Upper Shu'aiba reservoirs in northwestern Oman, *GeoArabia*, 19(4), 145–182, 2014.

917 Hacker, B. R. and Mosenfelder, J. L.: Metamorphism and deformation along the emplacement thrust of the Samail
918 ophiolite, Oman, *Earth Planet. Sci. Lett.*, 144(3–4), 435–451, doi:10.1016/S0012-821X(96)00186-0, 1996.

919 Hacker, B. R., Mosenfelder, J. L. and Gnos, E.: Rapid emplacement of the Oman ophiolite: Thermal and
920 geochronologic constraints, *Tectonics*, 15(6), 1230–1247, 1996.

921 von Hagke, C., Cederbom, C. E., Oncken, O., Stöckli, D. F., Rahn, M. K. and Schlunegger, F.: Linking the northern
922 Alps with their foreland: The latest exhumation history resolved by low-temperature thermochronology, *Tectonics*,
923 31(5), n/a-n/a, doi:10.1029/2011TC003078, 2012.

924 Hanna, S. S.: The Alpine deformation of the Central Oman Mountains, *Geol. Soc. London, Spec. Publ.*, 49(1),
925 341–359, doi:10.1144/GSL.SP.1992.049.01.21, 1990.

926 Hansman, R. J., Ring, U., Thomson, S. N. and Brok, B. Den: Late Eocene uplift of the Al Hajar Mountains, Oman,
927 supported by stratigraphy and low-temperature thermochronology, *Tectonics*, doi:10.1002/2017TC004672, 2017.

928 Hansman, R. J., Albert, R., Gerdes, A. and Ring, U.: Absolute ages of multiple generations of brittle structures by
929 U-Pb dating of calcite, *Geology*, doi:10.1130/G39822.1, 2018.

930 Hassanzadeh, J. and Wernicke, B. P.: The Neotethyan Sanandaj-Sirjan zone of Iran as an archetype for passive
931 margin-arc transitions, *Tectonics*, 25(3), 586–621, doi:10.1002/2015TC003926, 2016.

932 Hilgers, C., Kirschner, D. L., Breton, J. P. P. and Urai, J. L.: Fracture sealing and fluid overpressures in limestones
933 of the Jabal Akhdar dome, Oman mountains, *Geofluids*, 6(2), 168–184, doi:10.1111/j.1468-8123.2006.00141.x,
934 2006.

935 Hillier, S., Mátyás, J., Matter, A. and Vasseur, G.: Illite/smectite diagenesis and its variable correlation with
936 vitrinite reflectance in the Pannonian Basin, *Clays Clay Miner.*, 43(2), 174–183,
937 doi:10.1346/CCMN.1995.0430204, 1995.

938 Holland, M., Urai, J. L., Muechez, P. and Willemse, E. J. M.: Evolution of fractures in a highly dynamic thermal,
939 hydraulic, and mechanical system - (I) Field observations in Mesozoic Carbonates, Jabal Shams, Oman Mountains,
940 *GeoArabia*, 14(1), 57–110, 2009.

941 Homewood, P., Razin, P., Grélaud, C., Droste, H., Vahrenkamp, V., Mettraux, M. and Mattner, J.: Outcrop
942 sedimentology of the Natih Formation, northern Oman: A field guide to selected outcrops in the Adam Foothills
943 and Al Jabal al Akhdar areas, *GeoArabia*, 13(3), 39–120, 2008.

944 Immenhauser, A. and Scott, R. W.: An estimate of Albian sea-level amplitudes and its implication for the duration
945 of stratigraphic hiatuses, *Sediment. Geol.*, 152(1–2), 19–28, doi:10.1016/S0037-0738(02)00260-9, 2002.

946 Immenhauser, A., Schlager, W., Burns, S. J., Scott, R. W., Geel, T., Lehmann, J., van der Gaast, S. and Bolder-
947 Schrijver, L. J. A. J. a.: Late Aptian to late Albian sea-level fluctuations constrained by geochemical and biological
948 evidence (Nahr Umr Formation, Oman), *J. Sediment. Res.*, 69(2), 434–446, doi:10.2110/jsr.69.434, 1999.

949 Jacobs, J., Thomas, R. J., Ksienzyk, A. K. and Dunkl, I. I.: Tracking the Oman Ophiolite to the surface - New

950 fission track and (U-Th)/He data from the Aswad and Khor Fakkan Blocks, United Arab Emirates, *Tectonophysics*,
951 644, 68–80, doi:10.1016/j.tecto.2014.12.018, 2015.

952 Jirman, P., Geršlová, E., Kalvoda, J. and Melichar, R.: 2d basin modelling in the eastern variscan fold belt (Czech
953 Republic): influence of thrusting on patterns of thermal maturation, *J. Pet. Geol.*, 41(2), 175–188,
954 doi:10.1111/jpg.12699, 2018.

955 De Keijzer, M., Hillgartner, H., Al Dhahab, S. and Rawnsley, K.: A surface-subsurface study of reservoir-scale
956 fracture heterogeneities in Cretaceous carbonates, North Oman, *Geol. Soc. London, Spec. Publ.*, 270(1), 227–244,
957 doi:10.1144/GSL.SP.2007.270.01.15, 2007.

958 Ketcham, R. A.: Forward and Inverse Modeling of Low-Temperature Thermochronometry Data, *Rev. Mineral.*
959 *Geochemistry*, 58, 275–314, doi:10.2138/rmg.2005.58.11, 2005.

960 Ketcham, R. A., Mora, A. and Parra, M.: Deciphering exhumation and burial history with multi-sample down-well
961 thermochronometric inverse modelling, *Basin Res.*, 30, 48–64, doi:10.1111/bre.12207, 2018.

962 Koehrer, B., Zeller, M., Aigner, T., Poepfelreiter, M., Milroy, P., Forke, H. and Al-Kindi, S.: Facies and
963 stratigraphic framework of a Khuff outcrop equivalent: Saiq and Mahil formations, Al Jabal al-Akhdar, Sultanate
964 of Oman, *GeoArabia*, 15(2), 91–156, 2010.

965 Koehrer, B., Aigner, T. and Poppelreiter, M.: Field-scale geometries of Upper Khuff reservoir geobodies in an
966 outcrop analogue (Oman Mountains, Sultanate of Oman), *Pet. Geosci.*, 17(1), 3–16, doi:10.1144/1354-079310-
967 009, 2011.

968 Kouketsu, Y., Mizukami, T., Mori, H., Endo, S., Aoya, M., Hara, H., Nakamura, D. and Wallis, S.: A new approach
969 to develop the Raman carbonaceous material geothermometer for low-grade metamorphism using peak width, *Isl.*
970 *Arc*, 23, 33–50, doi:10.1111/iar.12057, 2014.

971 Levina, M., Horton, B. K., Fuentes, F. and Stockli, D. F.: Cenozoic sedimentation and exhumation of the foreland
972 basin system preserved in the Precordillera thrust belt (31–32°S), southern central Andes, Argentina, *Tectonics*,
973 33(9), 1659–1680, doi:10.1002/2013TC003424, 2014.

974 Lippard, S. J., Smewing, J. D., Rothery, D. a. and Browning, P.: The geology of the Dibba zone, northern Oman
975 mountains - a preliminary study, *J. Geol. Soc. London.*, 139(1), 59–66, doi:10.1144/gsjgs.139.1.0059, 1982.

976 Loosveld, R. J. H., Bell, A. and Terken, J. J. M.: The Tectonic Evolution of Interior Oman, *GeoArabia*, 1(1), 28–
977 51 [online] Available from: [http://search.ebscohost.com/login.aspx?direct=true&db=geh&AN=1998-
978 061521&site=ehost-live&scope=cite](http://search.ebscohost.com/login.aspx?direct=true&db=geh&AN=1998-061521&site=ehost-live&scope=cite), 1996.

979 Lünsdorf, N. K.: Raman spectroscopy of dispersed vitrinite - methodical aspects and correlation with reflectance,
980 *Int. J. Coal Geol.*, 153(1), 75–86, doi:10.1016/j.coal.2015.11.010, 2016.

981 Lünsdorf, N. K., Dunkl, I., Schmidt, B. C., Rantitsch, G. and von Eynatten, H.: The thermal history of the Steinach
982 Nappe (eastern Alps) during extension along the Brenner Normal Fault system indicated by organic maturation
983 and zircon (U-Th)/ He thermochronology, *Austrian J. Earth Sci.*, 105(3), 17–25, 2012.

984 Lünsdorf, N. K., Dunkl, I., Schmidt, B. C., Rantitsch, G. and von Eynatten, H.: Towards a Higher Comparability
985 of Geothermometric Data Obtained by Raman Spectroscopy of Carbonaceous Material. Part 2: A Revised
986 Geothermometer, *Geostand. Geoanalytical Res.*, 41(4), 593–612, doi:10.1111/ggr.12178, 2017.

987 Lutz, R., Littke, R., Gerling, P. and Bönnemann, C.: 2D numerical modelling of hydrocarbon generation in
988 subducted sediments at the active continental margin of Costa Rica, *Mar. Pet. Geol.*, 21(6), 753–766,
989 doi:10.1016/j.marpetgeo.2004.03.005, 2004.

990 Mair, D., Lechmann, A., Herwegh, M., Nibourel, L. and Schlunegger, F.: Linking Alpine deformation in the Aar

991 Massif basement and its cover units – the case of the Jungfrau–Eiger mountains (Central Alps, Switzerland), *Solid*
992 *Earth*, 9(5), 1099–1122, doi:10.5194/se-9-1099-2018, 2018.

993 Mann, a., Hanna, S. S. and Nolan, S. C.: The post-Campanian tectonic evolution of the Central Oman Mountains:
994 Tertiary extension of the Eastern Arabian Margin, *Geol. Tectonics Oman Reg.*, 49(1), 549–563,
995 doi:10.1144/gsl.sp.1992.049.01.33, 1990.

996 Mashhadi, Z. S., Rabbani, A. R. and Kamali, M. R.: Geochemical characteristics and hydrocarbon generation
997 modeling of the Kazhdumi (Early Cretaceous), Gurpi (Late Cretaceous) and Pabdeh (Paleogene) formations,
998 Iranian sector of the Persian Gulf, *Mar. Pet. Geol.*, 66, 978–997, doi:10.1016/J.MARPETGEO.2015.08.008, 2015.

999 Mattern, F. and Scharf, A.: Postobductional extension along and within the Frontal Range of the Eastern Oman
1000 Mountains, *J. Asian Earth Sci.*, 154, doi:10.1016/j.jseas.2017.12.031, 2018.

1001 Le Metour, J., Rabu, D., Tegye, M., Bechennec, F., Beurrier, M. and Villey, M.: Subduction and obduction: two
1002 stages in the EoAlpine tectonometamorphic evolution of the Oman Mountains, *Geol. Soc. London, Spec. Publ.*,
1003 49(1), 327–339, doi:10.1144/GSL.SP.1992.049.01.20, 1990.

1004 Mouthereau, F.: Timing of uplift in the Zagros belt/Iranian plateau and accommodation of late Cenozoic Arabia -
1005 Eurasia convergence, *Geol. Mag.*, 148(5–6), 726–738, doi:10.1017/S0016756811000306, 2011.

1006 Mozafari, M., Swennen, R., Balsamo, F., Clemenzi, L., Storti, F., El Desouky, H., Vanhaecke, F., Tueckmantel,
1007 C., Solum, J. and Taberner, C.: Paleofluid Evolution In Fault-Damage Zones: Evidence From Fault-Fold
1008 Interaction Events In the Jabal Qusaybah Anticline (Adam Foothills, North Oman), *J. Sediment. Res.*, 85(12),
1009 1525–1551, doi:10.2110/jsr.2015.95, 2015.

1010 Muchez, P., Marshall, J. D., Touret, J. L. R. and Viaene, W. a.: Origin and migration of palaeofluids in the Upper
1011 Visean of the Campine Basin, northern Belgium, *Sedimentology*, 41(1), 133–145, doi:10.1111/j.1365-
1012 3091.1994.tb01395.x, 1994.

1013 Neumaier, M.: Structural Restoration and Basin and Petroleum Systems Modeling: Case Studies from the Monagas
1014 Fold and Thrust Belt, Venezuela and the Moroccan Atlantic Margin, Dissertation, RWTH Aachen University.,
1015 2015.

1016 Nibourel, L., Berger, A., Egli, D., Luensdorf, N. K. and Herwegh, M.: Large vertical displacements of a crystalline
1017 massif recorded by Raman thermometry, *Geology*, 46(10), 879–882, doi:10.1130/G45121.1, 2018.

1018 Nicolas, A. and Boudier, F. F.: Structural contribution from the Oman ophiolite to processes of crustal accretion
1019 at the East Pacific Rise, *Terra Nov.*, 27(2), 77–96, doi:10.1111/ter.12137, 2015.

1020 Nolan, S. C., Skelton, P. W., Clissold, B. P. and Smewing, J. D.: Maastrichtian to early Tertiary stratigraphy and
1021 palaeogeography of the Central and Northern Oman Mountains, *Geol. Soc. London, Spec. Publ.*, 49(1), 495–519,
1022 doi:10.1144/gsl.sp.1992.049.01.31, 1990.

1023 Nöth, S., Karg, H. and Littke, R.: Reconstruction of Late Paleozoic heat flows and burial histories at the
1024 Rhenohercynian-Subvariscan boundary, Germany, *Int. J. Earth Sci.*, 90(2), 234–256, doi:10.1007/s005310000114,
1025 2001.

1026 Oliver, J.: Fluids expelled tectonically from orogenic belts: Their role in hydrocarbon migration and other geologic
1027 phenomena, *Geology*, 14(February), 99–102, 1986.

1028 Oxburgh, E. R. and Turcotte, D. L.: Thermal gradients and regional metamorphism in overthrust terrains with
1029 special reference to the Eastern Alps, *Schweizerische Mineral. und Petrogr. Mitteilungen*, 54(2/3), 642–662, 1974.

1030 Philip, J., Borgomano, J. and Al-Maskiry, S.: Cenomanian–Early Turonian carbonate platform of Northern Oman:
1031 stratigraphy and palaeo-environments, *Palaeogeogr. Palaeoclimatol. Palaeoecol.*, 119, 77–92, 1995.

1032 Pöppelreiter, M. C., Schneider, C. J., Obermaier, M., Forke, H. C., Koehrer, B. and Aigner, T.: Seal turns into
1033 reservoir: Sudair equivalents in outcrops, A1 Jabal al-Akhdar, Sultanate of Oman, *GeoArabia*, 16(1), 69–108,
1034 2011.

1035 Poupeau, G., Saddiqi, O., Michard, A., Goffé, B. and Oberhänsli, R.: Late thermal evolution of the Oman
1036 Mountains subophiolitic windows: Apatite fission-track thermochronology, *Geology*, 26(12), 1139–1142, 1998.

1037 Pratt, R., Smewing, D., Swansea, S. A., Pratt, B. R. and Smewing, J. D.: Jurassic and Early Cretaceous platform
1038 margin configuration and evolution, central Oman Mountains, *Geol. Soc. London, Spec. Publ.*, 49(1), 69–88,
1039 doi:10.1144/GSL.SP.1992.049.01.06, 1990.

1040 Rabu, D., Le Metour, J., Bechennec, F., Beurrier, M., Villey, M. and Bourdillon-Jeudy de Grissac, C.: Sedimentary
1041 aspects of the Eo-Alpine cycle on the northeast edge of the Arabian Platform (Oman Mountains), *Geol. Soc.
1042 London, Spec. Publ.*, 49(1), 49–68, doi:10.1144/GSL.SP.1992.049.01.05, 1990.

1043 Rantitsch, G. and Rainer, T.: Thermal modeling of Carboniferous to Triassic sediments of the Karawanken Range
1044 (Southern Alps) as a tool for paleogeographic reconstructions in the Alpine-Dinaridic-Pannonian realm, *Int. J.
1045 Earth Sci.*, 92(2), 195–209, doi:10.1007/s00531-003-0312-4, 2003.

1046 Reiners, P. W.: Zircon (U-Th)/He Thermochronometry, *Rev. Mineral. Geochemistry*, 58(1936), 151–179,
1047 doi:10.2138/rmg.2005.58.6, 2005.

1048 Reutter, K.-J., Teichmüller, M. and Teichmüller, R.: The Coalification Pattern in the Northern Apennines and its
1049 Palaeogeothermic and Tectonic Significance, *Geol. Rundschau/Geologische Rundschau*, 72(3), 861–894, 1988.

1050 Rioux, M., Bowring, S., Kelemen, P., Gordon, S., Miller, R. and Dudás, F.: Tectonic development of the Semail
1051 ophiolite: High-precision U-Pb zircon geochronology and Sm-Nd isotopic constraints on crustal growth and
1052 emplacement, *J. Geophys. Res. Solid Earth*, 118(5), 2085–2101, doi:10.1002/jgrb.50139, 2013.

1053 Rioux, M., Garber, J., Bauer, A., Bowring, S., Searle, M., Kelemen, P. and Hacker, B.: Synchronous formation of
1054 the metamorphic sole and igneous crust of the Semail ophiolite: New constraints on the tectonic evolution during
1055 ophiolite formation from high-precision U–Pb zircon geochronology, *Earth Planet. Sci. Lett.*, 451, 185–195,
1056 doi:10.1016/j.epsl.2016.06.051, 2016.

1057 Robertson, A.: The transition from a passive margin to an Upper Cretaceous foreland basin related to ophiolite
1058 emplacement in the Oman Mountains, *Geol. Soc. Am. Bull.*, 99, 633–653, doi:10.1130/0016-7606(1987)99<633,
1059 1987.

1060 Rolandone, F., Lucazeau, F., Leroy, S., Mareschal, J.-C., Jorand, R., Goutorbe, B. and Bouquerel, H.: New heat
1061 flow measurements in Oman and the thermal state of the Arabian Shield and Platform, *Tectonophysics*, 589, 77–
1062 89, doi:10.1016/j.tecto.2012.12.034, 2013.

1063 Roure, F., Andriessen, P., Callot, J. P., Faure, J. L., Ferket, H., Gonzales, E., Guilhaumou, N., Lacombe, O.,
1064 Malandain, J., Sassi, W., Schneider, F., Swennen, R., Vilasi, N., Box, P. O., Gonzales, E., Guilhaumou, N.,
1065 Lacombe, O., Malandain, J., Sassi, W., Schneider, F., Swennen, R. and Vilasi, N.: The use of palaeo-thermo-
1066 barometers and coupled thermal, fluid flow and pore-fluid pressure modelling for hydrocarbon and reservoir
1067 prediction in fold and thrust belts, *Geol. Soc. London, Spec. Publ.*, 348(1), 87–114, doi:10.1144/SP348.6, 2010.

1068 Saddiqi, O., Michard, A. N., Goffé, B. R., Poupeau, G. É. and Oberhänsli, R. O.: Fission-track thermochronology
1069 of the Oman Mountains continental windows, and current problems of tectonic interpretation, *Bull. la Soc. Geol.
1070 Fr.*, 177(3), 127–143, doi:10.2113/gssgfbull.177.3.127, 2006.

1071 Schito, A., Corrado, S., Trolese, M., Aldega, L., Caricchi, C., Cirilli, S., Grigo, D., Guedes, A., Romano, C., Spina,
1072 A. and Valentim, B.: Assessment of thermal evolution of Paleozoic successions of the Holy Cross Mountains

1073 (Poland), *Mar. Pet. Geol.*, 80, 112–132, doi:10.1016/J.MARPETGEO.2016.11.016, 2017.

1074 Schito, A., Andreucci, B., Aldega, L., Corrado, S., Di Paolo, L., Zattin, M., Szaniawski, R., Jankowski, L. and
1075 Mazzoli, S.: Burial and exhumation of the western border of the Ukrainian Shield (Podolia): a multi-disciplinary
1076 approach, *Basin Res.*, 30, 532–549, doi:10.1111/bre.12235, 2018.

1077 Scott, R. W.: Chronostratigraphy of the Cretaceous carbonate shelf, southeastern Arabia, *Geol. Soc. London, Spec.*
1078 *Publ.*, 49(1), 89–108, doi:10.1144/GSL.SP.1992.049.01.07, 1990.

1079 Searle, M. P.: Sequence of thrusting and origin of culminations in the northern and central Oman Mountains, *J.*
1080 *Struct. Geol.*, 7(2), 129–143, doi:10.1016/0191-8141(85)90127-0, 1985.

1081 Searle, M. P. and Cox, J. O. N.: Subduction zone metamorphism during formation and emplacement of the Semail
1082 ophiolite in the Oman Mountains, *Geol. Mag.*, 139(03), 241–255, doi:10.1017/S0016756802006532, 2002.

1083 Searle, M. P., Warren, C. J., Waters, D. J. and Parrish, R. R.: Subduction zone polarity in the Oman Mountains:
1084 implications for ophiolite emplacement, *Geol. Soc. London, Spec. Publ.*, 218(1), 467–480,
1085 doi:10.1144/GSL.SP.2003.218.01.24, 2003.

1086 Searle, M. P., Warren, C. J. J., Waters, D. J. and Parrish, R. R.: Structural evolution, metamorphism and
1087 restoration of the Arabian continental margin, Saih Hatat region, Oman Mountains, *J. Struct. Geol.*, 26(3), 451–
1088 473, doi:10.1016/j.jsg.2003.08.005, 2004.

1089 Searle, M. P. M. P.: Structural geometry, style and timing of deformation in the Hawasina Window, Al Jabal al
1090 Akhdar and Saih Hatat culminations, Oman Mountains, *GeoArabia*, 12(2), 99–130, 2007.

1091 Secor, D. T. jr.: Role of fluid pressure in jointing, *Am. J. Sci.*, 263(October), 633–646, 1965.

1092 Stenhouse, P.: *Reactive Transport and Fluid Pathways in Fracture-Controlled Flow Systems*, (Doctoral
1093 Dissertation), Australian National University., 2014.

1094 Sweeney, J. J. and Burnham, A. K.: Evaluation of a Simple Model of Vitrinite Reflectance Based on Chemical
1095 Kinetics, *Am. Assoc. Pet. Geol. Bull.*, 74(10), 1559–1570, 1990.

1096 Teichmüller, R. and Teichmüller, M.: Relations between coalification and palaeogeothermics in Variscan and
1097 Alpidic foredeeps of western Europe, *Lect. Notes Earth Sci.*, 5, 1986.

1098 Terken, J. M. J.: The Natih petroleum system of north Oman, *GeoArabia*, 4(2), 157–180, 1999.

1099 Terken, J. M. J., Frewin, N. L., Indrelid, S. L. and Indrelin, S. L.: Petroleum systems of Oman: Charge timing and
1100 risks, *Am. Assoc. Pet. Geol. Bull.*, 85(10), 1817–1845, 2001.

1101 Vahrenkamp, V. C.: Chemostratigraphy of the Lower Cretaceous Shu'aiba Formation: A delta-13C reference
1102 profile for the Aptian Stage from the southern Neo-Tethys Ocean, *GeoArabia*, 1, 107–137, 2010.

1103 Velde, B. and Lanson, B.: Comparison of I/S transformation and maturity of organic matter at elevated
1104 temperatures, *Clays Clay Miner.*, 41(2), 178–183, 1993.

1105 Vermeesch, P.: How many grains are needed for a provenance study?, *Earth Planet. Sci. Lett.*, 224(3–4), 441–451,
1106 doi:10.1016/J.EPSL.2004.05.037, 2004.

1107 Virgo, S.: Aspects of crack-seal vein system evolution. (Doctoral Dissertation). Retrieved from [http://nbn-](http://nbn-resolving.de/urn/resolver.pl?urn=urn:nbn:de:hbz:82-opus-33858)
1108 [resolving.de/urn/resolver.pl?urn=urn:nbn:de:hbz:82-opus-33858](http://nbn-resolving.de/urn/resolver.pl?urn=urn:nbn:de:hbz:82-opus-33858)., RWTH Aachen University., 2015.

1109 Virgo, S. and Arndt, M.: Evolution of a crack-seal calcite vein network in limestone: a high resolution structural,
1110 microstructural and geochemical study from the Jebel Akhdar high pressure cell, Oman Mountains, (Diploma
1111 Thesis), RWTH Aachen [online] Available from: <http://darwin.bth.rwth-aachen.de/opus3/volltexte/2010/3385/>,
1112 2010.

1113 Virgo, S., Arndt, M., Sobisch, Z. Z. and Urai, J. L.: Development of fault and vein networks in a carbonate

1114 sequence near Hayl al-Shaz, Oman Mountains, *GeoArabia*, 18(2), 99–136 [online] Available from:
1115 <http://www.gulfpetrolink.net/publication/vol18.php>, 2013.

1116 Visser, W.: Burial and thermal history of Proterozoic source rocks in Oman, *Precambrian Res.*, 54(1), 15–36,
1117 doi:10.1016/0301-9268(91)90066-J, 1991.

1118 Warburton, J., Burnhill, T. J., Graham, R. H. and Isaac, K. P.: The evolution of the Oman Mountains Foreland
1119 Basin, *Geol. Soc. London, Spec. Publ.*, 49(1), 419–427, doi:10.1144/GSL.SP.1992.049.01.26, 1990.

1120 Warren, C. J., Parrish, R. R., Searle, M. P. and Waters, D. J.: Dating the subduction of the Arabian continental
1121 margin beneath the Semail ophiolite, Oman, *Geology*, 31(10), 889, doi:10.1130/G19666.1, 2003.

1122 Warren, C. J., Parrish, R. R., Waters, D. J. and Searle, M. P.: Dating the geologic history of Oman's Semail
1123 ophiolite: insights from U-Pb geochronology, *Contrib. to Mineral. Petrol.*, 150(4), 403–422, doi:10.1007/s00410-
1124 005-0028-5, 2005.

1125 Wygrala, B. P.: Integrated study on an oil field in the southern po basin, northern italy, *Berichte der*
1126 *Kernforschungsanlage Jülich*, 2313(October), 217, 1989.

1127

1128